

**Republic of Iraq
Ministry of Higher Education
and Scientific Research
AL-Nahrain University
College of Science**



Maximum Power Point Tracking approach based on Temperature for PV Surfaces using PSPICE program

A Thesis

Submitted to the College of Science, Al-Nahrain University in Partial
Fulfillment of the Requirements for Degree of Master of Science in
Physics.

By

Harith Mohammed Saeed Hamed

B.Sc., Al-Nahrain University (2014)

Supervised by

Dr. Zainab M. Kubba

March 2017

Rajab 1438

Supervisor's Certification

I certify that this thesis entitled "*Maximum Power Point Tracking approach based on temperature for PV surfaces using PSPICE program*" was prepared by "*Harith Mohammed Saeed Hamed*", under our supervision at the College of Science - Al-Nahrain University as a partial fulfillment of the requirements for the Degree of Master of Science in Physics Science.

Signature:




Name: **Dr. Zainab M. Younis**

Scientific Degree: **Assistant Professor**

Date: **5/4/2017**

In view of the available recommendation, I forward this project for debate by the examination committee.

Signature:



Name: **Dr. Saad Naji Abood**

Scientific Degree: **Professor**

Title: **Head of Physics Science Department**

College of Science / Al Nahrain University.

Date: **5/4/2017**

Committee Certification

We, the examining committee certify that we have read this thesis entitled "*Maximum Power Point tracking approach based on temperature for PV surfaces using PSPICE program*" and examined the student "*Harith Mohammed Saeed Hamed*" in its contents and that in our opinion, it is accepted for the Degree of Master of Science in Physics Science.

Signature: 

Name: **Dr. Emad Al-Shakarchi**

Scientific Degree: **Professor**

Date: **9**/4/2017

(Chairman)

Signature: 

Name: **Dr. Ali H. Al-Hamdani**

Scientific Degree: **Assistant Professor**

Date: **9**/4/2017

(Member)

Signature: 

Name: **Dr. Wisam J. Aziz**

Scientific Degree: **Assistant Professor**

Date: **10**/4/2017

(Member)

Signature: 

Name: **Dr. Zainab M. Younis**

Scientific Degree: **Assistant Professor**

Date: **5** /4/ 2017

(Member/ Supervised)

I, hereby certify upon the decision of the examining committee.

Signature:

Name: **Dr. Hadi M. A. Abood**

Scientific Degree: **Professor**

Title: **Dean of College of Science**

Date: **1** / 2017

DEDICATION

***TO MY FATHER AND MY
FAMILY WHOSE VALUES
LIT THE WAY***

Acknowledgment

Praise is to Allah lord of the creation. Best prayer and peace be unto, the prophet Muhammed messenger of Allah, and his pure holy descendant, and Nobel companions.

Then, I would like to express my gratitude to my supervisors Dr. Zainab M. Kubba and for her valuable guidance and constant help through the course of this work.

My personal thank to the Staff of Physics Department at Al-Nahrain University for providing the opportunity and financial support to accomplish this study.

My deep gratitude to my friend who were very patient and encouraging during the period of my study.

Harith

10/ 4 / 2017

Abstract

This research study the effect of Photovoltaic surface temperature on Photovoltaic panel output characteristics. First, circuit simulator PSPICE was used to compose Photovoltaic panel model at 75 W, 4.8 A and 21 V. Then, study the behavior of it under varying conditions (solar insolation, environmental temperature and PV panel surface temperature). ABM feature of PSPICE was used to include the above parameters in PV PSPICE model and produced temperature dependent voltage. The voltage converted to current with galvanic insolation by element Gpjoy with gain 0.8. The model defined as hierarichal block in PSPICE library and could be called as individual source for any applications.

After studying the effect of PV surface temperature on its (I-V) curves specially the position of the maximum power point, this temperature was used to keep tracking of the optimal voltage for the PV panel at the MPP. Therefore DC -DC boost converter was used to achieve this purpose.

Boost converter was raise a PV panel voltage from 17 V to 34 V for all variation of surface temperature from 300 K to 350 K at frequency 10 KHz and $\Delta V_o = 5$ V.

List of Contents

Contents		
Abstract		II
List of Contents		III
List of Figures		V
List of Tables		VIII
List of Symbols		VIII
List of Abbreviations		IX
Chapter One “General Introduction”		
1.1	Introduction	2
1.2.1	Advantages of Photovoltaic	3
1.2.2	Disadvantages of photovoltaic	4
1.3	Types of Photovoltaic systems	4
1.4	Basics principles of Photovoltaic system	4
1.4.1	The effect of light	6
1.5	Literature overview	7
1.6	The Aim	12
1.7	Thesis overview	12
Chapter Two “Description of photovoltaic system”		
2.1	PV modeling	15
2.2	The Physics of PV solar cell	17
2.3	The Operation Temperature	19

2.4	Electrical Power Converters	22
2.4.1	Boost Converter	23
2.4.2	Boost Converter Operation principles	24
2.4.3	Critical inductance	28
2.4.4	Output capacitance	28
2.5	Maximum Power Point Tracking Algorithms	29
2.5.1	Temperature method	31
Chapter three “Simulation Results of The Proposed PV Model and System Design”		
3.1	Introduction	36
3.2	Design of photovoltaic panel in PSPICE	36
3.3	Hierarchical Block	52
3.4	Electrical Boost Converter	59
3.4.1	Design of Boost Converter	59
3.5	Maximum power point tracking technique	61
3.5.1	Control signal	61
3.5.2	PWM Signal gate drive circuit	63
3.6	Results	67
Chapter Four “Conclusion and future work”		
4.1	Conclusion	77
4.2	Future work	78

References	80
------------	----

List of Figures

Figure No.	Caption	Page No.
2-1	Single diode model of a PV cell (equivalent PV circuit).	16
2-2	Basics boost converter circuit.	24
2-3	The Operation Principles of Boost Converter (at switch on).	25
2-4	The Operation Principles of Boost Converter (at switch off).	26
2-5	Typical input and output data related to MPPT algorithms.	32
3-1	The basic blocks of building Photovoltaic system.	37
3-2	The voltage cell as a function of the saturation current I_S .	38
3-3	The circuit diagram used to determine R_S .	38
3-4	The voltage cell as a function of internal resistance R_S	39
3-5	The created PV panel as represented on Orcad-PSPICE.	41
3-6	The (I-V) curve of the panel under STC.	44
3-7	The (I-V) curves of the PV panel at different temperature under a constant irradiation $1000\text{W}/\text{m}^2$.	45
3-8	The (I-V) curves of the PV panel at surface temperature under a constant irradiation $1000\text{W}/\text{m}^2$.	46
3-9	The (I-V) curves of the PV panel at different irradiation under a constant temperature $T=25\text{ C}^\circ$.	47
3-10	The (P-V) curve of the PV panel under STC.	48

3-11	The (P-V) curves of the PV panel at different surface temperature under a constant irradiation $1000\text{W}/\text{m}^2$	49
3-12	The (P-V) curves of the PV panel at different temperature under a constant irradiation $1000\text{W}/\text{m}^2$	50
3-13	The (P-V) curves of the PV panel at different irradiation under a constant temperature $T=25\text{ C}^\circ$.	51
3-14	The hierarchical block (part) of SP75 in state of optimum load condition.	52
3-15	The (I-V) curves of the Hierarchal PV panel at different surface temperature under a constant irradiation $1000\text{W}/\text{m}^2$.	53
3-16	The (I-V) curves of the Hierarchal PV panel at different temperature under a constant irradiation $1000\text{W}/\text{m}^2$	54
3-17	The (I-V) curves of the Hierarchal PV panel at different irradiation under a constant temperature $T=25\text{ C}^\circ$.	55
3-18	The (P-V) curves of the Hierarchal PV panel at different temperature under a constant irradiation $1000\text{W}/\text{m}^2$.	56
3-19	The (P-V) curves of the Hierarchal PV panel at different irradiation under a constant temperature $T=25\text{ C}^\circ$	57
3-20	The (P-V) curves of the Hierarchal PV panel at different surface temperature under a constant irradiation $1000\text{W}/\text{m}^2$.	58
3-21	The electrical circuit of the boost converter.	59
3-22	The (ABM) analog behavioral table with temperature sensor as {val}.	62
3-23	The Error amplifier with two input one from PV panel and another from ABM table.	63
3-24	The compater Op-Amp to produce square signals.	64

3-25	The total simulated circuit of PV system with temperature controlled at PSPICE.	65
3-26	The total simulated circuit of PV system with temperature controlled using 555 timer at PSPICE	66
3-27	Current from PV panel at different surface temperature	67
3-28	Output voltage from PV panel at different surface temperature.	67
3-29	Different surface temperature as input to ABM table	68
3-30	Output voltage from ABM table.	68
3-31	Control signal from Op-Amp(u7).	69
3-32	Saw tooth method signal for different surface temperature.	69
3-33	PWM-signal for different surface temperature from 555.	70
3-34	The inductor current in the boost converter for different surface temperature.	70
3-35	Boost converter output voltages from saw tooth method for different surface temperature.	72
3-36	Boost converter output current from saw tooth method for different surface temperature.	73
3-37	Boost converter output voltage by using 555 timer for different surface temperature.	74
3-38	Boost converter output current by using 555 timer for different surface temperature.	75

List of Tables

Table No.	Caption	Page No.
(2-1)	Duty cycle for maximum power point operation.	34

List of Symbols

Symbol	Description	Units
I_s	Saturation current	(A)
R_s	Parasitic resistance	(Ω)
E_g	Energy gap	(eV)
C_{j0}	Zero-bias p-n capacitance	(f)
N	Emission coefficient	Without
M	p-n grading coefficient	Without
V _J	p-n potential	(V)
F_c	Forward-bias depletion capacitance coefficient	Without
MPP	Maximum power point	Without
e	Electron charge	(eV)
K	Boltzmann constant	(J/k)

List of Abbreviations

Symbol	Description
XTI	Temperature exponent
IKF	High-injection knee current
ISR	Recombination current parameter
NR	Emission coefficient for ISR
BV	Reverse breakdown knee voltage
IBV	Reverse breakdown knee current



Chapter One

Chapter One

General Introduction and Literature Review

1.1 Introduction:

In past years, it has become increasingly clear that the present method of generating energy has no future. Thus, finiteness of resources is noticeably reflected in the rising prices of oil and gas. At the same time, we are it has been noticed the burn effects of fossil fuels. The melting of the glaciers, the rise of the ocean levels and the increase in weather extremes, as well as the nuclear catastrophe in Fukushima, all show that nuclear energy is not the path to follow in the future. Besides the unsolved final storage question, fewer and fewer people are willing to take the risk of large parts of their country being radioactive. Fortunately, there is a solution with a sustainable energy supply can be assured: renewable energy sources. These use infinite sources as a basis for energy supplies and can ensure a full supply with a suitable combination of different technologies such as biomasses, photovoltaics, wind power, and so on. A particular role in the number of renewable energies is played by photovoltaics. They permit an emission-free conversion of sunlight into electrical energy and, because of their great potential, will be an important pillar in future energy systems. However, the changeover of our energy supply will be a huge task that will only be mastered with the imagination and knowledge of engineers and technicians. [1]

Photovoltaic system is the technology that generates direct current (DC) electrical power measured in watts (W) or kilowatts (kW) from

semiconductors when they are illuminated by photons. As long as the light is shining on the solar cell (the name for the individual PV element), it generates electrical power. When the light stops, the electricity stops. Solar cells never need recharging like a battery. Some have been in continuous outdoor operation on Earth or in space for over 30 years [2].

Solar cells are typically made of semiconductor materials, which have weakly bonded electrons occupying a band of energy called the valence band. When energy exceeding a certain threshold, called the bandgap energy, is applied to a valence electron, now the electron is somewhat “free” to move around in a new energy band called the conduction band where it can “conduct” electricity through the material. Thus, the free electrons in the conduction band are separated from the valence band by the bandgap (measured in units of electron volts or eV). This energy needed to free the electron can be supplied by photons, which are particles of light [2].

1.2.1 Advantages of Photovoltaic

- No emission, combustion or radioactive waste (does not contribute perceptibly to global climate change or air/water pollution).
- Low operating costs (no fuel).
- No moving parts (no wear); theoretically everlasting.
- Ambient temperature operation (no high-temperature corrosion or safety issues).
- High reliability of solar modules (manufacturers' warranties over 20

years) [2].

1.2.2 Disadvantages of photovoltaic

- High initial (installed) costs.
- Unpredictable hourly or daily output. [2]

1.3 Types of Photovoltaic systems

- Systems That feed power directly into the utility grid.
- Stand - alone systems that charge batteries, perhaps with generator back-up. Where this type of photovoltaic was used in this project.
- Applications in which the load is directly connected to the Photovoltaic: case of water – pumping systems.

1.4 Basics principle of Photovoltaic system

The photovoltaic (PV) effect is the basis of the conversion of light to electricity in photovoltaic, or solar, cells. Described simply, the PV effect is as follows: Light, which is pure energy, enters a PV cell and imparts enough energy to some electrons (negatively charged atomic particles) to free them. A built-in-potential barrier in the cell acts on these electrons to produce a voltage (the so-called photovoltage), which can be used to drive a current through a circuit.

All matter is made from atoms. They, in turn, are composed of three kinds of particles: protons, neutrons, and electrons. Protons (positively charged) and electrons (negatively charged) attract each other; neutrons are not electrically attracted to either and are said to be neutral. The positively charged protons and the neutral neutrons reside in a nucleus, the close-packed center of the atom. The electrons-much lighter than the protons {or neutrons}-orbit the nucleus. Although an atom contains charged particles, overall it is electrically neutral because it has the same number of protons and electrons [3].

Different atoms have different numbers of protons. For every proton in an atom's nucleus, there is an electron orbiting the nucleus. The orbital locations (and the motion of the 'electrons about their own axis) are determined by the energy of the electrons. The electrons, in particular those furthest from the nucleus, interact with electrons from other atoms and determine the way in which like or dissimilar atoms combine into larger structures such as solids.

The silicon atom has fourteen electrons arranged in such a way that the outer four can be given to, accepted from, or shared with another atom. These four outer electrons are called valence electrons. Large numbers of silicon atoms, through their valence electrons, can bond together to form a solid. As a solid, each silicon atom usually shares each of its four valence electrons with another silicon atom. Each basic silicon unit, forming a tetrahedral

arrangement, thereby contains five atoms (the one silicon atom plus the four others it shares electrons with).

Each atom in the silicon solid is held in place at a fixed distance and angle with each of the atoms with which it shares a bond. This regular, fixed formation of a solid's atoms is called a crystal lattice. Solids can form from several differently shaped crystal lattices. (All solids are not crystalline, however; some can have multiple crystalline forms and/or none at all.) For silicon, the atoms are located so as to form the vertices of a cube with single atoms centered at each of the faces of the cubic pattern. The cubic arrangement repeats throughout the crystal [3]

1.4.1 The Effect of light

When light strikes a silicon crystal, it may be reflected, be absorbed, or may go right through. Let's concentrate on the light that is absorbed. Usually when light of relatively low energy is absorbed by a solid, it creates Light of greater energy can alter the electrical properties of the crystal. If such light strikes a bound electron, the electron is torn from its place in the crystal. This leaves behind a silicon bond missing an electron and frees an electron to move about in the crystal. A bond missing an electron, rather picturesquely, is called a hole. An electron free to move because free electrons are the means by which electricity flows. Both the conduction-band electrons and the holes play important parts in the electrical behavior of PV cells. Electrons and holes freed from their positions in the crystal in this manner are said to be light-generated electron-hole pairs. Move throughout the crystal is said to be in the crystal's conduction band, because free electrons are the means by which electricity

flows. Both the conduction-band electrons and the holes play important parts in the electrical behavior of PV cells. Electrons and holes freed from their positions in the crystal in this manner are said to be light-generated electron-hole pairs and finally generate the electricity [3].

1.5 Literature overview:

Practical solar cells have only been available since the mid-1950's, but the phenomena were discovered by French scientist Henri Becquerel in 1839. [4]

Emery and Burdick (1996) state that Photovoltaic (PV) cells and modules are often rated in terms of a set of standard reporting conditions defined by a temperature, spectral irradiance, and total irradiance. Because PV devices operate over a wide range of temperatures and irradiances. Emery Surveys the temperature dependence of crystalline and thin-film, state-of-the-art, research-size cells, modules, and systems measured by EI variety of methods. The various error sources and measurement methods that contribute to cause differences in the temperature coefficient for a given cell or module measured with various methods are discussed [5].

King (1997) proposed that the term "temperature coefficient" had been applied to several photovoltaic performance parameters, including voltage, current, and power. The procedure for measuring the coefficient(s) for modules and arrays are not yet standardized, and systematic influences are common in the test methods used to measure them. He described effective methods for determining temperature coefficients for cells, modules, and

array; identifies sources of systematic errors in measurements; and provides guidance for their application in system engineering. [6]

Park and Yu (2004), A Photovoltaic system(PV) had been studied and watched with keen interest due to a clean and renewable power source. The output power of PV system was not only unstable but uncontrollable, because the maximum power point tracking (MPPT) of PV system is still hard with the tracking failure under the sudden fluctuation of irradiance. Authors suggested that the optimal voltage for MPPT be obtained by only solar cell temperature. Having an eye on that the optimal voltage point of solar cell was in proportion to its panel temperature, with operating the power converter whose operating point keeps its input voltage to the optimal voltage imagined by the surface's temperature of PV panel. The maximum power point becomes tenderly possible to be tracked. In order to confirm the availability of the proposed control scheme both control methods were simulated not only on the various angle of sampling time of switching control but also with the real field weather condition. [7]

Nema (2009) presented a computer simulation based study of photovoltaic cells/modules using circuit simulator PSpice. The PSpice was an analogous/digital circuit simulator which calculates voltage and current in a circuit under variety of different circumstances. This feature of PSpice used to simulate a circuit based model for PV cells/ modules and then to conduct the behavior under varying conditions of solar insolation including shading effect, temperature, diode model parameters, series and shunt resistance. [8]

Coelho (2009) stated that photovoltaic applications were increasing rapidly; thus, an accurate photovoltaic module modeling was requested in order to allow photovoltaic plants simulations. Roberto presented a mathematical modeling to describe numerically photovoltaic modules and arrays, taking into account the radiation and temperature effects on output voltage, current and power. [9]

Kubba and Samir (2009) presented a theoretical study of photovoltaic and modeling techniques using equivalent circuits. The using of equivalent circuits was it possible to investigate the characteristics of PV cell. The method was used here is implemented in OrCAD pspice program. The same modeling technique is also applicable for modeling a PV module. The details are also given the method of measuring the panel parameters I_{SC} , R_S and I_S , several techniques described to create a new components (PV), in the orcad-
pspice simulator library that could be directly called by their equivalent circuits [10].

Coelho (2010) stated a method based on temperature measurements, in which the PV module of surface temperature was used to determine the maximum power point voltage and also Roberto state that the Maximum Power Point trackers (MPPT) were quite required in order to maximize the extracted power from power from photovoltaic generators. Since the PV module output power depends on environment conditions, the tracking algorithm must ensure velocity and accuracy. Traditionally, methods like

constant voltage, perturb and Observe (P, O) and Incremental and Conductance (IncCond) were widely employed and the choice of one or other depends on static and dynamic tracking features. [11]

Coelho, etal. (2010) showed that Maximum Power Point Trackers (MPPT) system are essential devices employed to maximize the power flow from photovoltaic module (or array) to a load in most application, the MPPT composed by a DC-DC converter interposed between the photovoltaic module and the load. Among the main DC-DC converters, the Buck-type and Boost-type were not proper for this purpose, since they cannot ensure that the operation point will match the maximum power point for every radiation and temperature conditions. On the other hand, as it will be demonstrated theoretically and by experimentation, the Buck-Boost, Cúk, Sepic, Zeta, or any other DC-DC converter with static transfer characteristic given by $D/(1-D)$, which were a natural solution in Maximum Power Point Tracking applications. [12]

Brito (2013) presented the evaluations among the most usual maximum power point tracking (MPPT) techniques, doing meaningful comparisons with respect to the amount of energy extracted from the photovoltaic (PV) panel [tracking factor (TF)] in relation to the available power, PV voltage ripple, dynamic response, and use of sensors. Using MatLab/Simulink and dSPACE platforms, a digitally controlled boost dc–dc converter was implemented and connected to an Agilent Solar Array E4350B simulator in order to verify the analytical procedures. The main experimental results were presented for conventional MPPT algorithms and improved MPPT algorithms named IC

based on proportional–integral (PI) and perturb and observe based on PI. Moreover, the dynamic response and the TF are also evaluated using a user-friendly interface, which is capable of online program power profiles and computes the TF. Finally, a typical daily insolation is used in order to verify the experimental results for the main PV MPPT methods. [13]

Hiwale, etal. (2014) showed that the maximum power point tracker battery charger is proposed for extracting maximum power from a photovoltaic panel to charge the battery. The output power of the PV system continuously varies with change in irradiance and temperature. It is very important to improve the efficiency of charger. There were number of maximum power point tracking (MPPT) methods available to operate the PV system at maximum power point. The proposed system had used Perturb & Observe (P&O) MPPT algorithm for the design and implementation. When the irradiance and temperature are constant or slowly varying, the P&O method tracks MPP steadily and calculate the operating point at which the battery was capable of producing maximum power. In this method, the controller provides the PWM signal to adjust the voltage, adjustment is done by Buck converter and measures power, if the power increases, further adjustments in that direction are tried until power no longer increases [14].

Gauri, etal. (2016) show that for extracting maximum power from photovoltaic panel to charge battery. There are number of maximum power point tracking (MPPT) methods available to operate the PV system at maximum power point. The proposed system had been used Perturb and

Observe (P and O) MPPT algorithm for the design and implementation. A simulation study of maximum power point tracking (MPPT) for photovoltaic systems using perturb and observe algorithm. Maximum power point tracking (MPPT) is used in photovoltaic (PV) systems to maximize the photovoltaic array output power [15].

1.6 The Aim

The aim of this project is to study the effect of PV surface temperature on PV panel output characteristics. And also, to reach the maximum power point trackers (MPPT) by calculating and estimating the effect of the photovoltaic panel surface temperature on the output power of the photovoltaic system by designing an electrical circuit to control the Photovoltaic panel output. by using OrCAD PSPICE simulation program.

1.7 Thesis overview

In chapter one of the thesis issues a historical review was presented to show the extent of research interest in this field.

Chapter two describes the principles and electrical parameters of the PV cell (DC-DC converters types, the design of the boost converter), and the OrCAD Pspice model for PV cell will be presented.

The simulation of the PV panel with temperature effect within the OrCAD PSpice simulator will be presented in chapter three.

Finally, chapter four will give the conclusions and suggestions to continue and extend this work in the future.



Chapter Two

CHAPTER TWO

Description of the photovoltaic system

2.1 PV modeling

A photovoltaic module was modelled using single diode equivalent circuit. The various parameters which influence the characteristic of a cell are classified as environmental parameters as irradiance and temperature, internal parameter as ideality constant, energy band- gap and charge of electron, electrical parameter like open circuit voltage, short circuit current, series resistance, and shunt resistance [16].

A PV array consists of several photovoltaic cells in series and parallel connections. Series connections are responsible for increasing the voltage of the module whereas the parallel connection is responsible for increasing the current in the array [17].

A PV array comprises individual PV cells connected into a unit of suitable power rating. Its characteristic are determine by multiplying the voltage of an individual cell by the number of cells connected in series and multiplying the current by the number of cells connected in parallel. Three important operating points are open-circuit voltage, short circuit current and Maximum Power Point (MPP) [18]

Typically, a solar cell can be modeled by a current source and an inverted diode connected in parallel to it as shown in the figure (2-1). It has a series and parallel resistance. Series resistance is due to hindrance in the path of flow of electrons from n to p junction and parallel resistance is due to the leakage current [19].

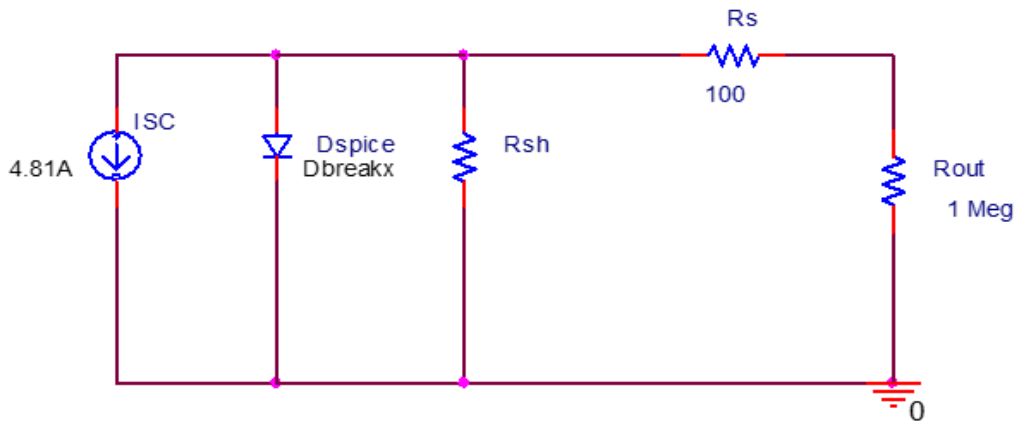


Figure 2-1: Single diode model of a PV cell (equivalent PV circuit).

The output current from the photovoltaic array is [18]

$$I = I_{sc} - I_d \dots\dots\dots (2-1)$$

$$I_d = I_s (e^{q V_d / K T} - 1) \dots\dots\dots (2-2)$$

Where: I_s the reverse saturation current of the diode

q: is the electron charge

V_d : is the voltage across the diode

K: is Boltzmann constant ($1.38 * 10^{-19}$ J/K)

T: is the junction temperature in Kelvin (K).

then

$$I = I_{sc} - I_s (e^{q(V+IR_s)/nkT} - 1) \dots\dots\dots (2-3)$$

where, I is the photovoltaic cell current, V is the PV cell voltage, and n is the diode ideality factor.

2.2 The Physics of PV solar cell

Solar PV systems are power-generating devices that convert electromagnetic energy into electricity. This physical phenomenon is due to the cell's material properties [21].

The main component of a PV cell is silicon, which is a semiconductor: it is an insulator at low temperature and a conductor when the energy is available, in other words, when there is light.

A semiconductor such as silicon consists in three main areas: the valence band where electron e^- are bounded to the atoms, the band gap which is a forbidden space, and the conduction band where electrons are moving as negative carriers and participate in electricity generation.

For a valence electron to get to the conduction band there should be sufficient energy provided so that the electron can jump over the band gap, leaving a hole h^+ in the valence band. Hence, if the absorbed photon's energy is equal or superior to the band gap energy E_g , which is 1.1 eV or $1.7622 \cdot 10^{-19}$ J for silicon, the electron will be to the conduction band with a release of heat in the last case [20].

The energy carried by a photon is expressed as $E=h\nu$ or $E=hc/\lambda$. Thus, long wavelengths might not provide enough energy while the absorption of short wavelengths may generate heat [20].

Solar Photovoltaic (PV) systems generate electric power by absorbing electromagnetic energy. They have an efficiency of about 10-22%, and are heated by the remainder of energy.

These heat losses increase with higher incoming irradiance. The issue of the phenomenon is the module temperature directly influences the module's performances as the electric output power and the efficiency goes down as the module temperature rises. By studying the encapsulation scheme and the thermal modeling of a PV module, the heat transfer processes in the system can be understood and to know which parameters make the module temperature vary [20].

Finally, as the expression of the temperature is difficult to establish, a simplified formula has been used in order to calculate the performances of a given module under different environmental conditions [20].

PV-cell characteristics depend on insulation and temperature and surface temperature of photovoltaic panel. The P-V characteristics of a PV cell array can be obtained from its I-V characteristics [18].

2.3 The Operation Temperature

A PV module might be used in a variety of climates, and so is expected to withstand harsh environmental conditions such as dust, salt, sand, wind and snow [20].

A module is physically protected by the encapsulation structure, which needs to be carefully studied to provide a long life-time (usually between 15 and 20 years) [21].

PV modules that are currently available in the market have an efficiency ranging between 15% and 22%. The incident irradiance converted into electricity. The remainder is converted into thermal energy that heats the cells [21].

These heat losses cannot be estimated as they depend on the material's band gap and on the weather, i.e. the solar irradiance. However, a fraction of

the sunlight is reflected on the front cover of the cell: it doesn't contribute to either the electrical power generation or the heating of the cells [20].

Three heat transfer processes occur in a PV module: conduction of the heat losses through the encapsulates, heat convection at the module front and back surfaces and radiation to the surroundings [20].

The conversion efficiency of a PV module is affected by changes in the temperature and radiation levels. The higher the radiation levels, the higher will be the amount of energy. The issue concerning the low amount of absorbed radiation can be solved through the use of multi-junction solar cell. These PV cells combine different semiconductor materials that possess dissimilar response for distinct wavelengths of light. Therefore, the combination of different materials increases the total of absorbed radiation, reducing the amount that is converted into heat [21].

High radiation regions also have high local temperature. Seeing that, as proven by Mishra and Tiwari, all different types of PV cells are negatively affected by high temperature, leading to a decrease in the converted efficiency conversion of the PV system.

The main concern in order to improve the efficiency conversion should be about maintaining the PV module at a low temperature, rather than increasing PV cell conversion efficiency. Otherwise, high irradiation regions like Brazil will not fulfill its true PV potential, due the high local ambient temperature [22].

Fundamentally, the temperature coefficients for modules and large arrays should be directly related to the temperature coefficients for their individual cells. In principal, it should be possible to measure temperature coefficients for a large number of cells, average the values, and then calculate coefficients for modules and arrays using the average values. However, test results for modules and arrays often don't support this premise [23].

Systematic influences that occur during testing or system operation often result in apparent temperature coefficients that differ from anticipated values. Typically, the difference results from nonuniform temperature distributions and/or measured temperatures that are not indicative of actual cell temperatures [23].

The important role of the operating temperature is relation to the electrical efficiency of a photovoltaic (PV) device [22]. The correlations expressing the PV cell temperature (T) as a function of weather variables such as the ambient temperature (T_a), local wind speed, solar radiation, material and system dependent properties such as, glazing-cover transmittance and plate absorption [24].

The short-circuit current of solar cells is not strongly temperature-dependent. It tends to increase a slightly increasing temperature. This can be attributed to increased light absorption, since semiconductor band gaps generally decrease when the enough energy available. The other cell parameters, the open-circuit voltage and the fill factor, both decrease [25].

2.4 Electrical Power Converters

The dc-dc converters are widely used in regulated switch-mode dc power supplies and in dc motor drive applications. Often the input to these converters is unregulated dc voltage, which is obtain by rectifying the line voltage, and therefore it will fluctuate due to changes in the line-voltage magnitude. Switch-mode dc-to-dc converters are used to convert the unregulated dc input into a controlled dc output at a desired voltage level [26].

The role of power electronic converters is to provide power to the user in a suitable form at high efficiency. The power electronic converters are needed in PV systems to convert DC voltage to the required values and to convert from DC to AC and vice versa. In addition, they control the charging and discharging of batteries in systems where batteries are storage elements.

There are many types of DC -DC converters as follow:

- 1- Step-down (buck) converter.
- 2- Step-up (boost) converter.
- 3- Step-down step-up (buck- boost) converter.
- 4- Cuk converter.

5- Full-bridge converter.

In this work was focused on boost converter to achieve the desired voltage.

2.4.1 Boost Converter

The Boost converter is another simple power electronic converter and basically consists of a voltage source, an inductor, a power electronic switch (usually a MOS- FET or an IGBT) and a diode. It usually also has a filter capacitor to smoothen the output. Its function is to step up DC voltage to bring it to a desired level. [28]

In the source side, it has been used a boost convertor connected to a solar panel in order to enhance the output voltage so that it can be used for different applications like motor load. By changing the duty cycle of the boost converter appropriately it can match the source impedance with that of the load impedance [27].

Fig. 2-2 illustrates the basic circuit of a Boost converter. However, in this example the switching transistor is a power MOSFET, both Bipolar power transistors and MOSFETs are used in power switching, the choice being determined by the current, voltage, switching speed and cost considerations. [28]

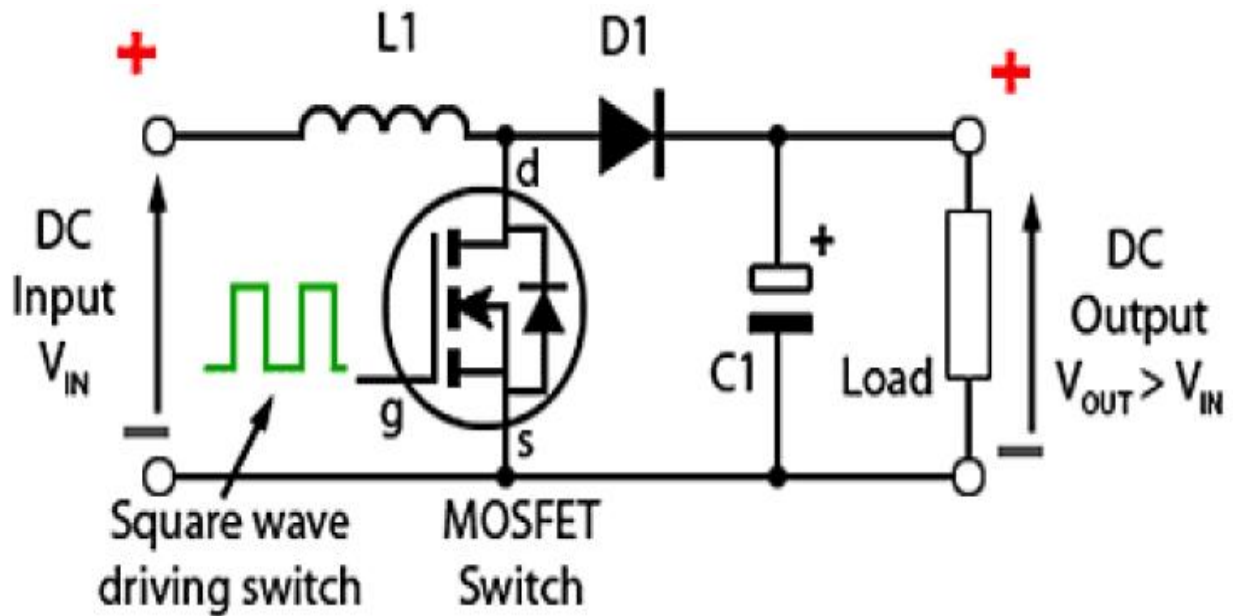


Figure 2-2: Basics boost converter circuit [28].

2.4.2 Boost Converter Operation principles

Fig 2-3 illustrates the circuit action during the initial high period of the high frequency square wave applied to the MOSFET gate at start up. During this time MOSFET conducts, placing a short circuit from the right-hand side of L1 to the negative input supply terminal. Therefore, a current flow between the positive and negative supply terminals through L1, which stores energy in its magnetic field [28].

There is virtually no current flowing in the remainder of the circuit as the combination of D1, C1 and the load represent a much higher impedance than the path directly through the heavily conducting MOSFET. [28]

Fig.2-3 shows the circuit action during MOSFET ON periods after the initial startup. Each time the MOSFET conducts, the cathode of D_1 is more positive than its anode, due to the charge on C_1 . D_1 is therefore turned off so the output of the circuit is isolated from the input, however the load continues to be supplied with $V_{IN} + V_L$ from the charge on C_1 [28]. Although the charge C_1 drains away through the load during this period, C_1 is recharged each time the MOSFET switches off, so maintaining an almost steady output voltage across the load [28].

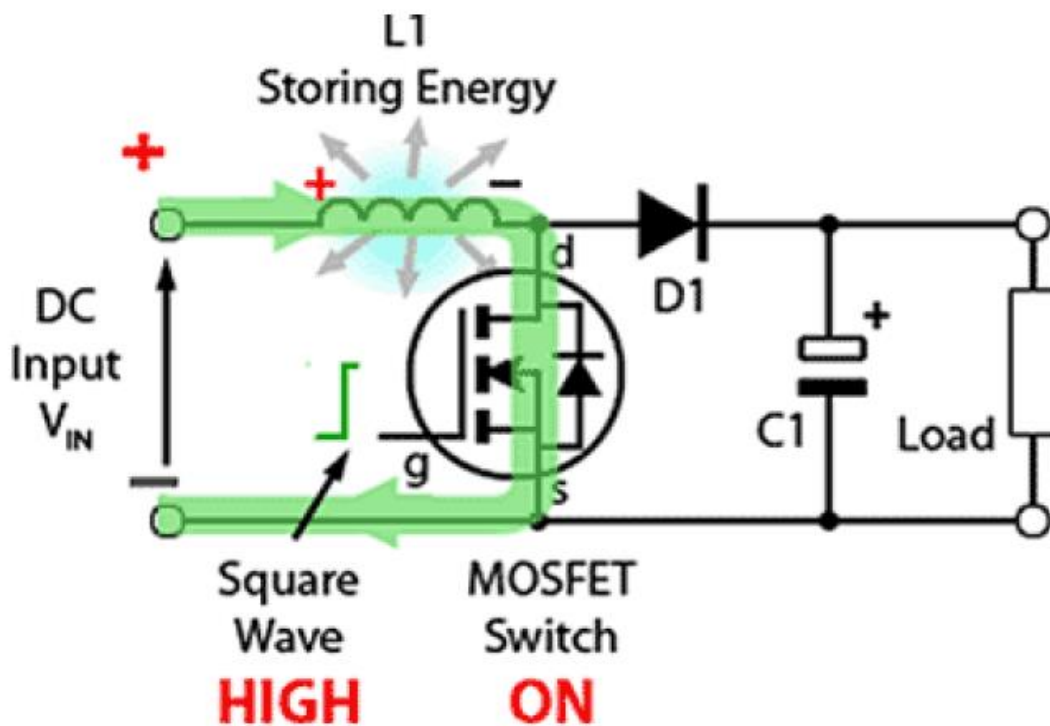


Figure 2-3: The Operation Principles of Boost Converter (at switch on) [28].

Fig. 2-4 shows the current path during the low period of the switching square wave cycle. As the MOSFET is rapidly turned off the sudden drop in current causes L1 to produce a back e.m.f. in the opposite polarity to the voltage across L1 during the on period, to keep current flowing [28].

This results in two voltages, the supply voltage V_{IN} and the back e.m.f. (V_L) across L1 in series with each other. This higher voltage ($V_{IN} + V_L$), now that there is no current path through the MOSFET, forward biases D1. The resulting current through D1 charges up C1 to $V_{IN} + V_L$ minus the small forward voltage drop across D1, and also supplies the load [28].

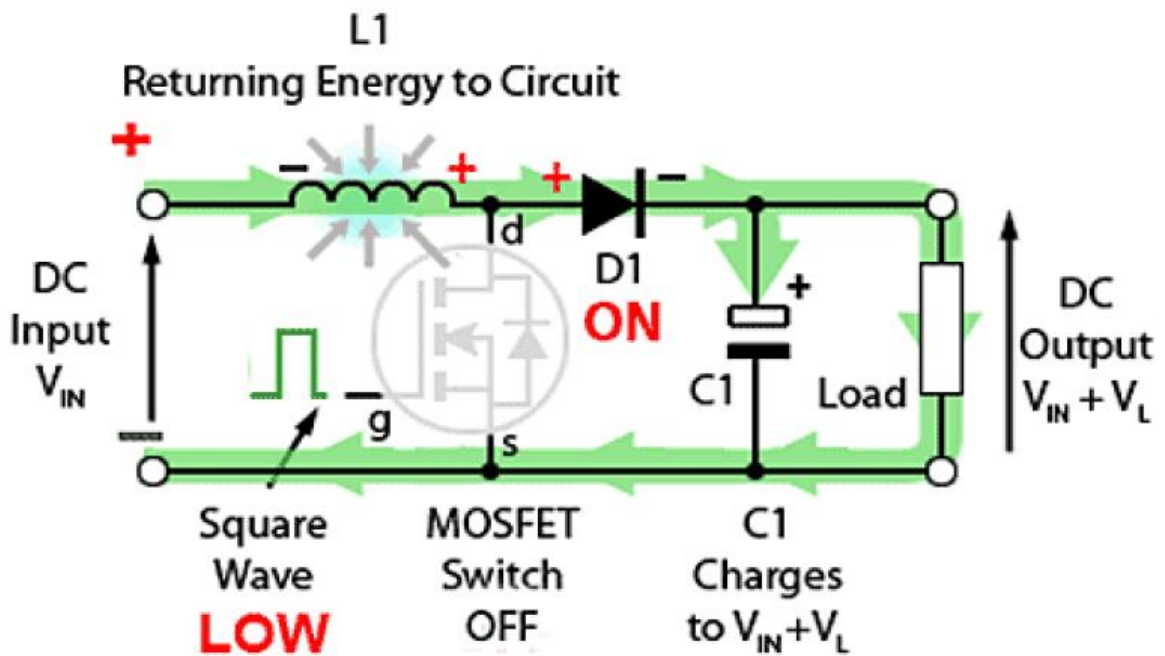


Figure 2-4: The Operation Principles of Boost Converter (at switch off)

[28].

The Boost converter may be described mathematically through the following equations [29].

When switch closed (ON) then

$$V_L = V_{IN} = L (dI/ dT) \dots\dots\dots (2-5)$$

$$V_{IN} = L * (I_{Max} - I_{Min}) / DT \dots\dots\dots (2-6)$$

$$(V_{IN}/ L)/ DT = I_{Max} - I_{Min} \dots\dots\dots (2-7)$$

$$I_{Max} = I_{Min} + (V_{IN}/L) DT \dots\dots\dots (2-8)$$

Now if switch is open (Off)

$$-V_{IN} + V_L + V_O = 0 \dots\dots\dots (2-9)$$

$$V_O = V_{IN} - V_L \dots\dots\dots (2-10)$$

$$V_O = V_{IN} - L * (di_L/dt) \dots\dots\dots (2-11)$$

$$V_O = V_{IN} - L * (I_{MIN} - I_{Max}) / (T - DT) \dots\dots\dots (2-12)$$

$$-L (I_{Min} - I_{Max}) / (1-D) T = V_O - V_{IN} \dots\dots\dots (2-13)$$

$$I_{Max} = I_{Min} - (V_{IN} - V_O) / (L) * (1-D) T \dots\dots\dots (2-14)$$

Therefore, $V_O > V_{IN}$

$$I_{Max} = I_{Min} + (V_O - V_{IN}) / (L) * (1-D) T \dots\dots\dots (2-15)$$

Now eq. (2-8) equal to eq. (2-15)

$$I_{Min} + V_{IN}/(L) * DT = I_{Min} + (V_O - V_{IN}) / (L) * (1-D) T \dots\dots\dots (2-16)$$

Since

$$V_{Load} / V_{Module} = 1 / (1-D) \dots\dots\dots (2-17)$$

$$I_{Load} / I_{Module} = 1-D \dots\dots\dots (2-18)$$

Where:

D: duty cycle.

V_{Load} , I_{Load} : load voltage and load current.

V_{Module} , I_{Module} : module voltage and module temperature.

2.4.3 Critical inductance

The conduction mode of a power stage is a function of input voltage, output voltage, output current, and the value of the inductor. The value of inductor is given by the following equation [31].

$$L_{min} \geq (V_o * T_s) / (16 * I_o) \dots\dots\dots (2-19)$$

2.4.4 Output capacitance

In switching power supply power stages, the function of output capacitance is to store energy. The energy is stored in its electric field due to the voltage applied. Thus, qualitatively, the function of a capacitor is to attempt to maintain a constant voltage [30].

The output capacitance for a boost power stage is generally selected to limit output voltage ripple to the level required by the specification. The series

impedance of the capacitor and the power stage output current determine the output voltage ripple. The three elements of the capacitor that contribute to its impedance (and output voltage ripple) are equivalent series resistance (ESR), equivalent series inductance (ESL), and capacitance (C). The following discussion gives guidelines for output capacitor selection [30].

To determine the amount of capacitance needed as a function of output load current, I_o , switching frequency, f_s , and desired output voltage ripple, the following equation is used assuming all the output voltage ripple is due to the capacitor's capacitance. This is because the output capacitor supplies the entire output load current during the power stage on-state [30].

$$C \geq (I_o * D) / (f_s * \Delta V_o) \dots\dots\dots (2-20)$$

2.5 Maximum Power Point Tracking Algorithms

A typical solar panel converts only 15 to 20 percent of the incident solar irradiation into electrical energy. Maximum Power Point Trackers (MPPT) systems are essential devices employed to maximize the power flow from a photovoltaic module (or array) to a load. In most applications, the MPPT is composed by a DC-DC converter interposed between the photovoltaic module and the load [31].

The output power of a solar panel is a function of the temperature, the sunshine and the position of the panel. It is also function of the product of the voltage by the current. By varying one of these two parameters, voltage or current, the power can be maximized. Several MPPT methods exist in order to maximize this output power and to fix its value, in steady-state, at its high level [32].

Among the main DC-DC converters, the Buck-type and Boost-type are not proper for this purpose, since they cannot ensure that the operation point will match the maximum power point for every radiation and temperature conditions. On the other hand, as it will be demonstrated theoretically and by experimentation, the Buck-Boost, Cúk, Sepic, Zeta, or any other DC-DC converter with static transfer characteristic given by $D/(1-D)$, are a natural solution in Maximum Power Point Tracking applications [33].

Usually, the MPPT is achieved by interposing a DC-DC converter between the photovoltaic generator and the load, thus, acting on the converter duty cycle (D) it is possible to guarantee the operation point as being the MPP.

The photovoltaic (PV) module efficiency conversion affected by environmental condition, particularly by variation in temperature and radiation. There are several devices and techniques that allow a minimization of those effects and changes, by keeping the efficiency conversion at its highest level.

The most common techniques are the output current, voltage or both to calculate the maximum power technique. However, some MPPT systems recently appeared using the PV module temperature as an input to determine the MPP.

The choice of the algorithm depends on the time complexity the algorithm takes to track the MPP, implementation cost and the ease of implementation [34]. The two environmental conditions of solar insolation and temperature govern output of a PV cell. In this thesis as state previously focused on cell temperature effect (temperature method).

2.5.1 Temperature method

The tracking algorithm performance is fundamental for an efficient tracking response. Usually, the algorithm receives the PV module voltage and current as input data and defines the dc-dc converter duty cycle that establishes the system operating point on the MPP [36], as depicts Fig. 2-5

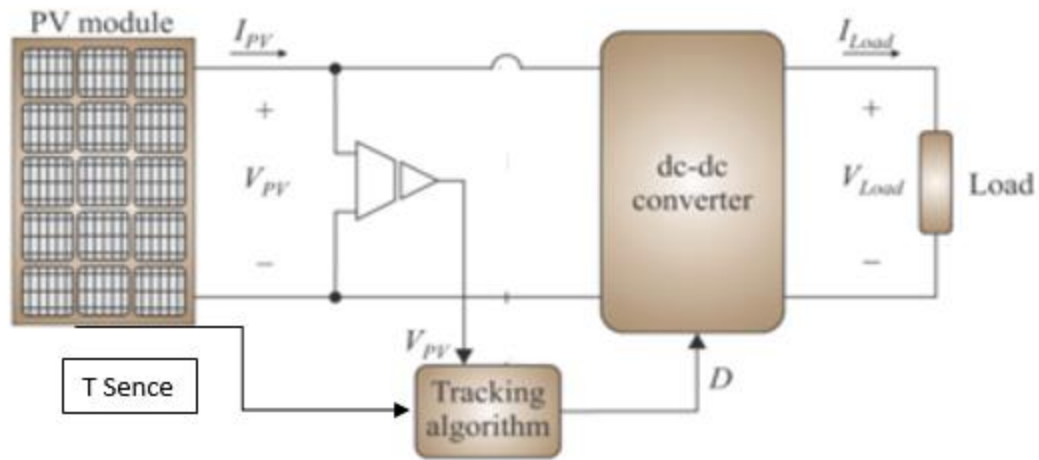


Figure 2-5: Typical input and output data related to MPPT algorithms.

The main aim of the proposed algorithm is to unify the simplicity of implementation of the constant voltage method with the velocity and accuracy tracking of the IncCond one [36].

Constant Voltage algorithm is the simplest way to impose the voltage across the photovoltaic terminals; however, the voltage value is clamped in a fixed value and the MPP is not always achieved [35].

On the other hand, IncCond algorithm allows varying the voltage across the photovoltaic device, fast and accurately, always matching the MPP; nevertheless, this algorithm is complex to be implemented. In the Maximum Power Point Tracking algorithm employing temperature sensor (MPPT-

temp), the current sensor is substituted by a temperature sensor, fixed on the photovoltaic back surface [35].

The development of an algorithm that employs temperature measurement is based on the fact that the output photovoltaic voltage is directly proportional to the temperature on the photovoltaic surface [36]. This algorithm is achieved by the following steps:

- 1- The PV panel surface temperature and output voltage are measured by sensors.
- 2- both sense values are set as input data for the tracking algorithm, whose output is the duty cycle of the DC-DC converter.

Table (2-1) index the simplicity of the temperature measurement algorithm.

It is possible directly set the duty cycle (D) and transfer the maximum power from PV panel to the load.

Power DC-DC Converter	Duty Cycle for operation on the MPP
Buck	$D_{MPP} = V_{load} / (V_{mpp} + (T - T^{STC})_{\mu V})$
Boost	$D_{MPP} = 1 - V_{load} / (V_{mpp} + (T - T^{STC})_{\mu V})$
Buck-Boost	$D_{MPP} = V_{load} / (V_{load} + V_{mpp} + (T - T^{STC})_{\mu V})$

Table (2-1) Duty cycle for maximum power point operation.



Chapter Three

CHAPTER THREE

Simulation Results of The PV Model

3.1 Introduction

In this chapter the PV panel has been simulated within the PSPICE simulator. Temperature of Photovoltaic panel is measured to estimate its effect on the maximum power point trackers (MPPT) of PV system. Details are also given to the methods of measuring the panel temperature and several techniques to create a new component PV in the Orcad-PSpice simulator library which will be called directly by their equivalent circuits.

3.2 Design of photovoltaic panel in PSPICE

Photovoltaic cells in Orcad-PSPICE program must be represented by diode device, where diode have the same characteristics of solar cells, it's also have two layers and it's a semiconductor device.

The block diagram in the fig. 3-1 below shows the full system with maximum power point tracking controller. The voltage source provides the panel voltage at different temperature.

CHAPTER THREE Simulation Results of The PV Module

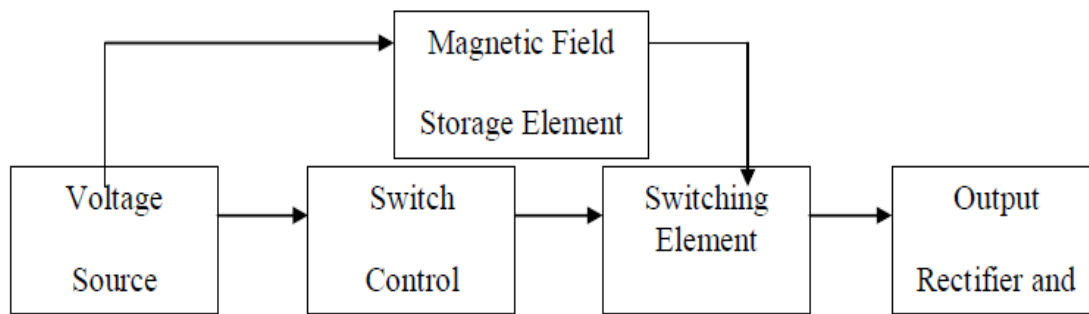


Figure 3-1: The basic blocks of building Photovoltaic system [37].

Firstly, the PSPICE PV model will be prepared to understand its operation and how to improve quality and add all the other parameters that is affected the PV panel.

It is possible to simulate a PV panel in OrCAD- PSPICE if I_s and R_s for the diode in a single cell model shown in fig. (2-1) in the previous chapter are calculated. Whereas the saturation current is calculated using a circuit shown in fig (2-1). From DC simulation results under open circuit voltage shown in fig (3-2) ($I_s = 436.96 \text{ PA}$ at $V_{OC} = 0.602 \text{ V}$).

The PSPICE model of the diode is built according to the saturation current I_s calculated above ($I_s = 436.96 \text{ PA}$, $N=1$, $R_s= 0.001\Omega$, $XTI = 3$, $IKF = 0A$, $E_g = 1.11\text{ev}$, $C_{jo} = 1\text{Pf}$, $M = 0.3333$, $V_j = 0.75\text{V}$, $F_c = 0.5$, $ISR = 0.1\text{PA}$, $NR= 2$, $BV = 100\text{V}$, $IBV=0.0001$

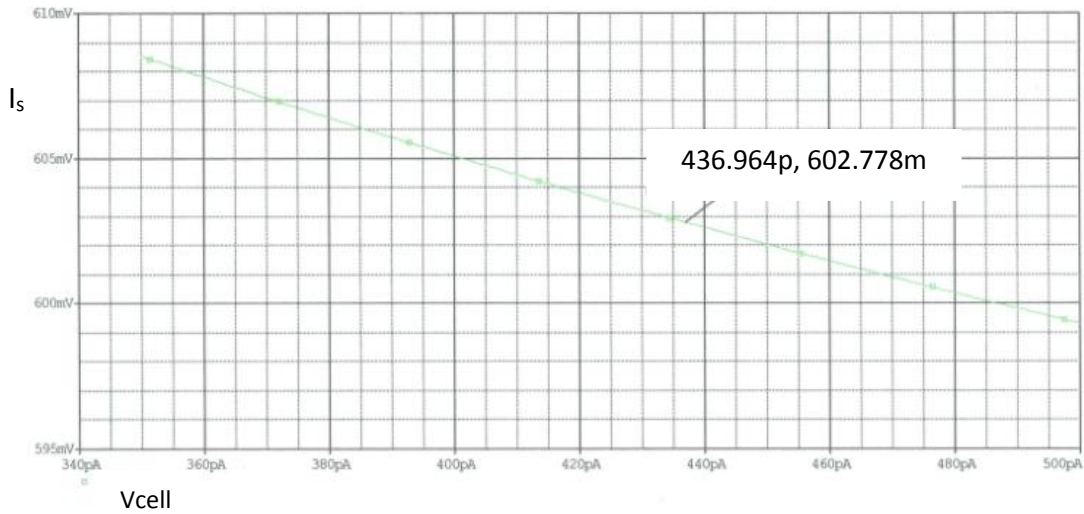


Figure 3-2: The voltage cell as a function of the saturation current I_s .

Series resistance was represented as R_{val} in fig. (3-3) and simulated under optimal load 16.652Ω . (P_{Max}/ I_L), and from DC analysis results shown in fig. (3-4) $R_s = 13.95\Omega$.

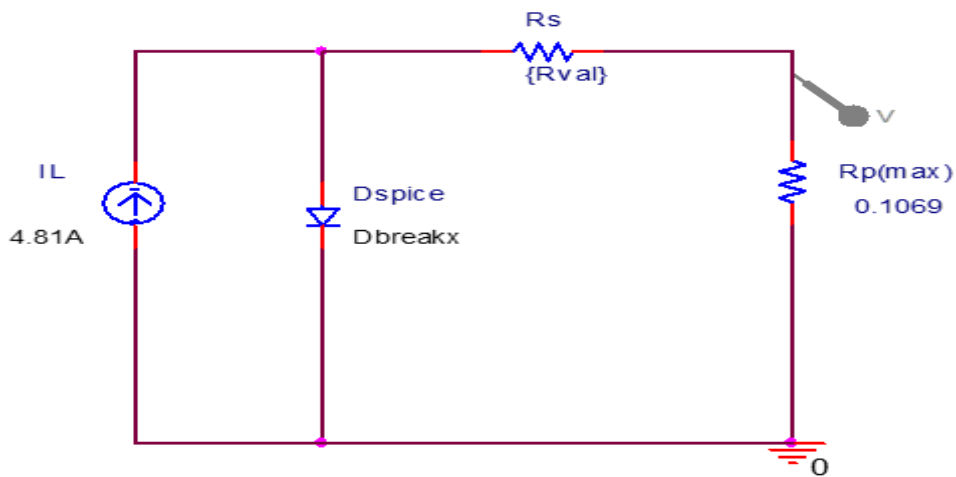


Figure 3-3: The circuit diagram used to determine R_s .

CHAPTER THREE **Simulation Results of The PV Module**

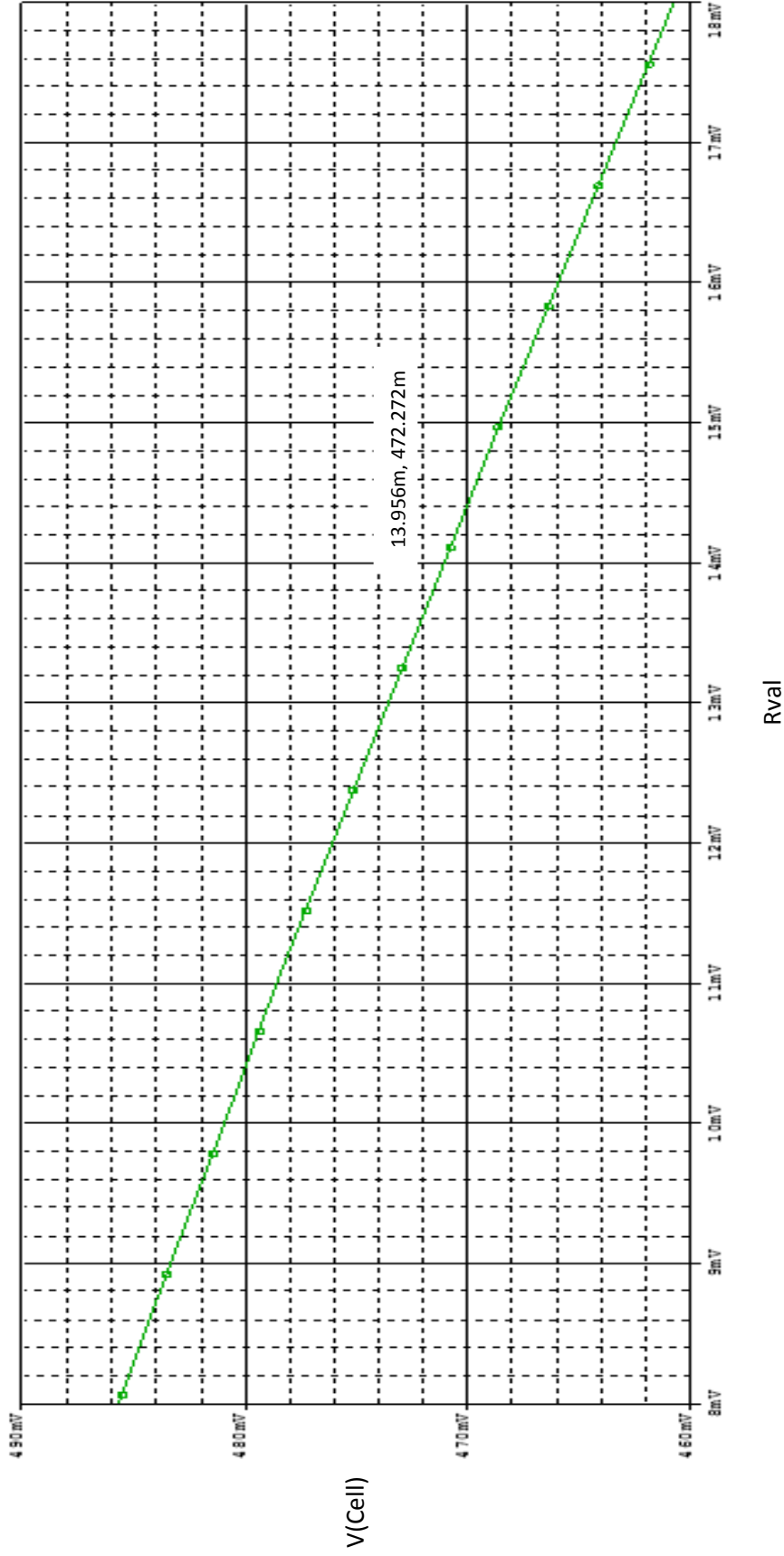


Figure 3-4: The voltage cell as a function of internal resistance R_s .

CHAPTER THREE Simulation Results of The PV Module

Right now, is possible to create the PV panel consist of 36 elementary cells in series as shown in fig (3-5). The value of R_s for whole model is the sum of the internal resistances of all the cells.

Temperature and solar radiation are the more important parameter affected the PV panel output. Therefore, these two parameters will be added to the previous model to improve it is behavior. This improvement will be helpful to verify different types of PV systems. To achieve this work the following equation (3-1) [38] was employed in the previous mathematical PV model as shown in fig. (3-4).

$$I_{PH} = [I_{SCR} + K_1 (T - 298) * (Irradiation / 1000)] \dots\dots (3-1)$$

Where:

K_1 : short circuit current temperature coefficient for SP75 equal 0.0017 A/C°. from data sheet.

I_{PH} : represented photovoltaic current (A).

T: cell temperature.

Irradiation: solar radiation (W/m²).

I_{SCR} : short circuit current (A).

CHAPTER THREE Simulation Results of The PV Module

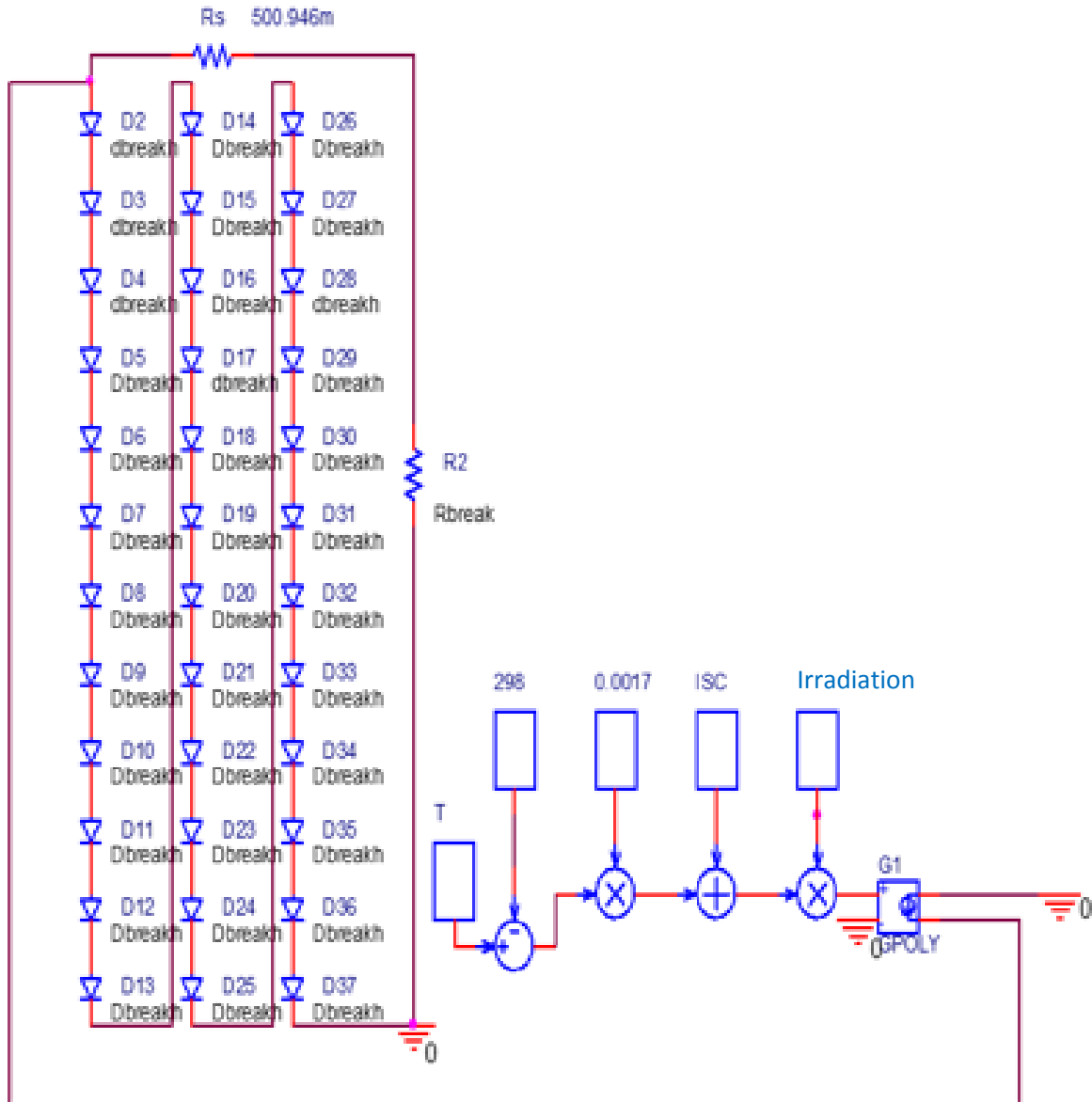


Figure 3-5: The created PV panel as represented on Orcad-PSpice.

CHAPTER THREE Simulation Results of The PV Module

ABM feature of PSPICE is used to include the above parameters in PSPICE model and produced temperature dependent voltage. This voltage converted to current with galvanic insulation by element Gpoy with gain (0.8).

The I-V and P-V characteristics of the created panel are shown in fig. (3-6), (3-7), (3-8) and (3-9) these curves provides that the PSPICE PV model could be used as a source of energy to the power circuit.

Fig. 3-6 shows the current-voltage curve, obtained from the DC analysis of the PV model. The optimal load replaced by R_{break} to obtain all value of I and V. The simulated model shows 21.7V open circuit voltage and 4.8A short circuit current and 75W maximum power at 25C° with 1000W/m² solar irradiation. Fig. (3-7) depicts (I-V) curves for different ambient temperature.

Next, the following figures (3-8) (3-9) depict the panel characteristics from this simulation at different surface temperature and irradiation respectively.

CHAPTER THREE Simulation Results of The PV Module

The power vs. voltage plot is described on fig. 3-9. It reveals that the value of PV model power varies greatly depending on its operation condition.

The location of the maximum power point in the (P-V) plane is not known beforehand and always changes dynamically dependence on irradiance and temperature.

Fig 3-10 shows the (P-V) curves for different temperatures at constant irradiance and fig. 3-11 shows the (P-V) curves for different irradiance value at constant temperature (25C^o). there is observer shift where the maximum power point occurred.

CHAPTER THREE **Simulation Results of The PV Module**

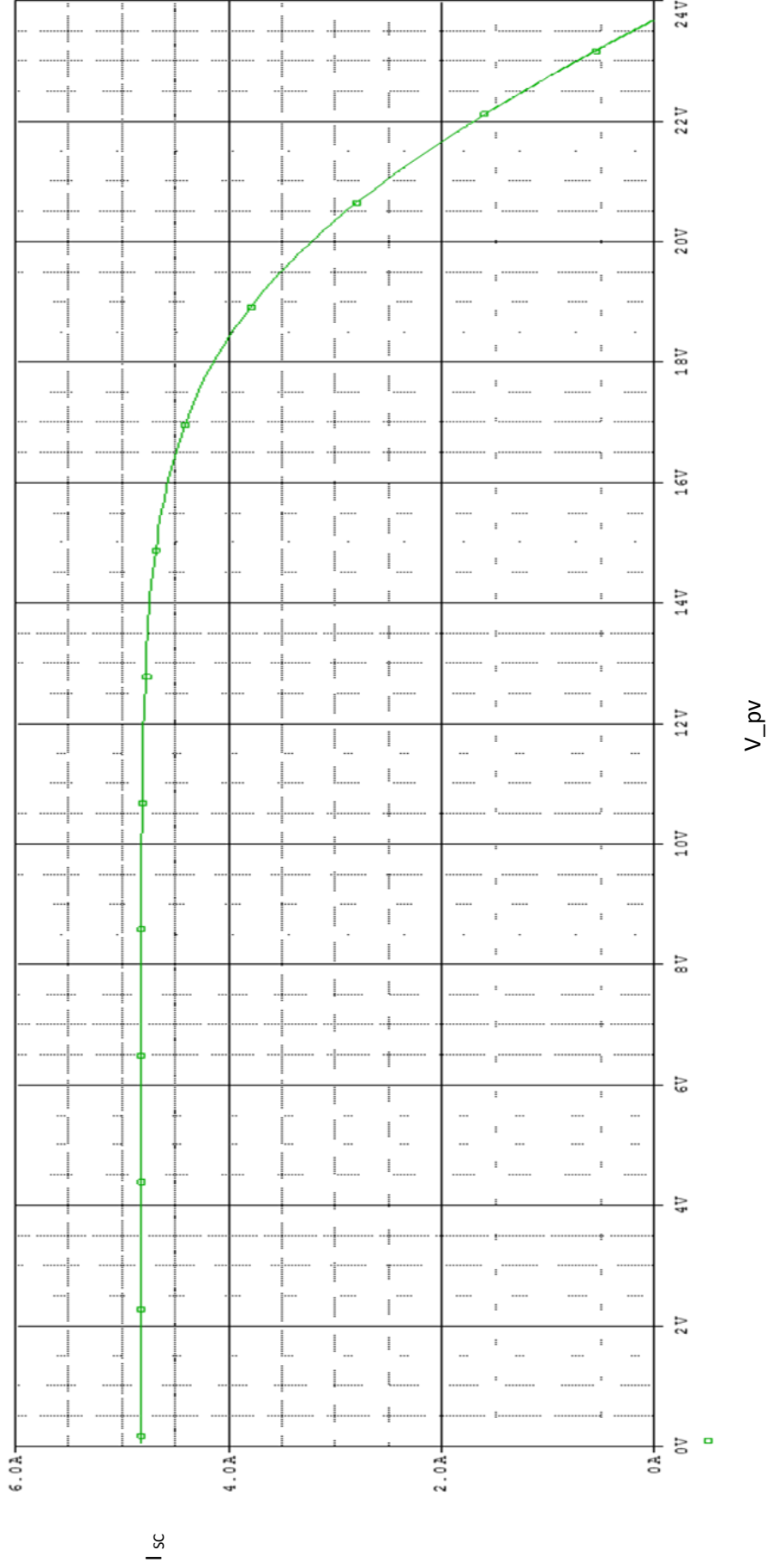


Figure 3-6: The (I-V) curve of the panel under STC.

CHAPTER THREE **Simulation Results of The PV Module**

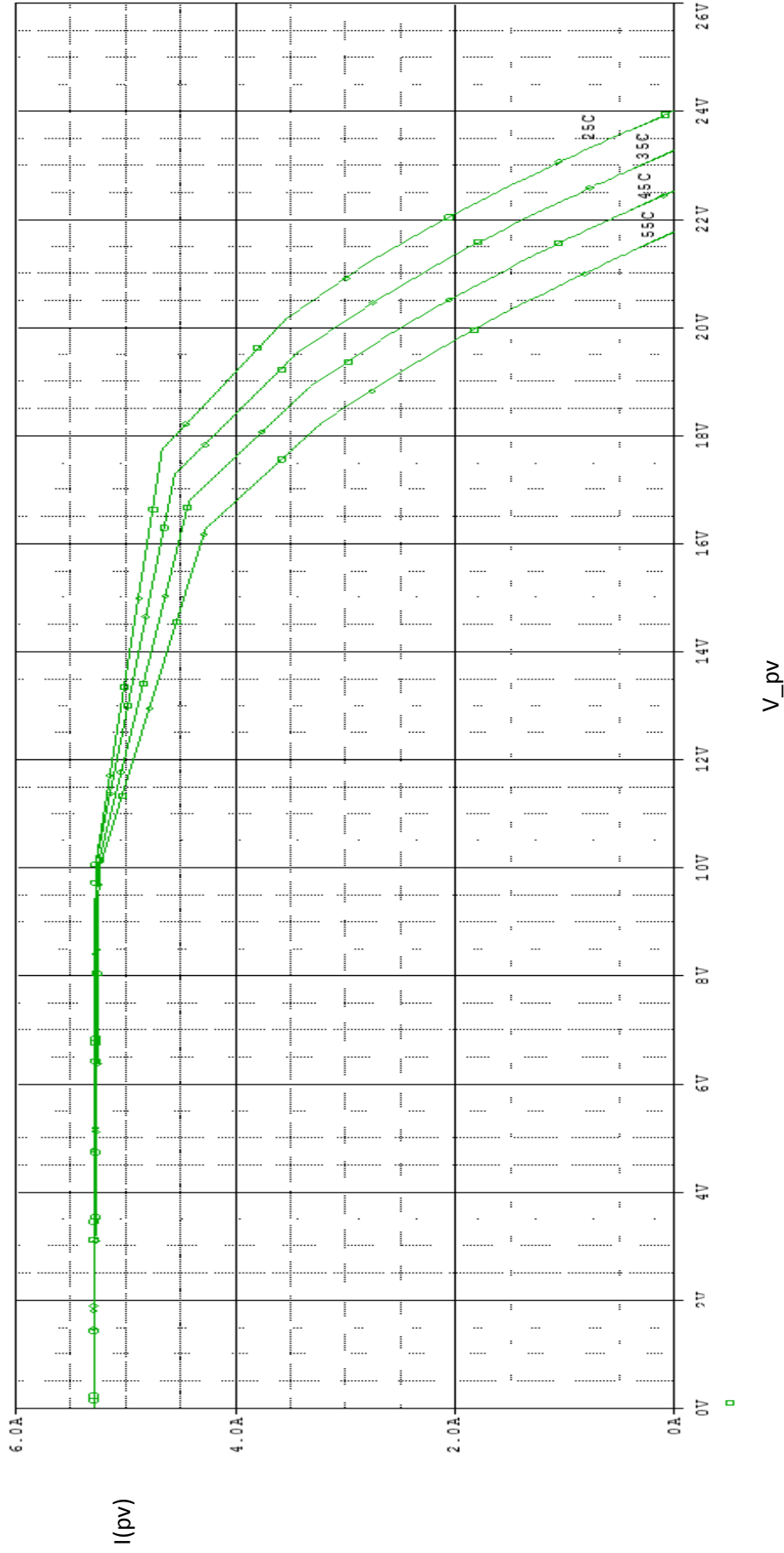


Figure 3-7: The (I-V) curves of the PV panel at different temperature under a constant irradiation 1000W/m².

CHAPTER THREE **Simulation Results of The PV Module**

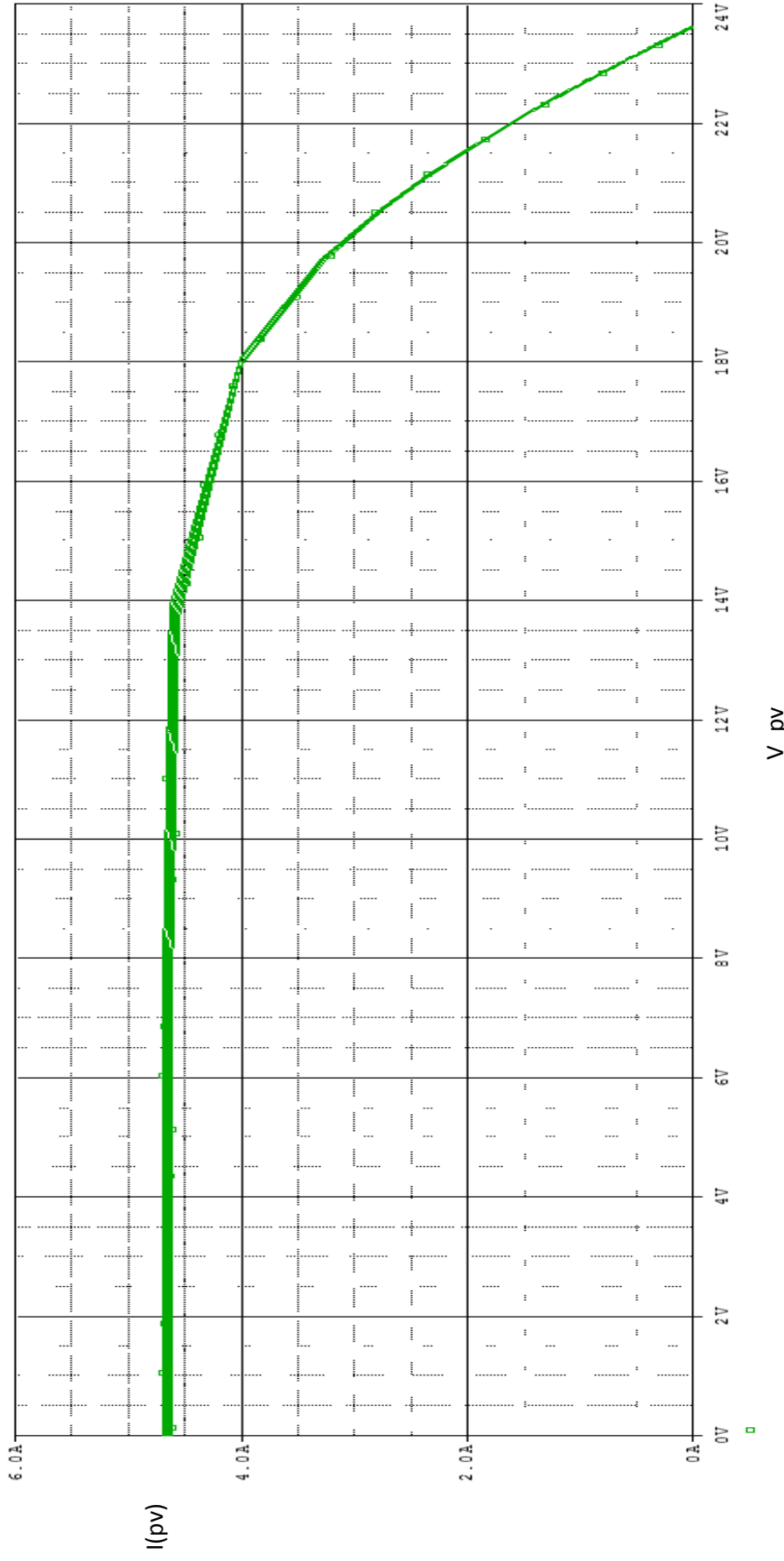


Figure 3-8: The (I-V) curves of the PV panel at different surface temperature under a constant irradiation 1000W/m².

CHAPTER THREE Simulation Results of The PV Module

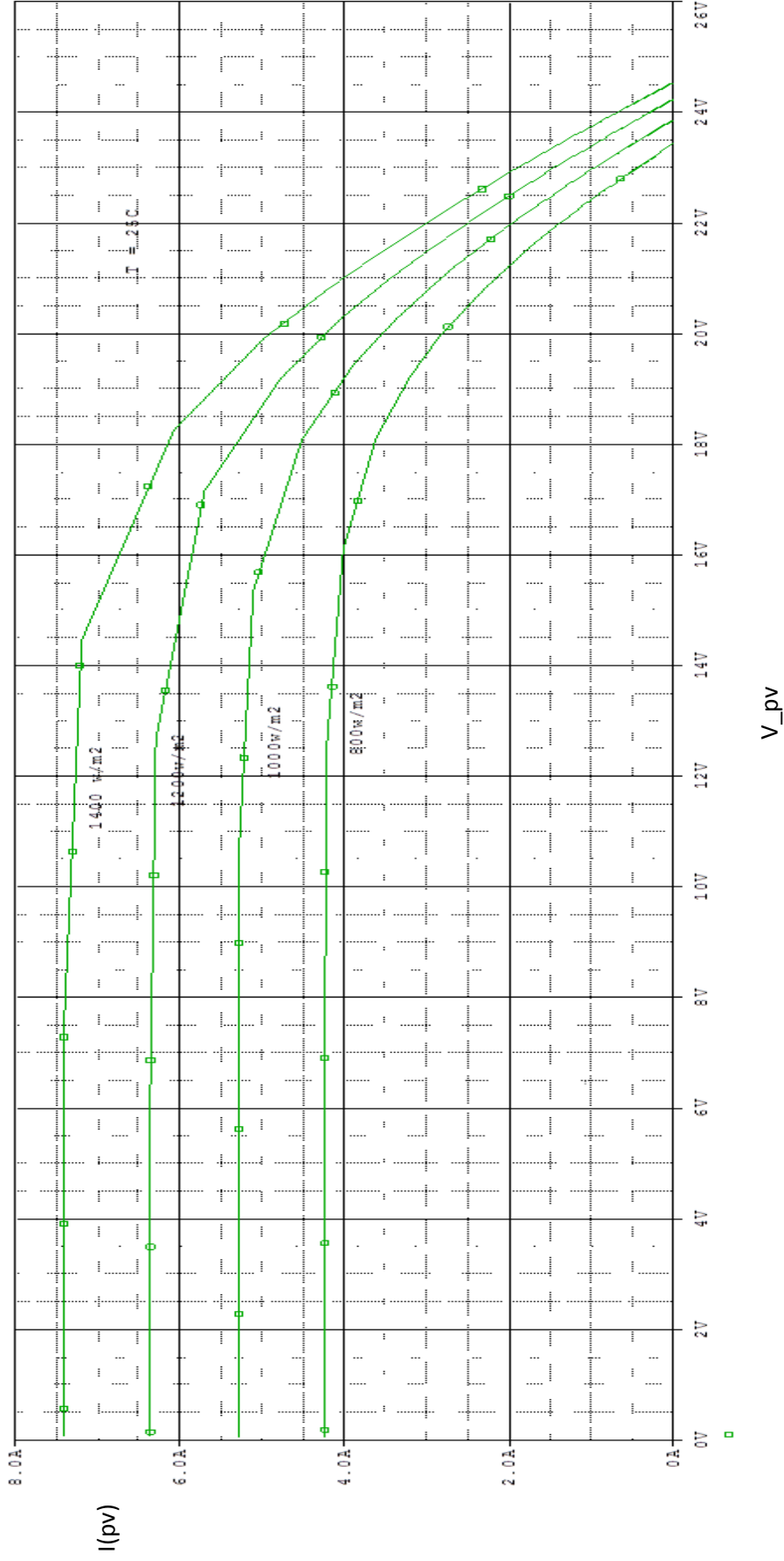


Figure 3-9: The (I-V) curves of the PV panel at different irradiation under a constant temperature $T=25^{\circ}\text{C}$.

CHAPTER THREE **Simulation Results of The PV Module**

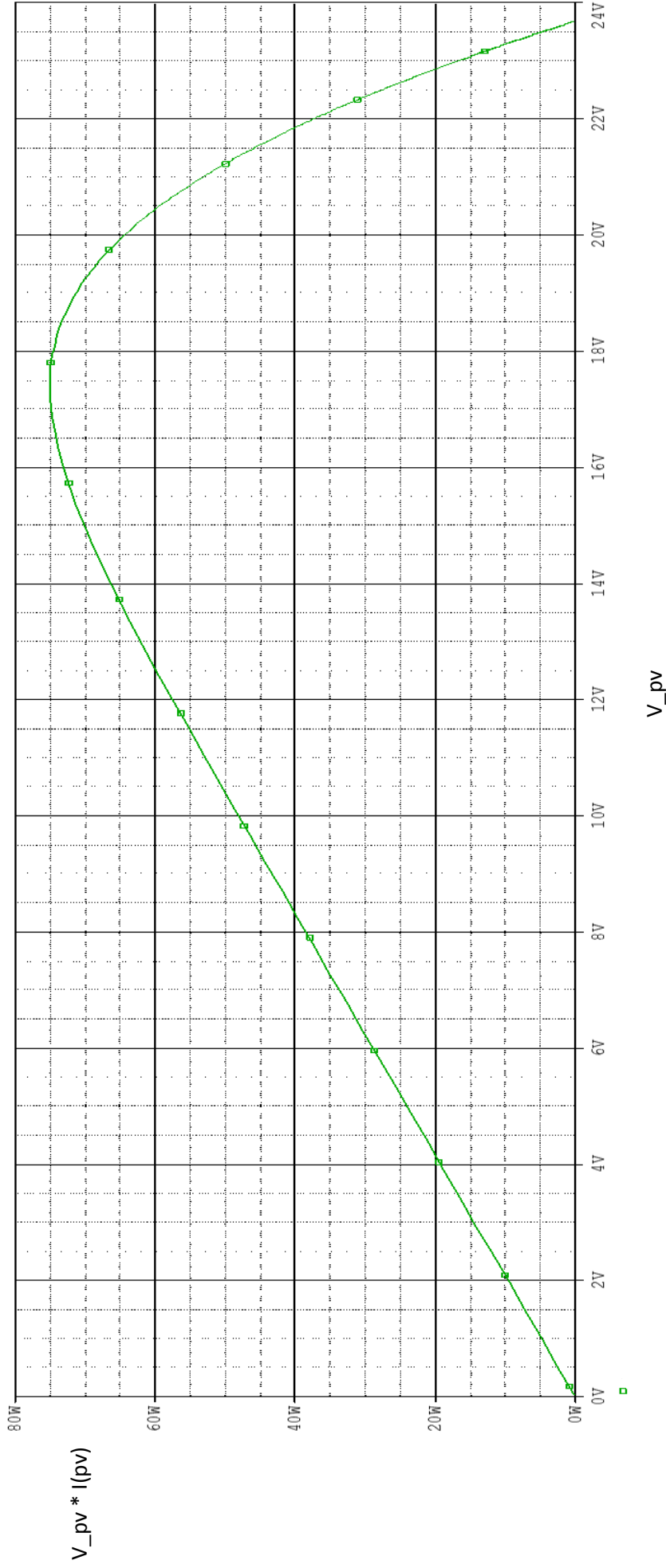


Figure 3-10: The (P-V) curve of the PV panel under STC.

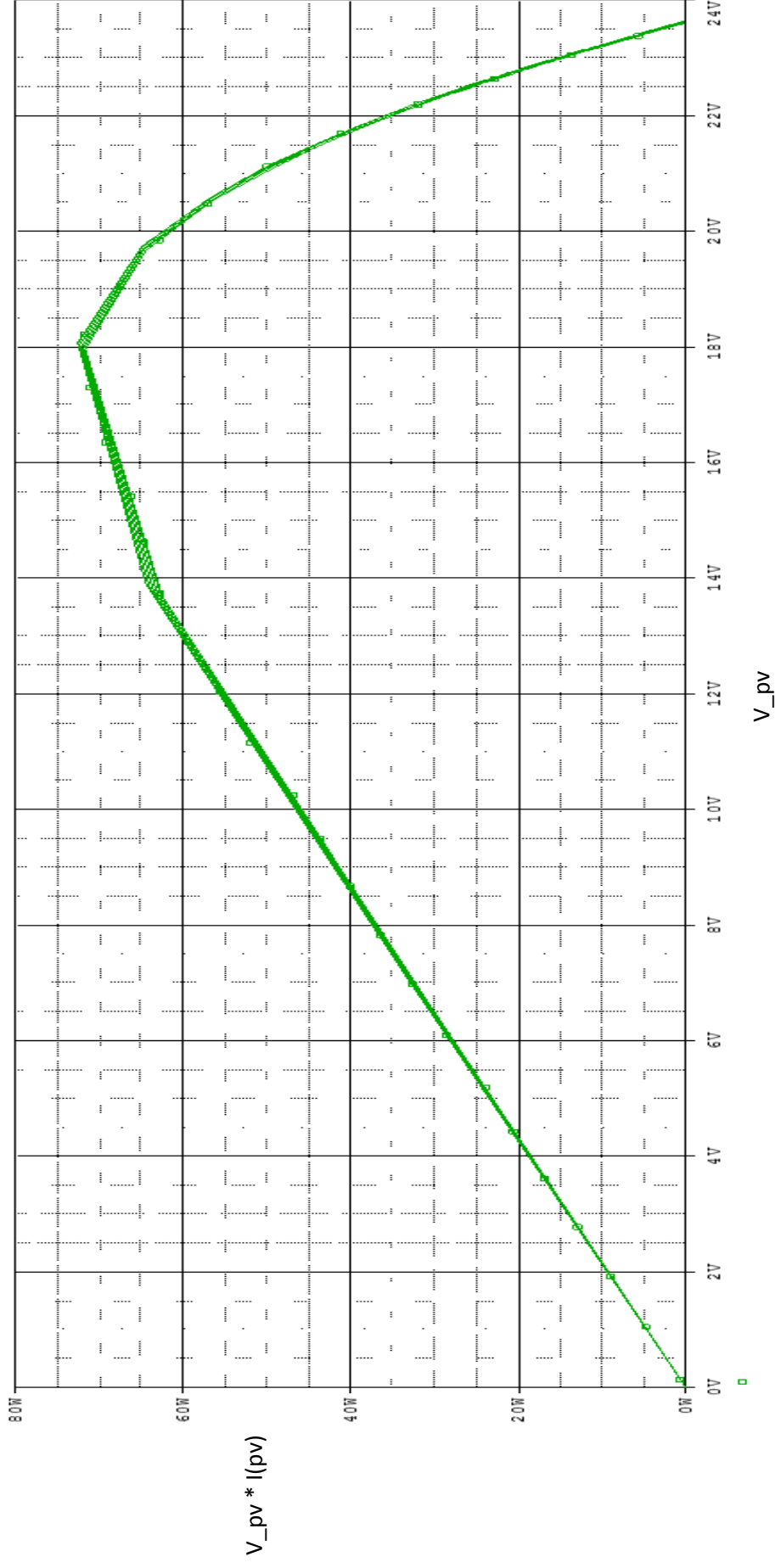


Figure 3-11: The (P-V) curves of the PV panel at different surface temperature under a constant irradiation 1000W/m².

CHAPTER THREE **Simulation Results of The PV Module**

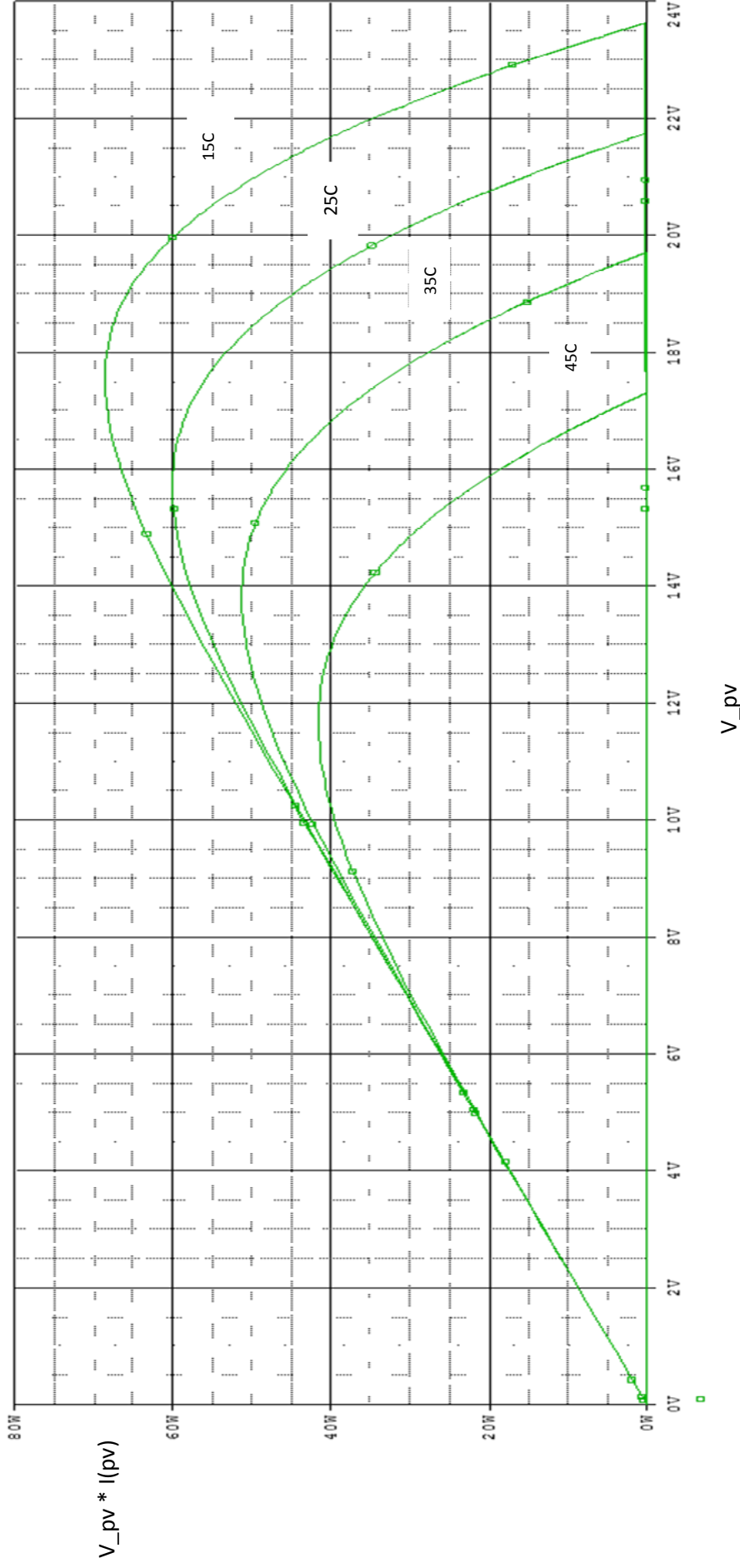


Figure 3-12: The (P-V) curves of the PV panel at different temperature under a constant irradiation 1000W/m².

CHAPTER THREE **Simulation Results of The PV Module**

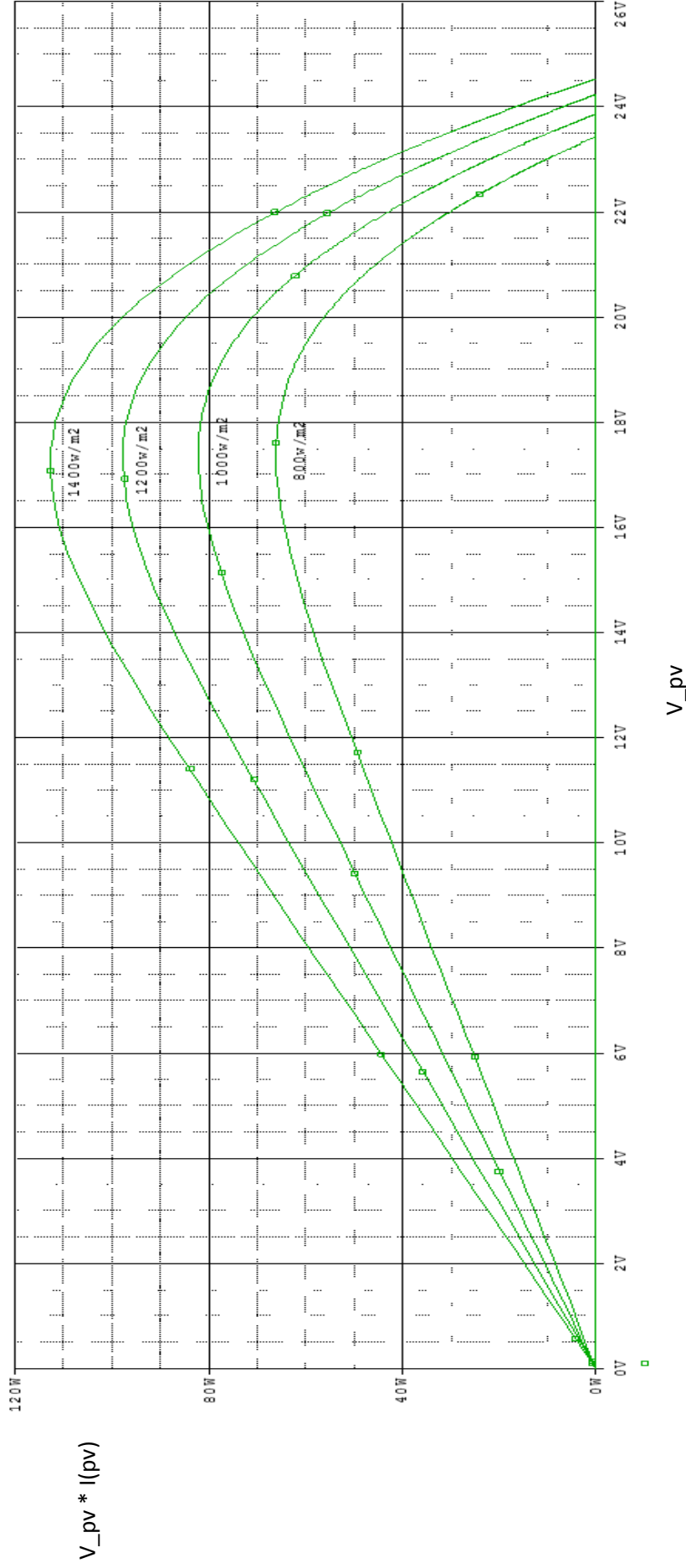


Figure 3-13: The (P-V) curves of the PV panel at different irradiation under a constant temperature T=25 C°.

3.3 Hierarchical Block

The model which described previously is very big so to minimize it an integrated part (hierarchical block) has been assumed as shown in figure 3-14 below.

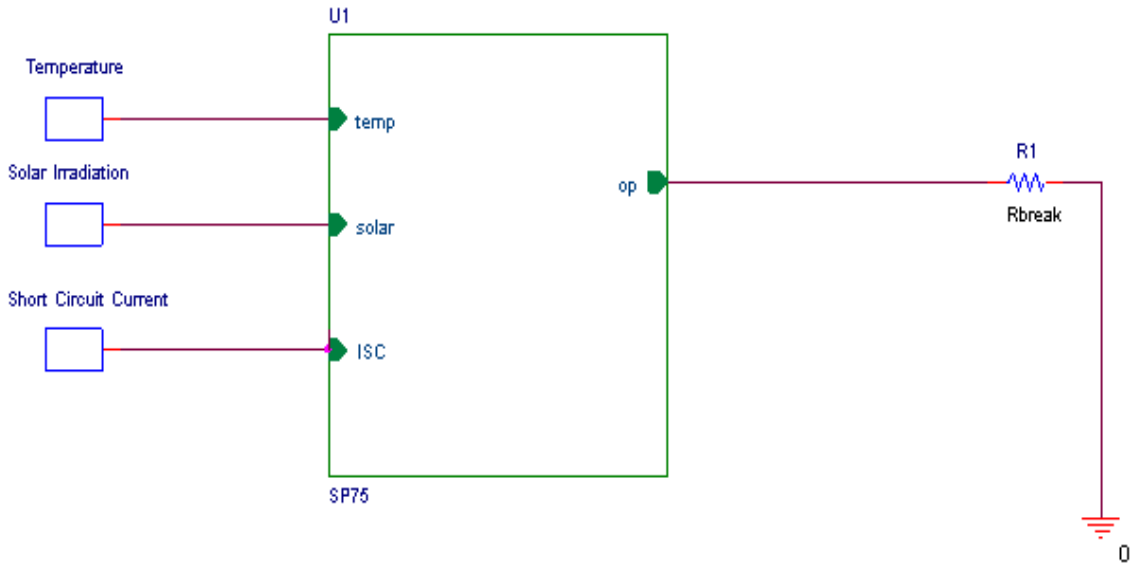


Fig 3-14: The hierarchical block (part) of SP75 in state of optimum load condition.

The result obtained from hierarchical part (figure 3-15, 3-16, 3-17, 3-18, 3-19 and 3-20) and pervious section figures are compatible. This part could be called from PSPICE library to use as PV source at any circuit.

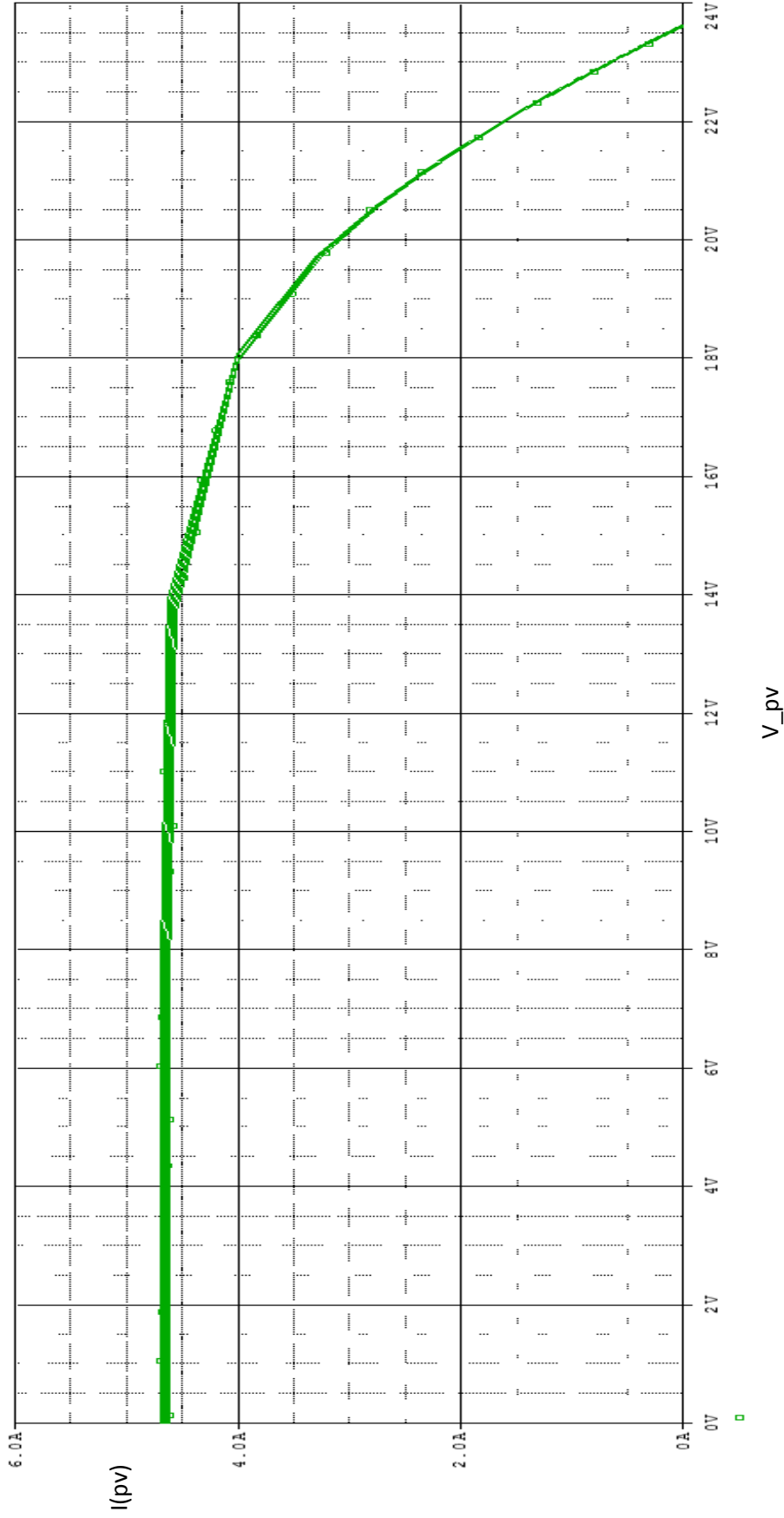


Figure 3-15: The (I-V) curves of the Hierarchal PV panel at different surface temperature under a constant irradiation 1000W/m².

CHAPTER THREE **Simulation Results of The PV Module**

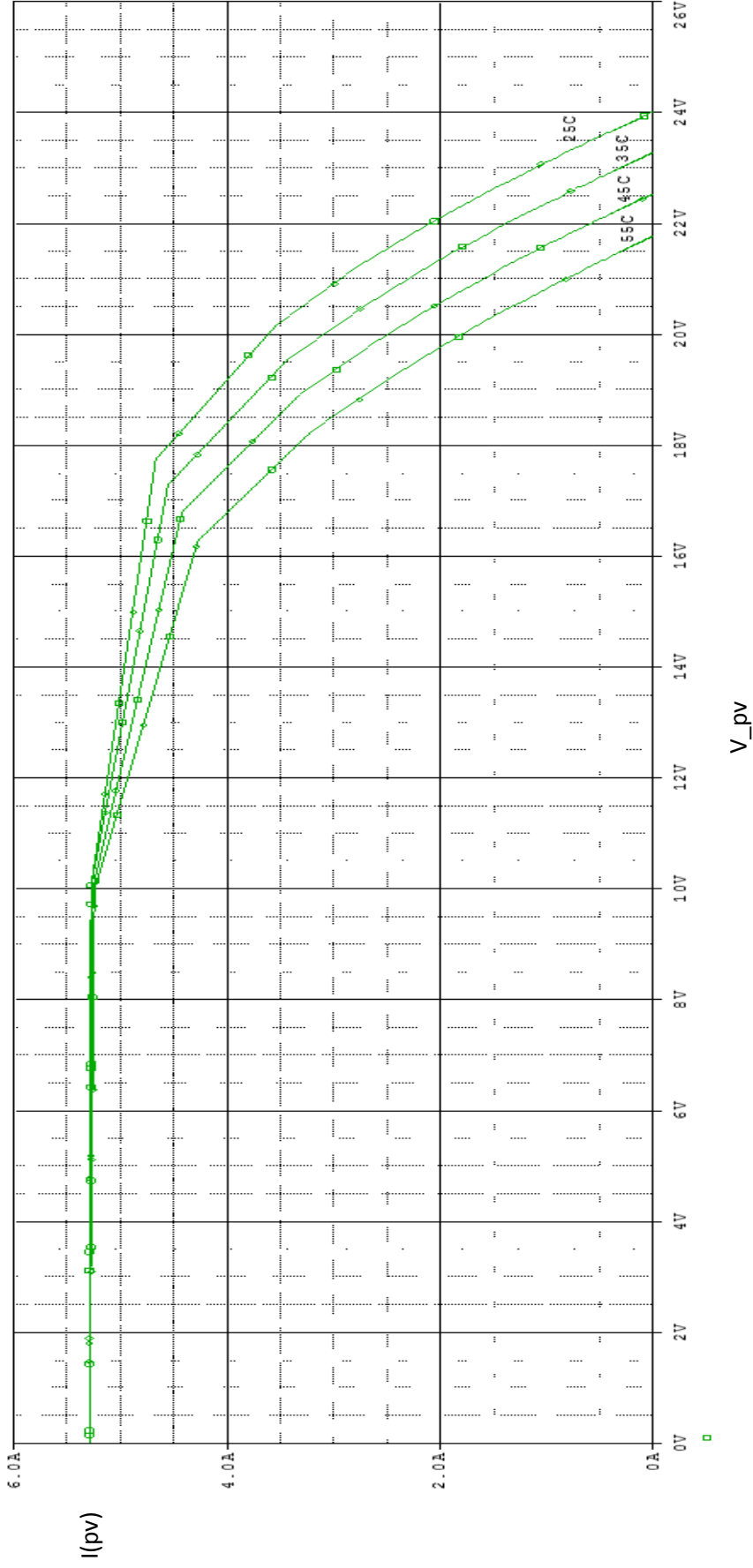


Figure 3-16: The (I-V) curves of the Hierarchical PV panel at different temperature under a constant irradiation $1000W/m^2$.

CHAPTER THREE Simulation Results of The PV Module

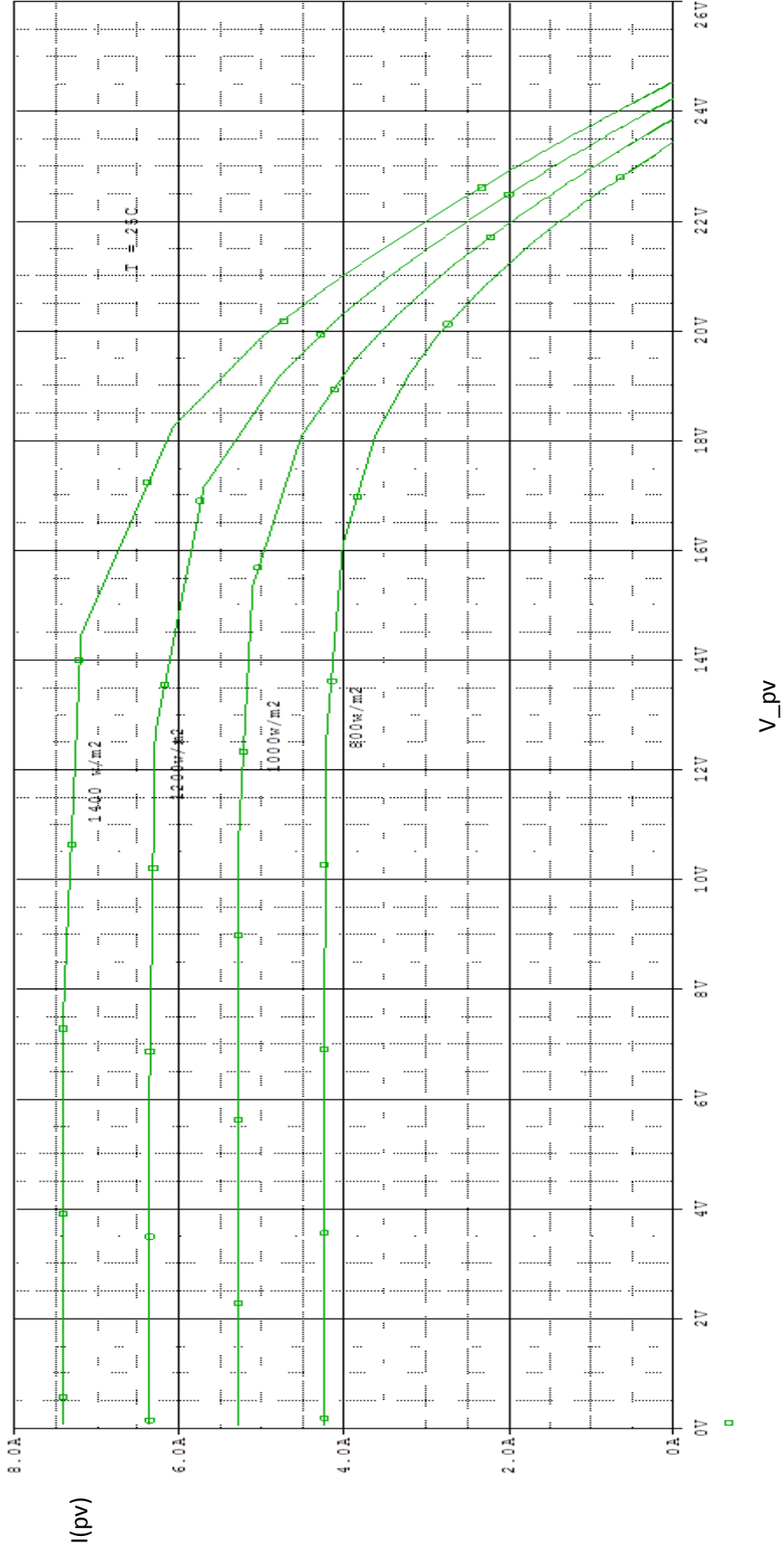


Figure 3-17: The (I-V) curves of the Hierarchical PV panel at different irradiation under a constant temperature $T=25^{\circ}\text{C}$.

CHAPTER THREE **Simulation Results of The PV Module**

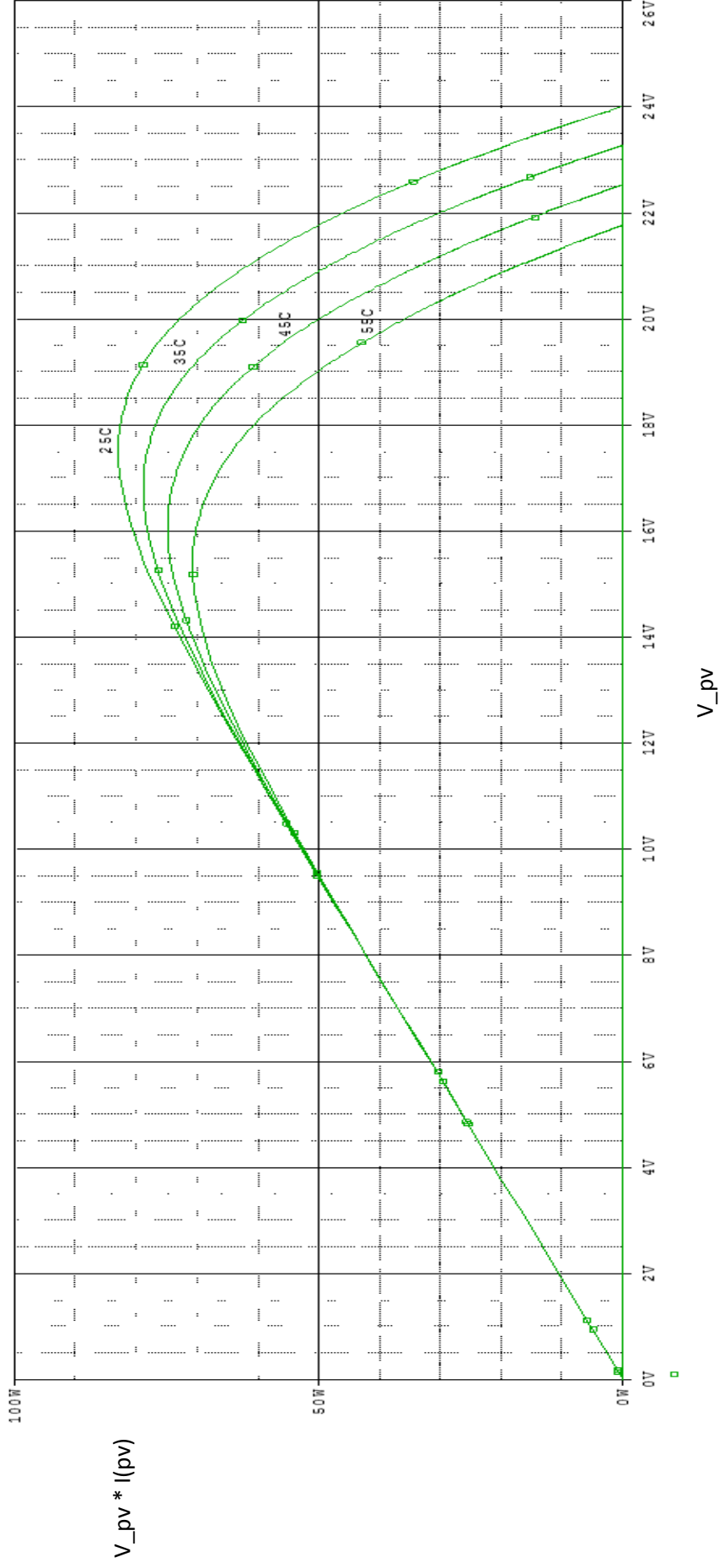


Figure 3-18: The (P-V) curves of the Hierarchical PV panel at different temperature under a constant irradiation 1000W/m².

CHAPTER THREE **Simulation Results of The PV Module**

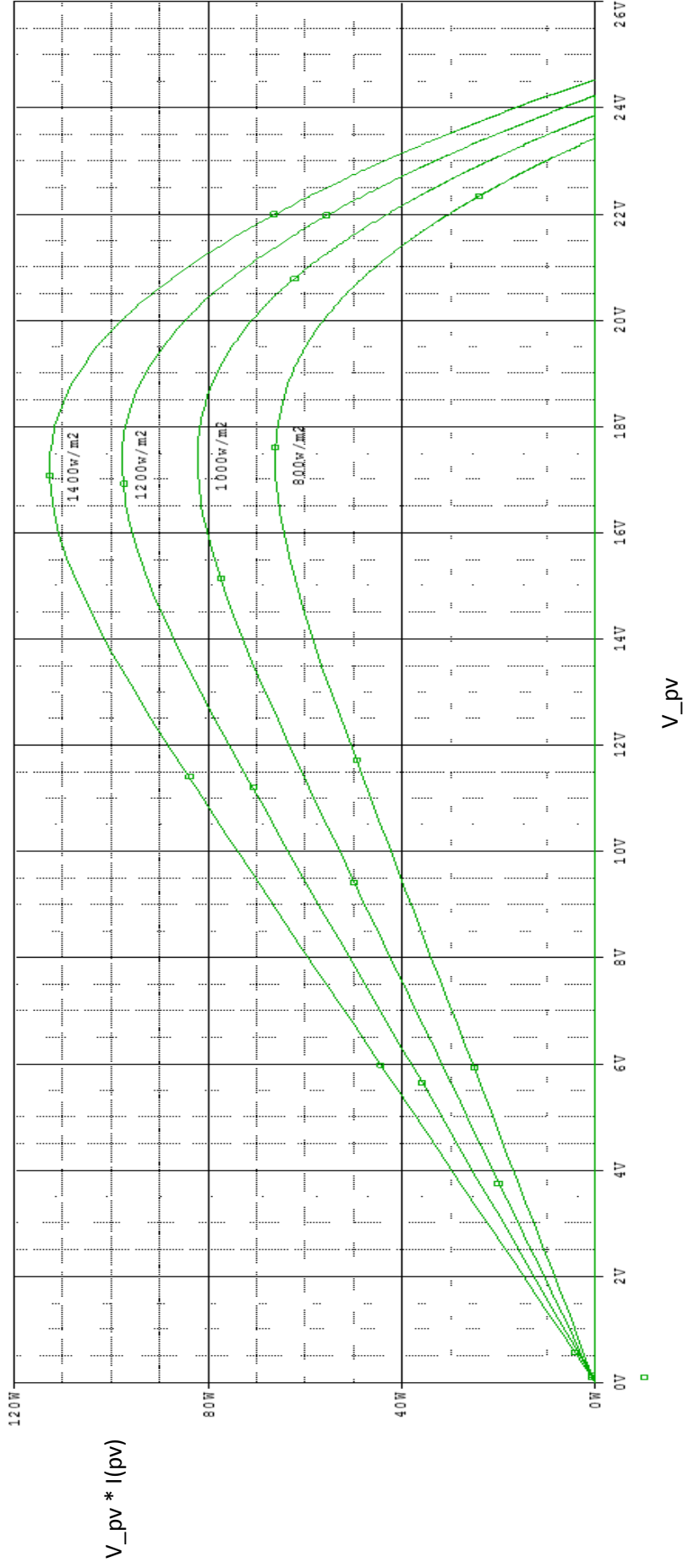


Figure 3-19: The (P-V) curves of the Hierarchical PV panel at different irradiation under a constant temperature $T=25\text{ }^{\circ}\text{C}$.

CHAPTER THREE **Simulation Results of The PV Module**

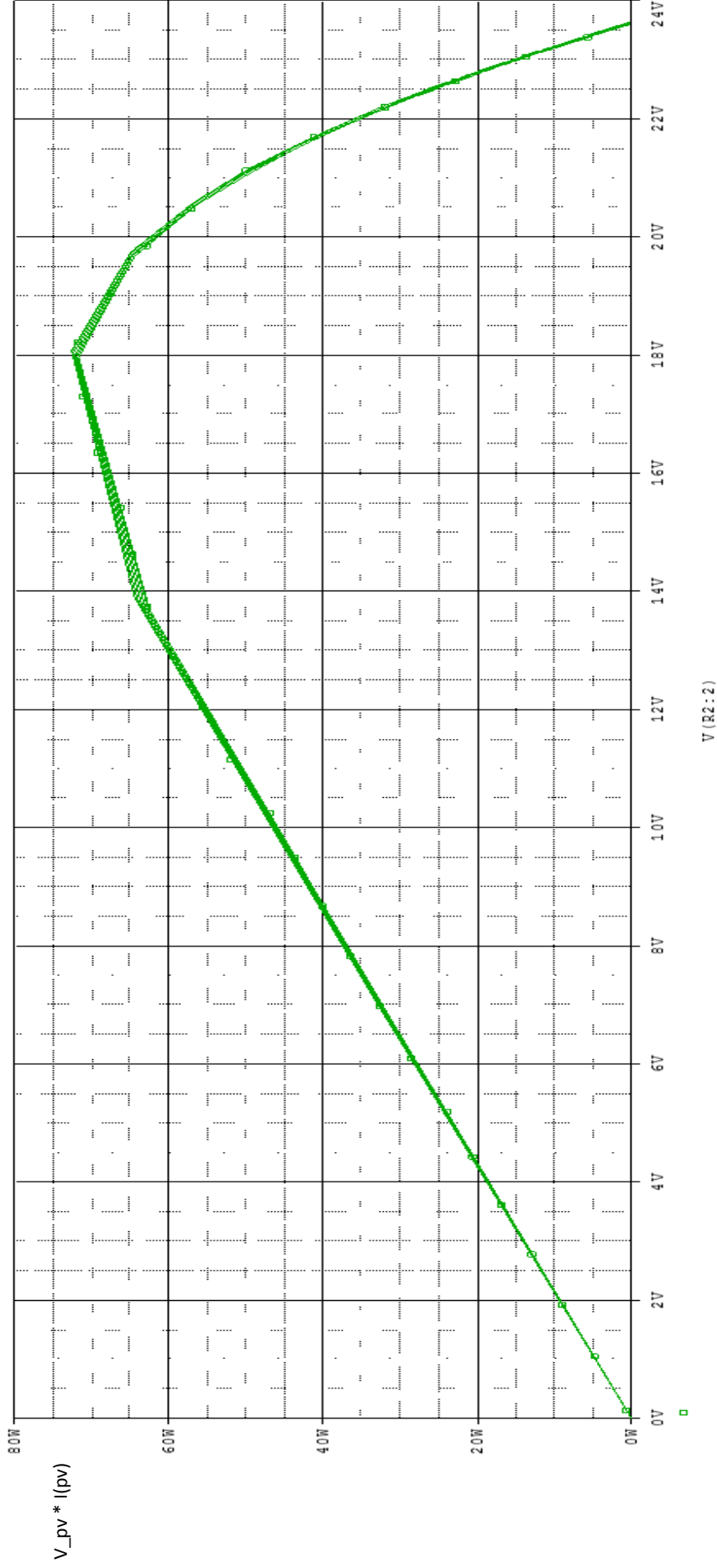


Figure 3-20: The (P-V) curves of the Hierarchical PV panel at different surface temperature under a constant irradiation 1000W/m².

3.4 Electrical Boost Converter

After studying the effect of PV surface temperature on its I-V curves specially the position of the MPP, this temperature will be used to keep tracking of the optimal voltage for the PV panels at the MPP. Therefore, DC-DC converter will be used to achieve this purpose.

3.4.1 Design of Boost Converter

Boost converter shown in fig (3-21) will be raise a PV panel voltages from (17 V) To (34 V). Assuming $I_O = 4.4 \text{ A}$, $f_s = 10 \text{ KHZ}$, $\Delta V_o = 5 \text{ V}$.

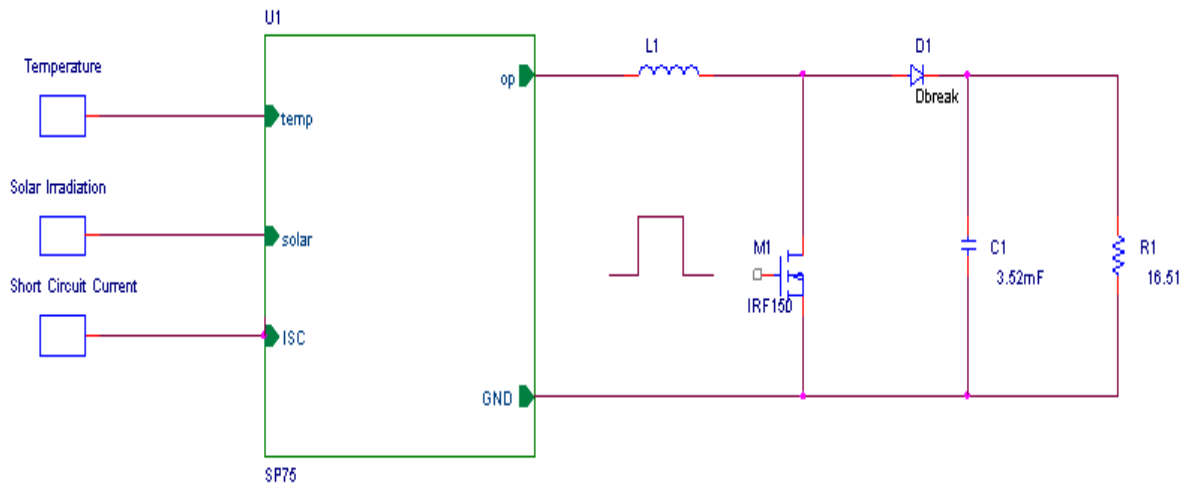


Figure 3-21: The electrical circuit of the boost converter.

Therefore,

CHAPTER THREE Simulation Results of The PV Module

$$R = (V_o)^2 / P = (34)^2 / 70 = 16.51 \Omega.$$

and the duty cycle from eq. (2-5)

$$D = 1 - (V_{IN} / V_o) = 0.5$$

The capacitor and the diode are used to achieve both a rectified and filtered output voltage.

The value of the capacitance is calculated from eq. (2-8) Let $\Delta V_o = 5 \text{ V}$

$$C = (I_o D) / (f_s \Delta V_o) \dots\dots\dots (3-2)$$

$$C = 3.52 \text{ mF}$$

The inductor shown in fig (3-17) works as a storage element is calculated from eq. (2-7)

$$L = (V_o T_s) / (16 I_o) \dots\dots\dots (3-3)$$

$$L = 0.103\text{mH}$$

IRF150 MOSFET is employed as a switching element in the circuit with data sheet in appendix (B).

3.5 Maximum power point tracking technique

3.5.1 Control signal

MPPT are employed with boost converter in order to set the MPP as operating point for large scale of irradiation and surface temperature.

As irradiation and PV surface temperature are changing during the day so, it is important to record these parameters. For this job PV surface temperature is the main factor to be recorded. Also, record the PV voltage to compare it with the actual Maximum voltages of the I-V curves for assigned temperature, to design a control signal for MOSFET gates of the converter.

First problem, that should be solved is how to represent the measured voltages in PSPICE program and the second one the design of the control signal.

First one will be solved by represent a measured PV surface temperature as {val} and from analog behavioral modeling (ABM) library table part will be used to convert the actual temperature to voltage as shown in the fig. 3-22.

CHAPTER THREE Simulation Results of The PV Module

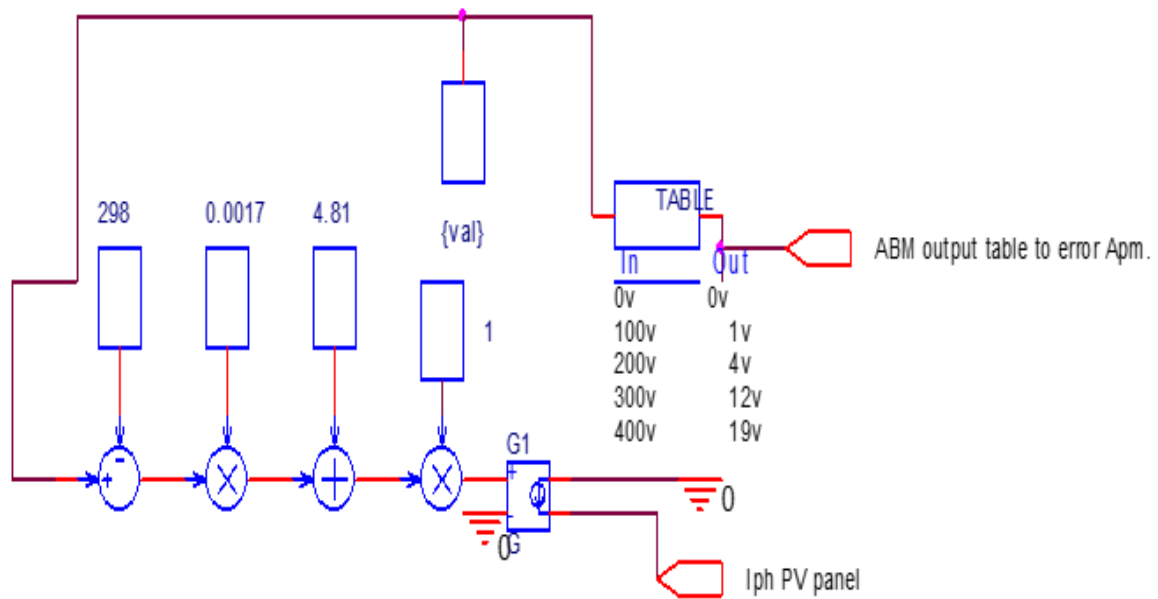


Figure 3-22: The (ABM) analog behavioral diagram with temperature sensor as {val}.

A second problem control signal, was achieved by comparing the output voltage for the PV panel with the voltage obtained from the output of the table by using Error amplifier as shown in fig. (3-23)

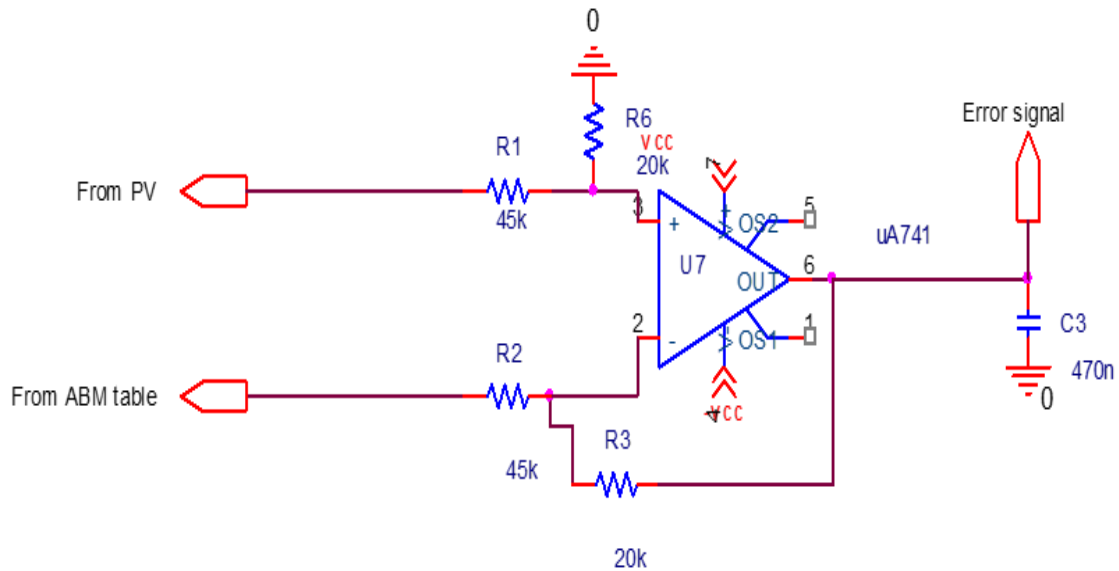


Figure 3-23: The Error amplifier with two input one from PV panel and another from ABM table.

3.5.2 PWM Signal gate drive circuit

Fig (3-24) show a sub circuit connected to gate drive circuit for converter MOSFET. This OP-Amp compare a saw tooth signal with an error signal obtained from Op-Amp fig (3-23) to produce a square wave with necessary duty ratio to drive the switching device of the converter.

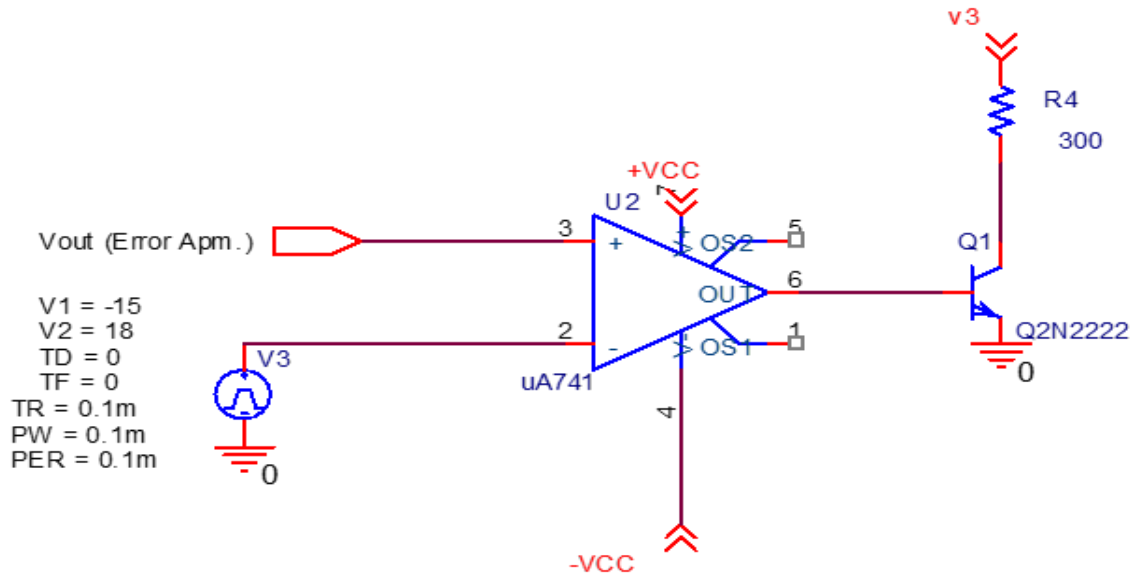


Figure 3-24: The computer Op-Amp to produce square signals.

Transistor Q2 provide a square pulse of suitable voltage and current to the gate of transistor M5.

For the same purpose 555 timer was tasted as PWM the control signal from fig. (3-24) is applied to the control pin (no. 5 in 555 timer)

Finally, fig (3-25) and fig (3-26) explained the total simulated circuit of PV system with temperature controlled at PSPICE.

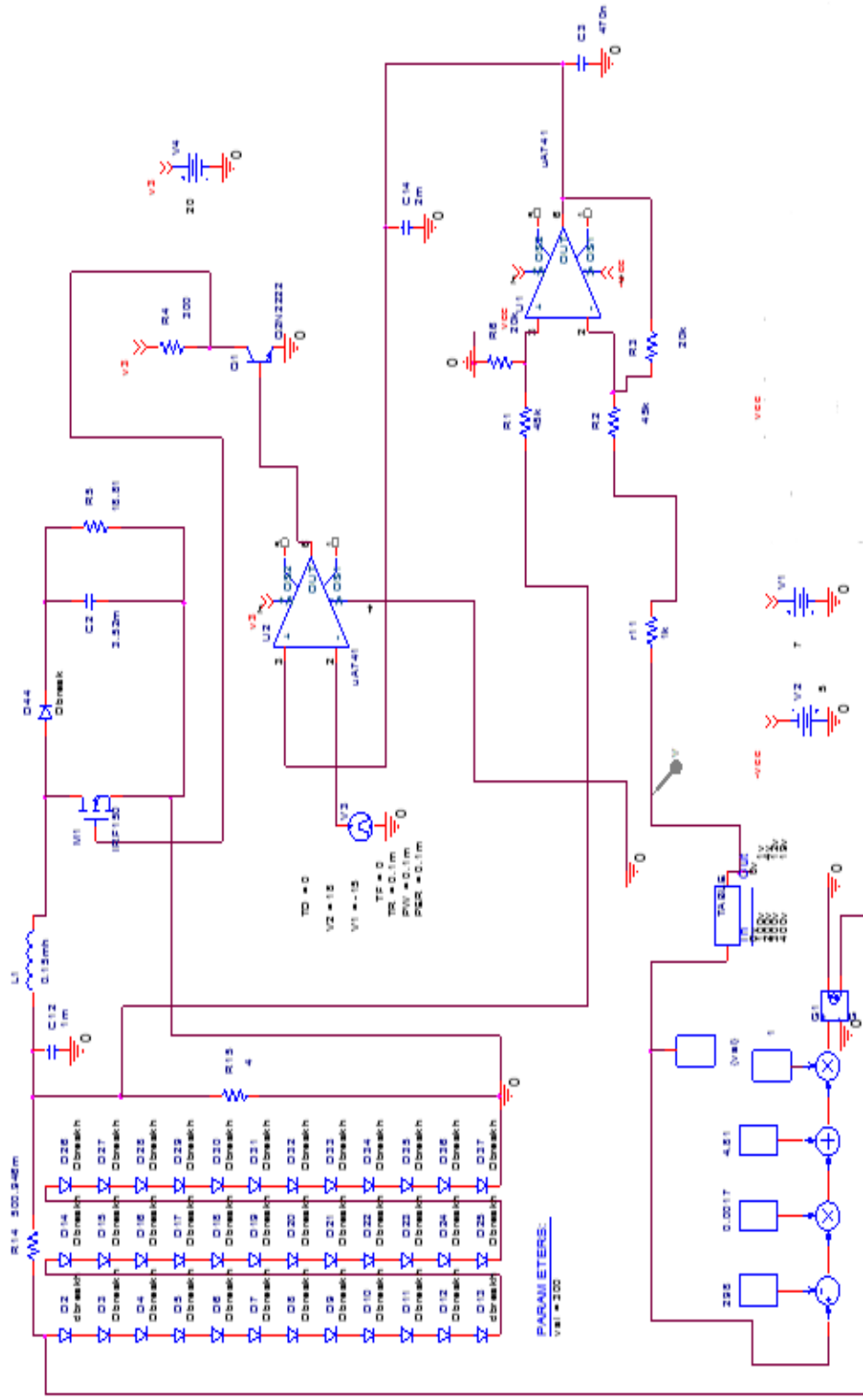


Figure 3-25: The total simulated circuit of PV system with temperature controlled at PSPICE.

CHAPTER THREE Simulation Results of The Proposed PV Module and System Design

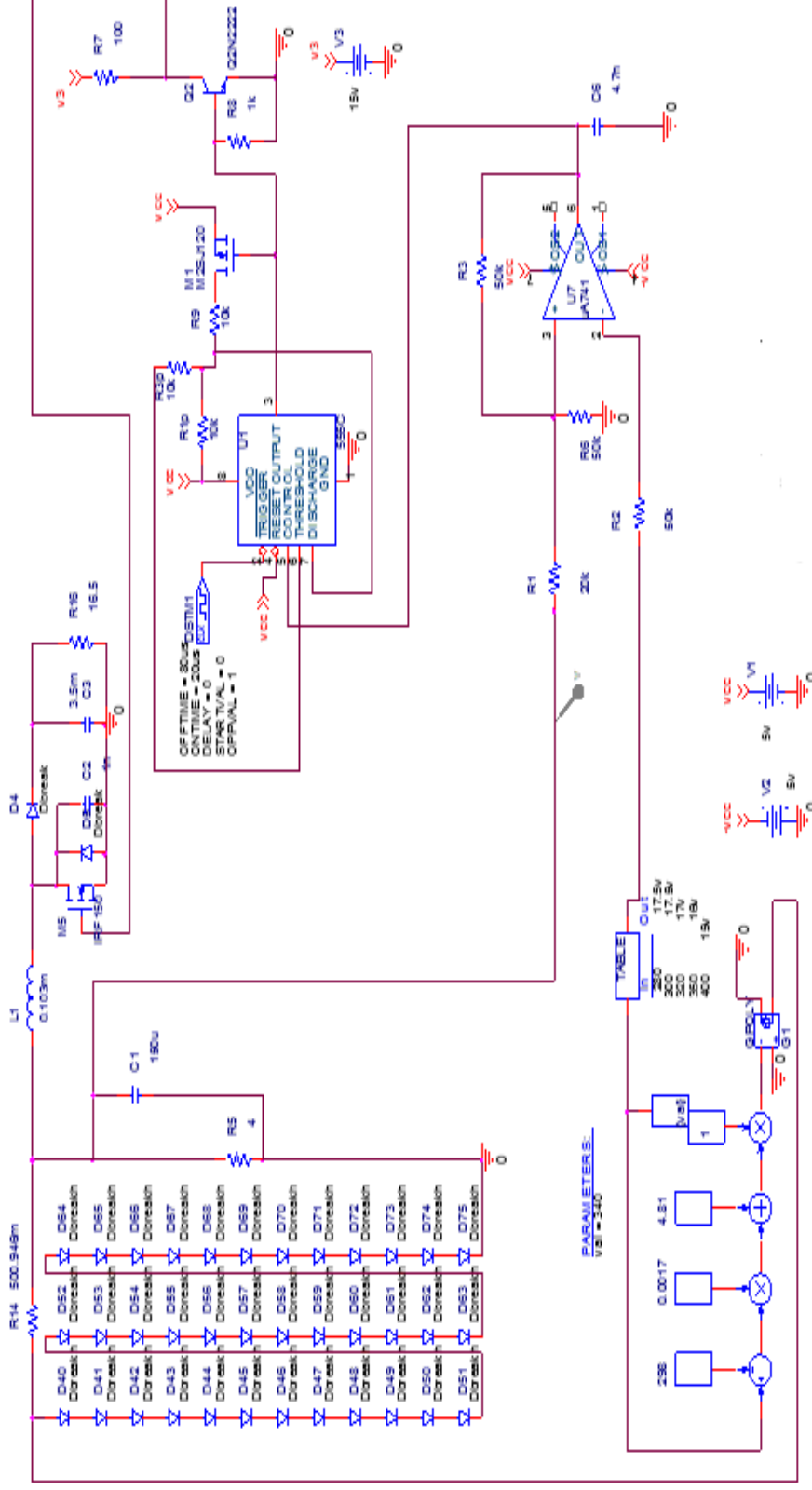


Figure 3-26: The total simulated circuit of PV system with temperature controlled using 555 timer at PSPICE

CHAPTER THREE Simulation Results of The Proposed PV Module and System Design

3.6 Results

Fig. (3-27) and fig. (3-28) represents the simulated I_{SC} and a simulated PV panel output voltage for different surface temperature

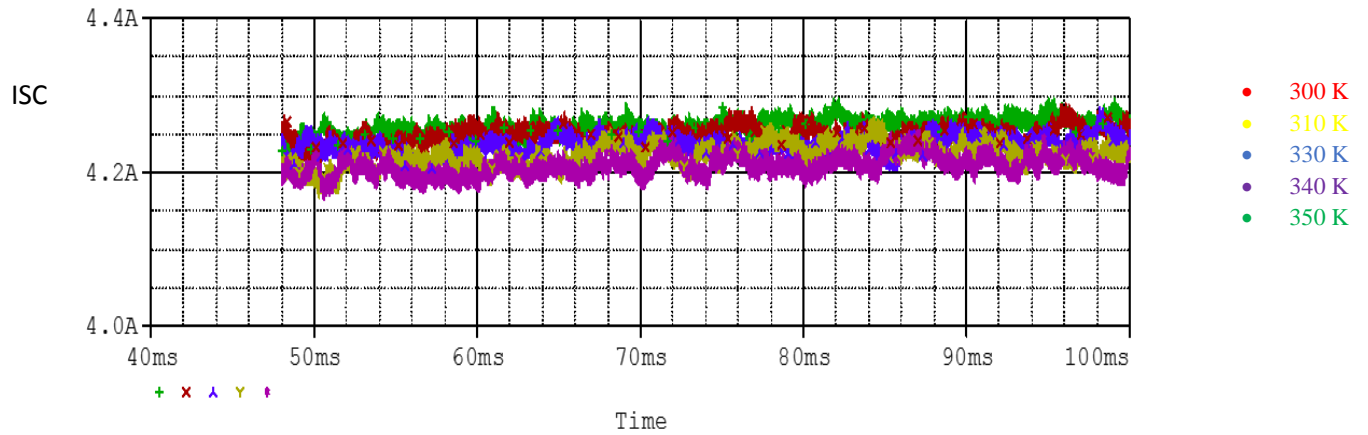


Figure 3-27: Current from PV panel at different surface temperature.

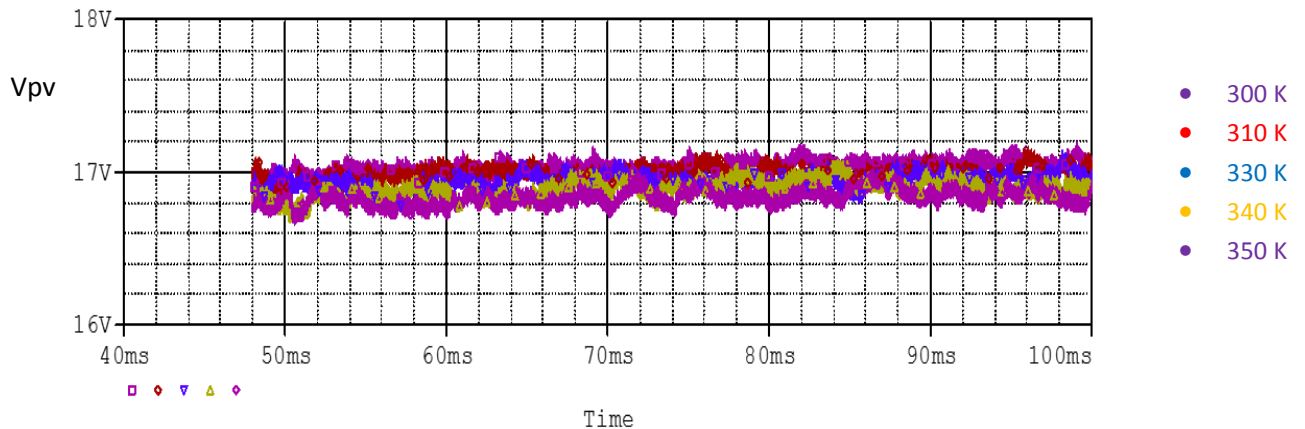


Figure 3-28: Output voltage from PV panel at different surface temperature.

CHAPTER THREE Simulation Results of The Proposed PV Module and System Design

Fig. (3-29) and represent the input of ABM table at different surface temperature of PV panel. Fig (3-30) shows the maximum voltage of PV panel for each change in surface temperature

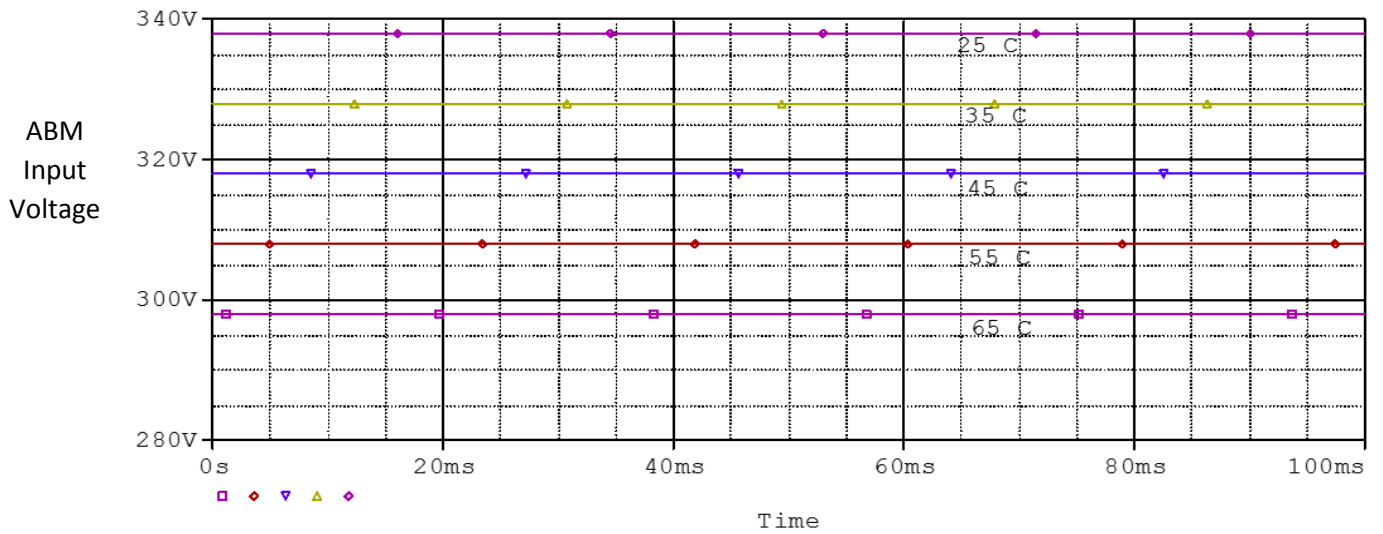


Figure 3-29: Different surface temperature as input to ABM table

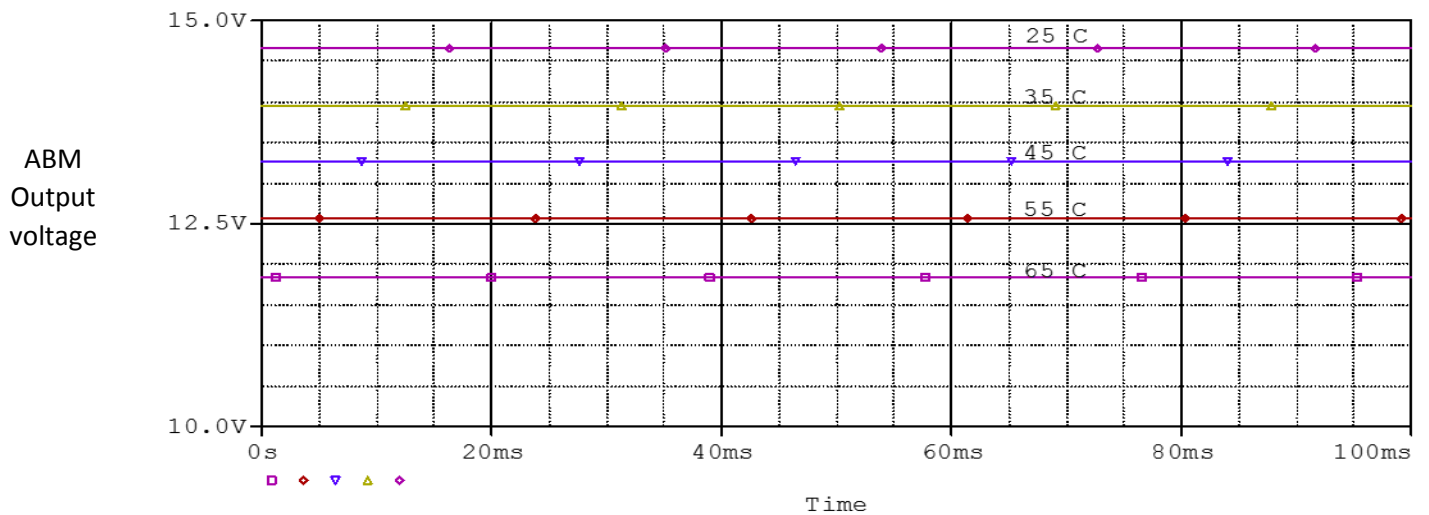
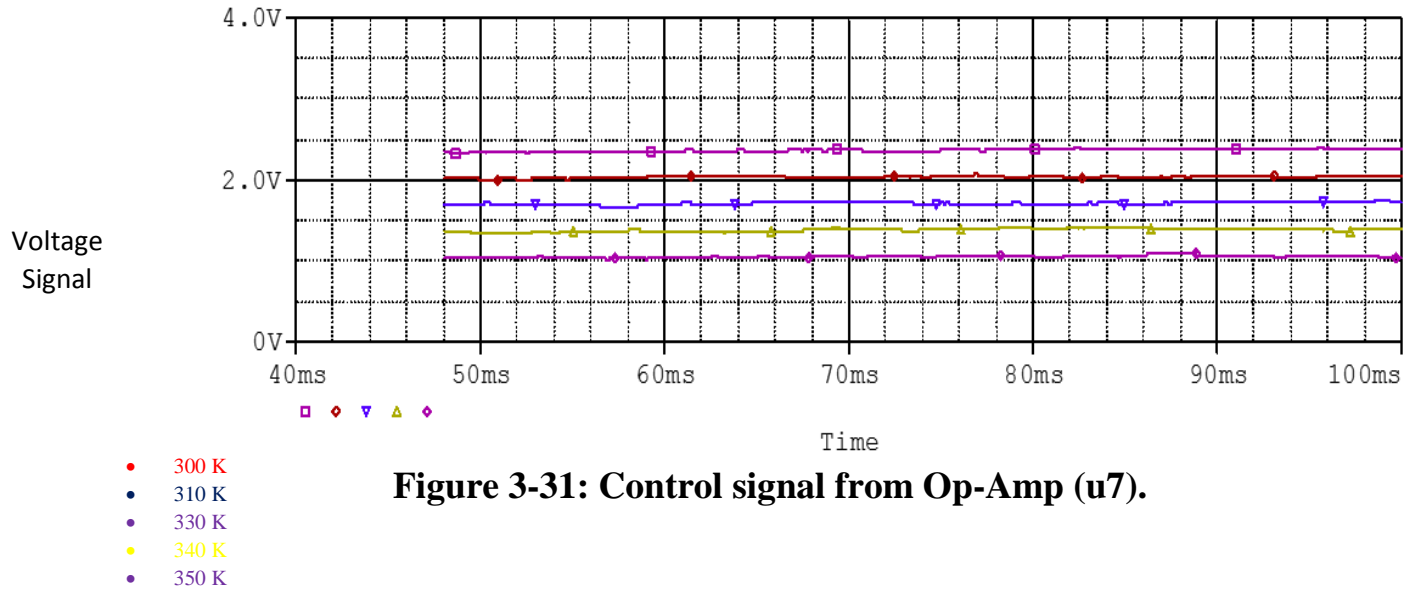


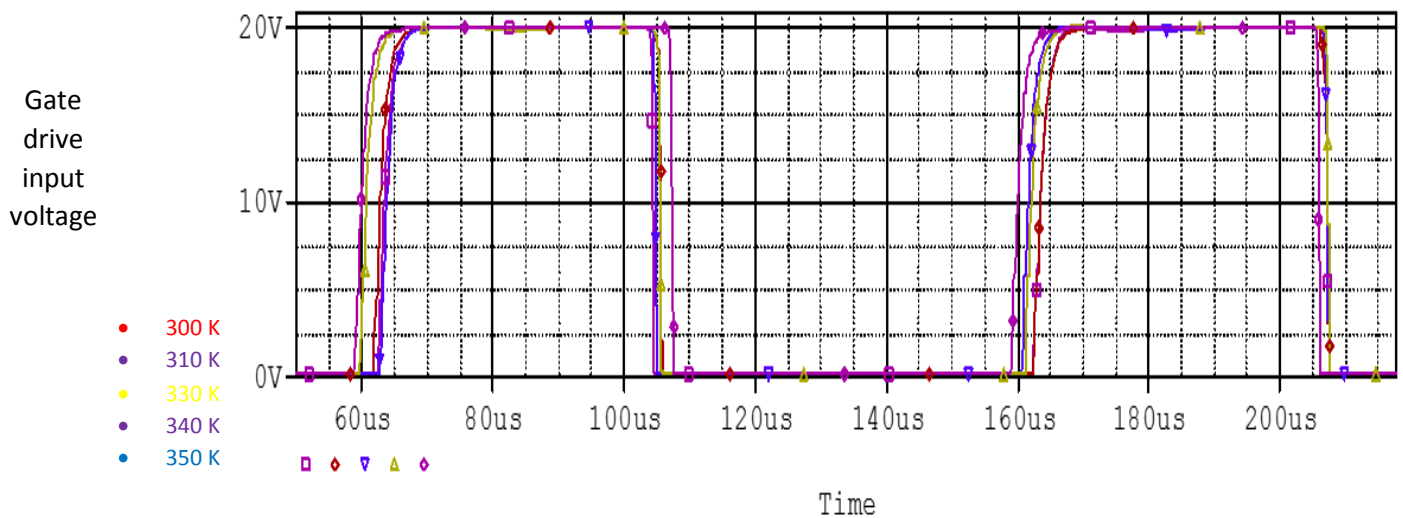
Figure 3-30: Output voltage from ABM table.

CHAPTER THREE Simulation Results of The Proposed PV Module and System Design

As seen in fig. (3-31) below the value of control signal confined between 0 V and 5 V according to VCC supply voltage of the error amplifier



as seen in the fig. (3-32), fig. (3-33) below a different duty cycle has been obtained from both tasted circuit 555 timer and saw tooth method.



CHAPTER THREE Simulation Results of The Proposed PV Module and System Design

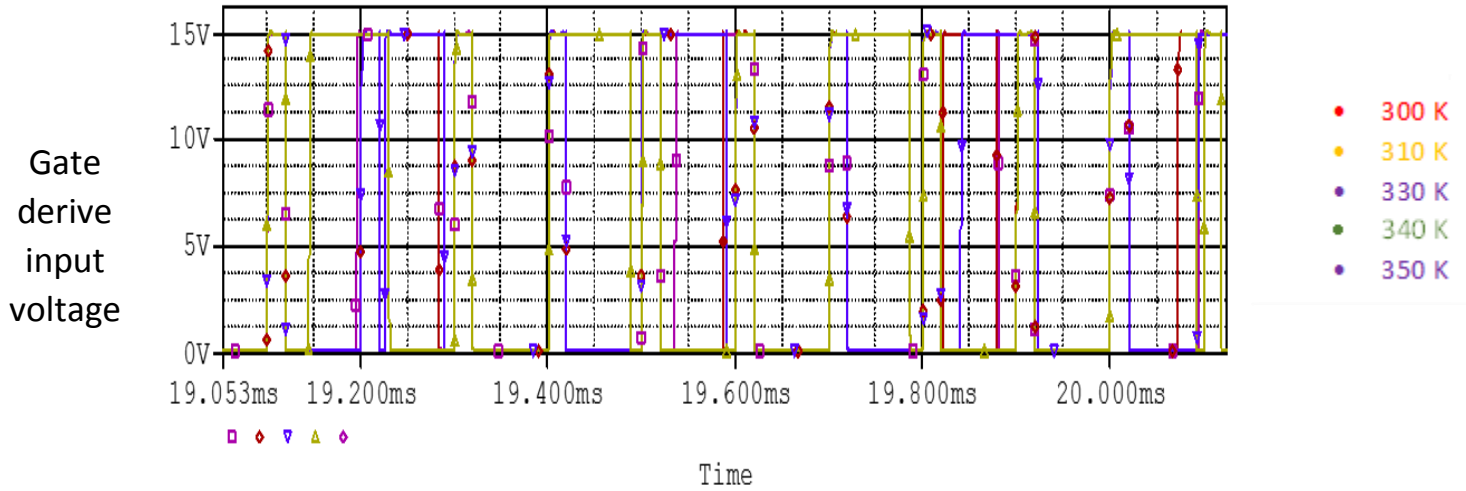


Figure 3-33: PWM signal for different surface temperature from 555C.

the current from the inductor in the boost converter is equal to 4.4 A as shown in fig. 3-34

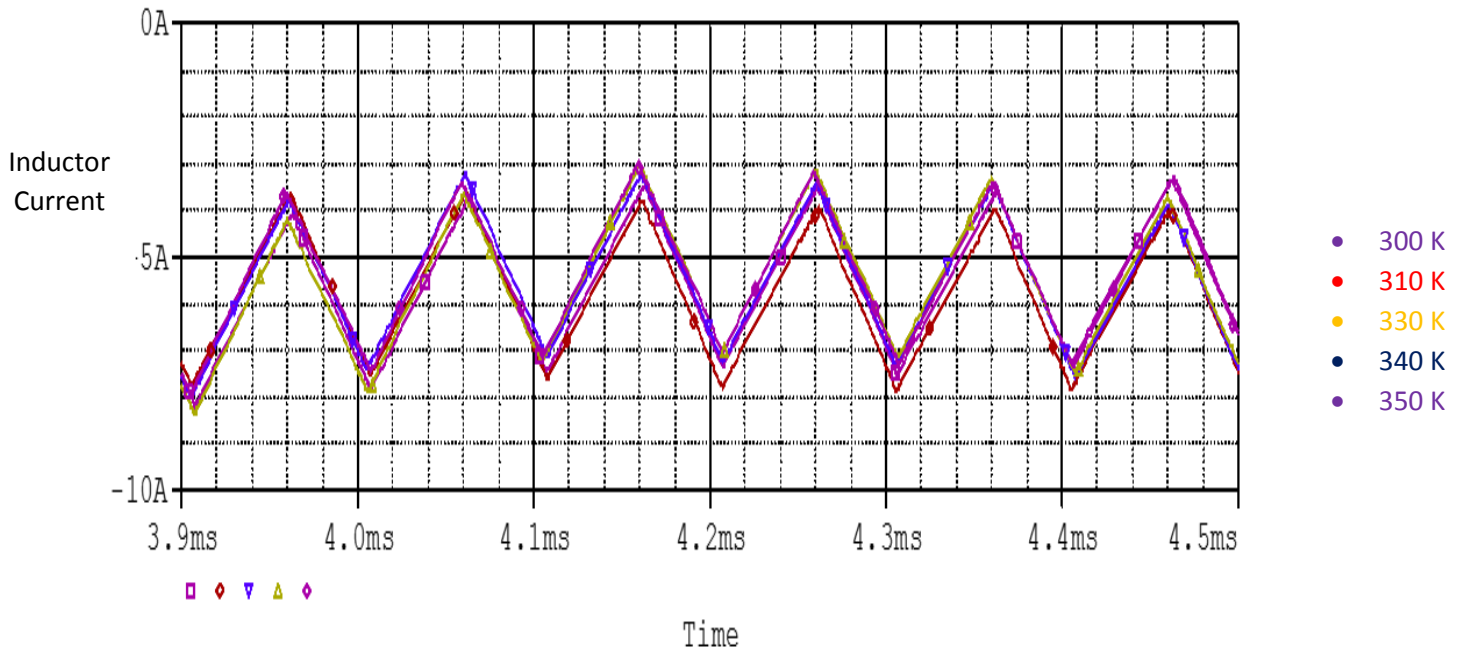


Figure 3-34: The inductor current in the boost converter for different surface temperature.

CHAPTER THREE Simulation Results of The Proposed PV **Module and System Design**

Fig. 3-35 and fig. 3-36 show the output voltage and current from boost converter for the designed PV system at different surface panel temperature. The output current value ranging from 1.65 to 1.75 A and the output voltage between 33V and 34V from saw tooth method. Fig. 3-37 fig. 3-38 shows the output voltage and current from boost converter in PV system by using 555 timer.

This method give us a good result in comparison with the first one because the converter output voltage and current are constant for all surface temperature.

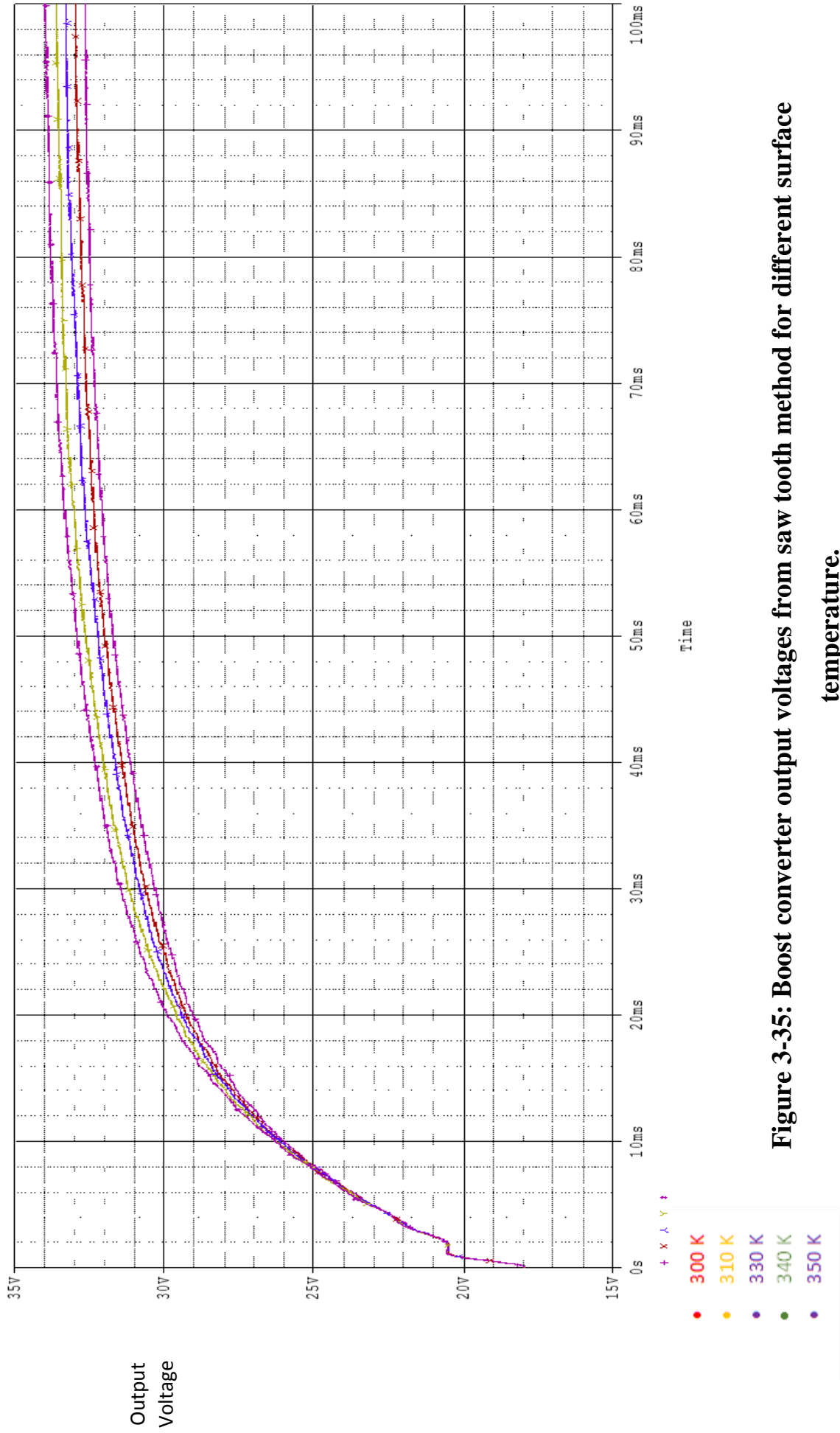


Figure 3-35: Boost converter output voltages from saw tooth method for different surface temperature.

CHAPTER THREE Simulation Results of The Proposed PV Module and System Design

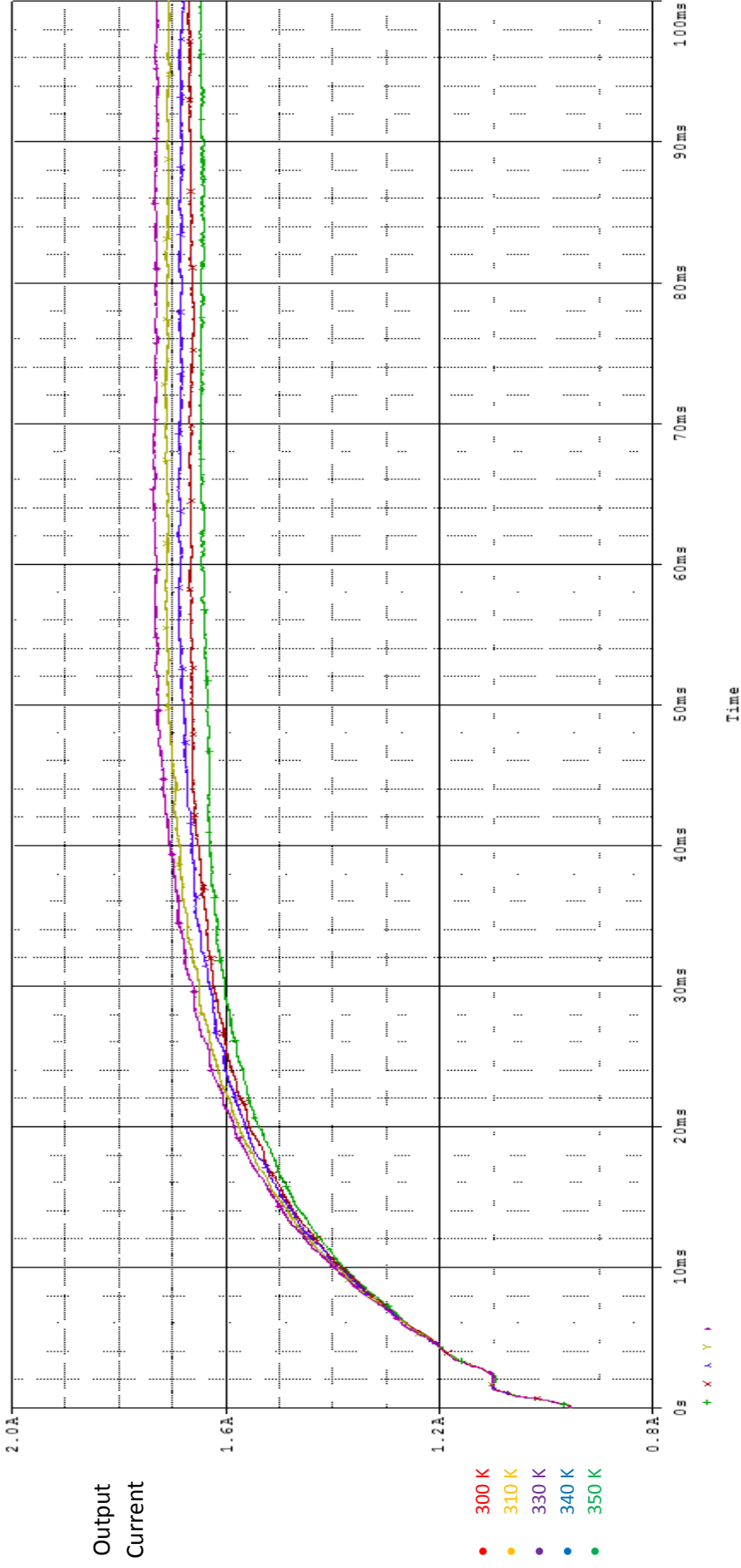


Figure 3-36: Boost converter output current from saw tooth method for different surface temperature.

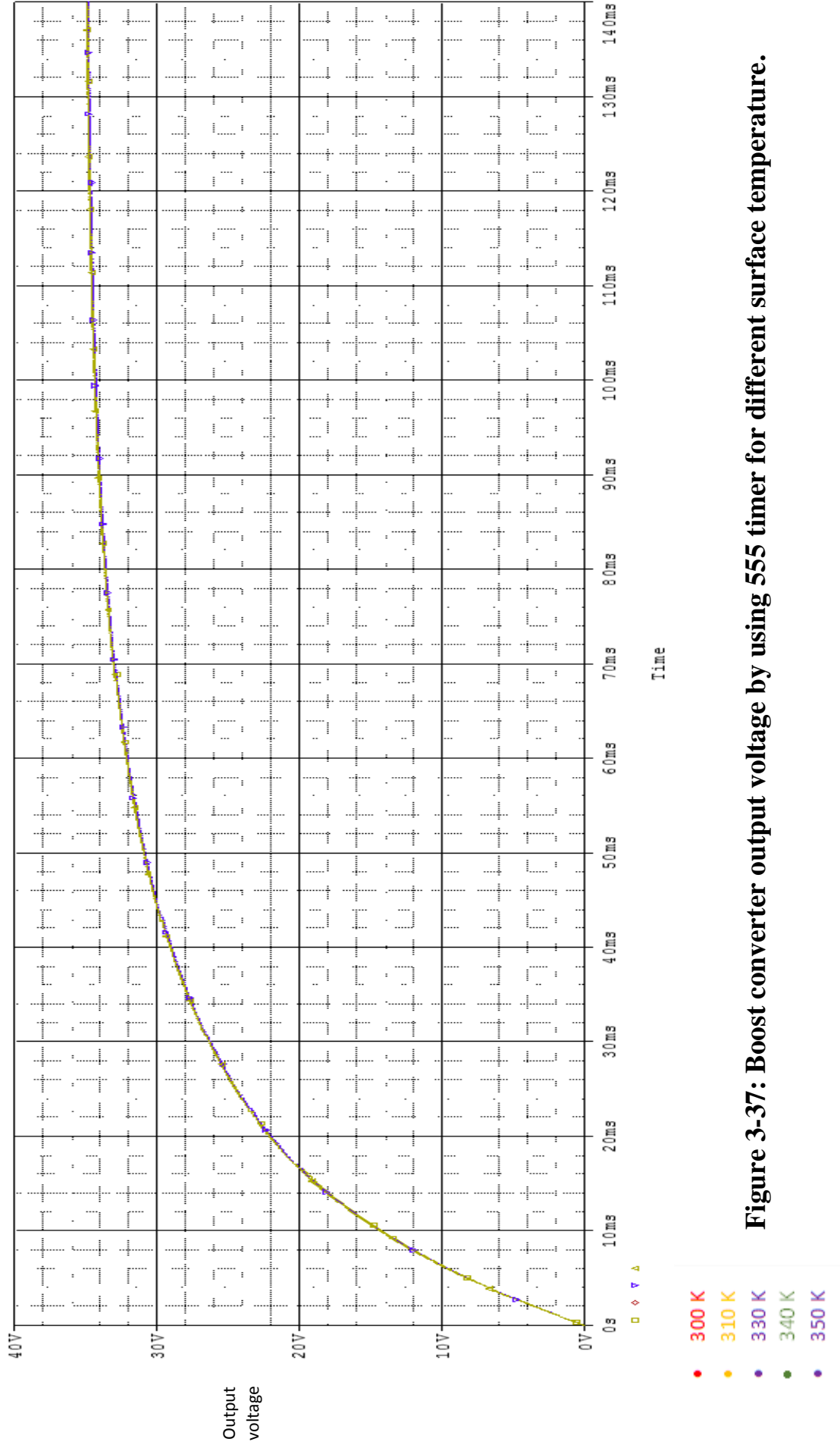


Figure 3-37: Boost converter output voltage by using 555 timer for different surface temperature.

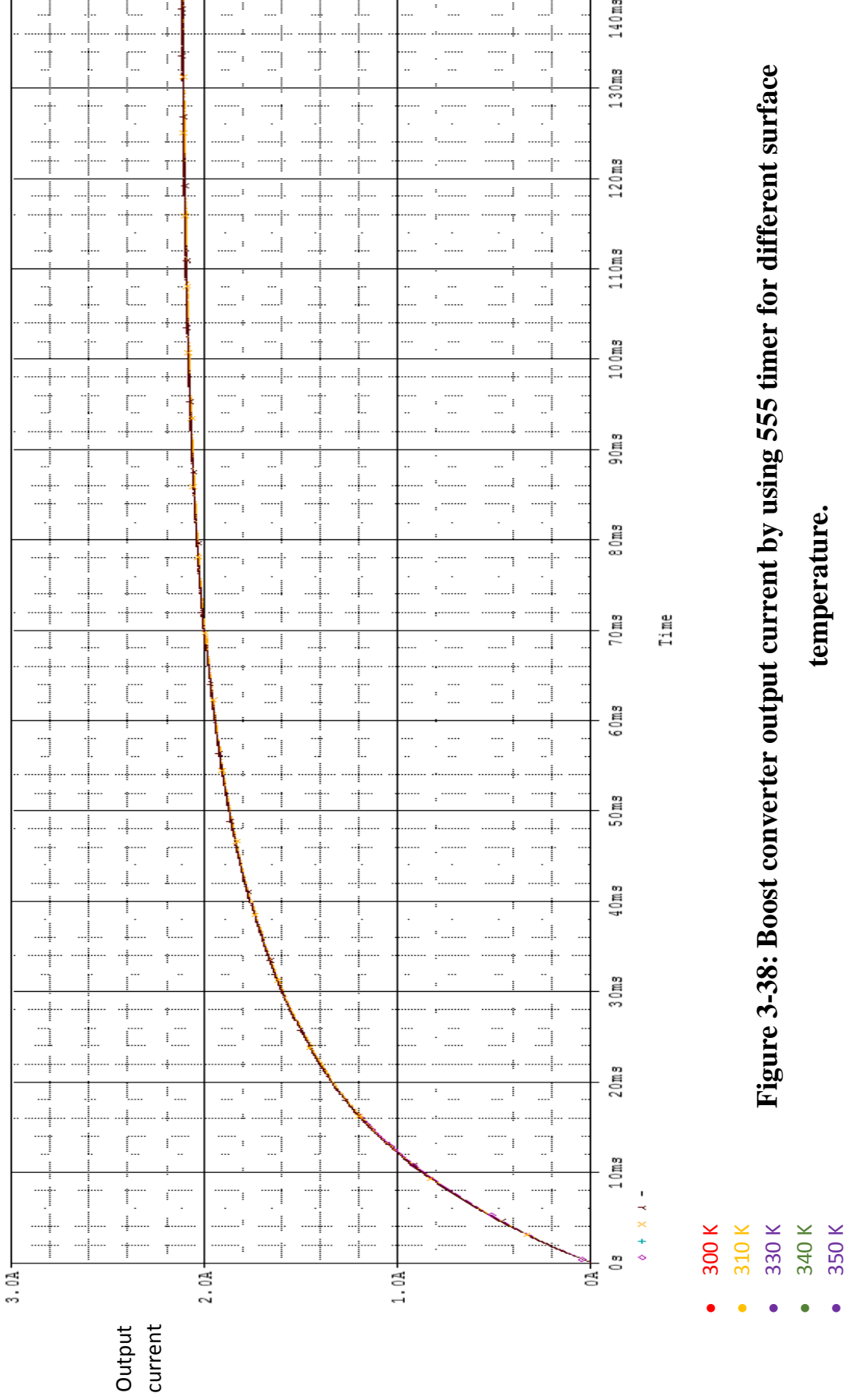


Figure 3-38: Boost converter output current by using 555 timer for different surface temperature.



Chapter Four

Chapter Four

Conclusions and future work

4.1 Conclusions

From the present study, the following points could be concluded:

1. PV panel model Defined as hierarchical block in PSPICE library. So, it could be called directly from PSPICE library as special source and used it for most PV systems applications.
2. In all MPPT techniques a PV voltage and current should be measured but for temperature technique just sensing the surface temperature. For this reason, this technique is used because it's easy and economical.
3. In temperature technique the MPP sensing this parameter at constant irradiation.
4. Boost converter gives better results with 555 timer as pulse width modulation. The output voltage equal to 34 V for temperature variation from 300 K to 350 K.

4.2 Future work

For future work, can recommend the introduction of the following open problem:

1. Present the effect of shading for single cell or more in Photovoltaic panel (I-V) and (P-V) curves. Also, study its effect on PV surface temperature.
2. Modify a PV panel model by adding tilt angle parameter.
3. Test PV panel model with other types converter with the same MPP techniques.
4. design and implantation the previous work experimentally to sensing surface temperature of PV panel.

A graphic of a scroll with a grey shadow on the left side. The word "References" is written in a bold, black, serif font in the center of the scroll.

References

[1] Wiley “Photovoltaics fundamentals, technologies and practice” Thomson, Digital, Noida, India, 2014.

[2] Heinrich Häberlin “Photovoltaics System Design and Practice”, John Wiley & Sons, Ltd, 2012.

[3] Cole Boulevard, etal “Basic Photovoltaic Principles and Methods”, Published by Technical Information Office Published February 1982.

[4] Cederblad Henrik, Fasselund Joar, Nordin Olof “nCube-power supply” thesis, Narvik University College, June 2003.

[5] K. Emery, J. Burdick, Y. Caiyem, D. Dunlavy, H. Field, B. Kroposki, T. Moriarty, L. Ottoson, S. Rummel, T. Strand, and M.W. Wanlass “Temperature Dependence of Photovoltaic Cells, Module, And Systems” 25th PVSC; Washington, D.C May 13-17, 1996.

[6] David L. King, Jay A. Kratochvil, and William E. Boyson “Temperature coefficient for PV modules and arrays: measurements methods, difficulties, and results” IEEE photovoltaic specialists conference, 1997.

[7] Minwon Park and In-Keun Yu “A study of the optimal voltage for mppt obtained by surface temperature of solar cell” The 30th Annual Conference of the IEEE Industrial Electronics Society, November 2 - 6, 2004, Busan, Korea.

[8] R.K. Nema, Savita Nema, and Gayatri Agnihotri “Computer Simulation based study of photovoltaic cells/modules and their experimental verification” international journal of recent trends in engineering, Vol 1, No. 3 May 2009.

[9] Roberto F. Coelho, Filipe Concer and Denizar C. Martins “A proposed photovoltaic module and array mathematical modeling destined to simulation” IEEE international symposium electronics,2009.

[10] Zainab M. Kubba and Zaid Samair “PSPICE MODEL OF THE PV PANEL” Journal of Al-Nahrain University, Vol.12, NO.3, September, 2009.

[11] Roberto F. Coelho, Filipe M. Concer, Denizar C. Martins “A MPPT approach based on temperature measurements applied in PV systems” 9th IEEE/IAS International Conference on Industry Applications, 2010.

[12] Roberto F. Coelho, Filipe M. Concer, Denizar C. Martins “A simplified analysis of DC-DC converters applied as maximum power point tracker in photovoltaic systems” IEEE international symposium on power electronics for distributed generation systems, 2010.

[13] Moacyr Aureliano Gomes de Brito, Luigi Galotto, Jr., Leonardo Poltronieri Sampaio, Guilherme de Azevedo e Melo, and Carlos Alberto Canesin “Evaluation of the main MPPT techniques for Photovoltaic applications” IEEE transactions on industrial electronics, Vol. 60, No. 3, March 2013.

[14] Anil S. Hiwale, Mugdha V. Patil and Hemangi Vinchurkar “An Efficient MPPT Solar Charge Controller” International Journal of Advanced Research in Electrical, Electronics and Instrumentation Engineering, Vol. 3, Issue 7, July 2014.

[15] Gaikwad Gauri, Kumbhar Sangita, Kokane Rohini and Suryawanshi Prashant “Enhancing the Efficiency of Solar Power System with Perturb and Observe Method” International Journal of Advanced Research in Electrical, Electronics and Instrumentation Engineering, Vol. 5, Issue 4, April 2016.

[16] Savitha P B, Shashikala M S and Puttabuddhi K L “Modelling of Photovoltaic Cell/Module under Environmental Disturbances using MATLAB /Simulink” International Journal of Engineering Trends and Technology (IJETT) – Vol. 9, NO.1 - Mar 2014.

[17] K. Subbulakshmi “Maximum Power Point Tracking Technique” Middle-East Journal of Scientific Research 20 (6): 728-733, 2014.

[18] Krismadinata, Nasrudin Abd. Rahim, Hew Wooi Ping and Jeyraj Selvaraj “Photovoltaic module modeling using simulink/matlab” Procedia Environmental Sciences 17 (2013) 537 – 546.

[19] Asmi Assis, Shinosh Mathew “Fundamentals and Modelling of a Solar PV System” International Journal of Advanced Research in Electrical, Electronics and Instrumentation Engineering. 4, Issue 6, June 2015.

[20] Gail-Angee Migan, " Study of the operating temperature of a PV module" Project report MVK160 Heat and Mass Transfere, Lund, Sweden, May 16, 2013.

[21] Abdennaceur Karoui and Ara Kechiantz “Quantum Mechanics Design of Two Photon Processes Based Solar Cells” published by Intech, 22, February, 2012.

[22] N.M. da Rocha, R.F. Coelho, J.C. Passos and D.C. Martins “Suggestion of Associating a PV MPPT Algorithm Based on Temperature Control with a PV Cooling System” IEEE , 2014.

[23] David L. King, Jay A. Kratochvil, and William E. Boyson “Temperature Coefficients for PV Modules and Arrays: Measurement Methods, Difficulties, and Results” 26th PVSC; Anaheim, CA, IEEE Sept. 3Wct. 3,1997.

[24] Skoplaki E, Palyvos JA. On the temperature dependence of photovoltaic module electrical performance: A review of efficiency/power correlations Solar Energy 2009; 83:614-24.

[25] Minwon Park and In-Keun Yu “A Study on the Optimal Voltage for MPPT obtained by Surface Temperature of Solar Cell” The 30th Annual Conference of the IEEE Industrial Electronics Society, Busan, Korea, November 2 - 6, 2004.

[26] Ali Emadi, Alireza Khaligh, Zhong Nie and Young Joo Lee “Integrated Power Electronic Converters and Digital Control” by Taylor and Francis group, 2009.

[27] Ioan Viorel Banu, Marcel Istrate “Modeling of Maximum Power Point Tracking Algorithm for Photovoltaic Systems” IEEE International conference and Exposition on electrical power engineering, Lasi, Romania, 2012.

[28] Shalini S. Durgam, Anuradha B. Musale, Sneha A. Balki, Payal S. Gahane, Asst. Prof. L. B. Awale “Ac Hybrid Charge Controller” Int. Journal of Engineering Research and Applications, Vol.5, Issue 3, Part 5, March 2015.

[29] Roberto F. Coelho "A Simplified Analysis of DC-DC Converters Applied as Maximum Power Point Tracker in Photovoltaic Systems" IEEE international symposium on power electronics for distributed generation system, Brazil, 2010

[30] Zainab Kubba, K. Al-Shara and E- Alshakarchi “Computer aided design and implementation of converter circuit applied for Photovoltaic system” Journal of engineering, Volume 4, No. 4, December 2008.

[31] Dr. Anil S. Hiwale, Mugdha V. Patil and Hemangi Vinchurkar “An Efficient MPPT Solar Charge Controller” International Journal of Advanced Research in Electrical, Electronics and Instrumentation Engineering” Vol. 3, Issue 7, July 2014.

[32] Nazih Moubayed, Ali El-Ali and Rachid Outbib “A comparison of two MPPT techniques for PV system” Wseas Transactions on Environment and Development Issue 12, Volume 5, December 2009.

[33] Roberto Faranda “Energy comparison of MPPT techniques for PV Systems”, Wseas Transactions on Power Systems, Issue 6, Volume 3, June 2008.

[34] Gaikwad Gauri, Kumbhar Sangita, Kokane Rohini and Suryawanshi Prashant “Enhancing the Efficiency of Solar Power System with Perturb and Observe Method” International Journal of Advanced Research in Electrical, Electronics and Instrumentation Engineering, Vol. 5, Issue 4, April 2016.

[35] Roberto Francisco Coelho and Denizar Cruz Martins “An Optimized Maximum Power Point Tracking Method Based on PV Surface Temperature Measurement” licensee InTech, 2012.

[36] Roberto F. Coelho, Filipe M. Concer and Denizar C. Martins “A MPPT Approach Based on Temperature Measurements Applied in PV Systems” ICSET, Kandy, Srilanka, 2010.

[37] Abdul Fathah “Design of a Boost Converter” Department of Electrical Engineering National Institute of Technology Rourkela-769008 (ODISHA) June-2013.

[38] R.K. Nema, Sativa Nema and Gayatri Agnihotri “Computer Simulation Based Study of Photovoltaic Cells/Modules and their Experimental Verification” International journal of recent trends in Engineering, Vol 1, No. 3, May 2009.

APPENDIX “A”

Shell Solar

Product Information Sheet

Shell SP75 Photovoltaic Solar Module

General

The Shell SP75 module contains 36 series connected 125 x 125 mm PowerMax® mono-crystalline silicon solar cells.

The Shell SP75 can generate a peak power of 75 watts at 17 volts.

The Shell SP75 solar module has been designed for grid connected and industrial applications.

Qualifications and Certificates

The Shell SP75 solar module meets the following requirements:

- IEC 61215
- UL - Listing 1703
- FM approved
- TÜV Isolation Class II

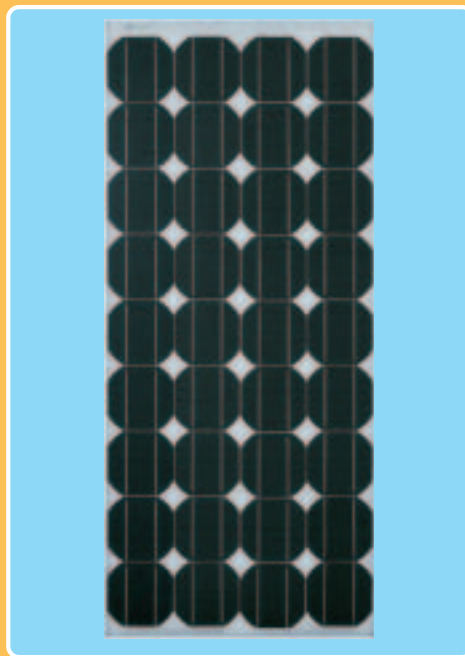


All Shell Solar modules are produced in ENISO 9001 certified factories.

Limited Warranties

- Peak Power for 25 years

Shell SP75 Module



Junction Box

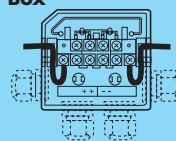
The junction box provides a high quality, dust protected and splash proof IP44-rated housing. The housing contains a rigid connection block with screw terminals and by-pass diodes providing "hot spot" protection for the solar cells.

ProCharger™-CR Junction Box

Maximum conductor cross-section: 4 mm²

Type of protection: IP44

Number of by-pass diodes: 2



Benefits

- PowerMax® mono-crystalline solar cells deliver maximum power output even under reduced light conditions providing more power where space is a limitation.
- The surface of the PowerMax® cell has a pyramidal textured surface to enable more light absorption and deliver exceptional efficiency.
- Highly transparent tempered glass delivers more power and ensures high impact resistance and protection against hail, snow, ice, and storms.
- Nearly 300MW of cumulative installed experience has been applied to the evolution of our mono-crystalline range to ensure that our products have a long and reliable service life backed by a 25 year warranty.



**ELECTRICAL EQUIPMENT,
CHECK WITH YOUR INSTALLER**

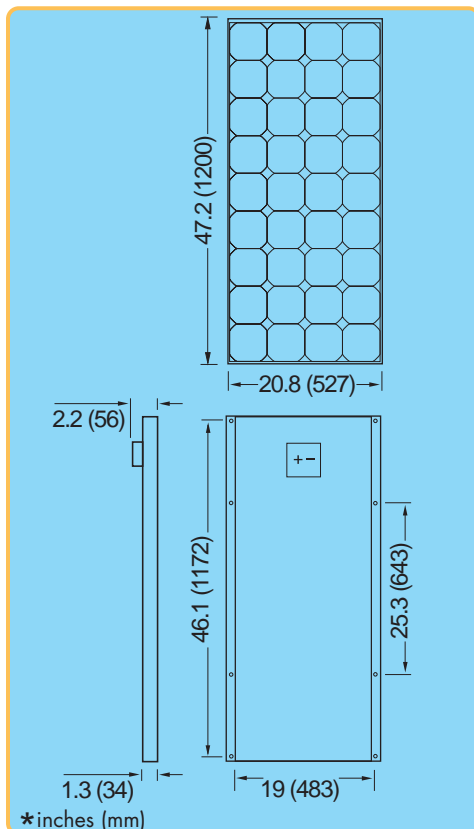
Due to continuous research and product improvement the specifications in this Product Information Sheet are subject to change without notice. Specifications can vary slightly. For installation and operation instructions, see the applicable manuals. No rights can be derived from this Product Information Sheet and Shell Solar assumes no liability whatsoever connected to or resulting from the use of any information contained herein.



Shell SP75 Photovoltaic Solar Module

Mechanical Specifications Module

A torsion and corrosion-resistant anodized aluminium frame ensures dependable performance, even under harsh weather conditions. Pre-drilled mounting holes are provided for ease of installation.



Outside dimensions (in)	47.2 x 20.8
Thickness (inc. junction box) (in)	2.2
Thickness (exc. junction box) (in)	1.3
Weight (lbs)	16.7

For installation instructions, please refer to the **Installation Manual** which is available from Shell Solar.

Electrical Characteristics

Data at Standard Test Conditions (STC)

STC: irradiance level 1000W/m², spectrum AM 1.5 and cell temperature 25°C

Rated power	P_r	75W
Peak power	P_{mpp}	75W
Peak power voltage	V_{mpp}	8.5*/17V
Peak power current	I_{mpp}	8.8*/4.4A
Open circuit voltage	V_{oc}	10.85*/21.7V
Short circuit current	I_{sc}	9.6*/4.8A
Series fuse rating		15A
Minimum peak power	$P_{mpp\ min}$	70W

The abbreviation 'mpp' stands for Maximum Power Point.

Typical data at Nominal Operating Cell Temperature (NOCT) conditions

NOCT: 800W/m² irradiance level, AM 1.5 spectrum, wind velocity 1m/s, T_{amb} 20°C

Temperature	T_{NOCT}	45°C
Mpp power	P_{mpp}	54W
Mpp voltage	V_{mpp}	7.8*/15.6V
Open circuit voltage	V_{oc}	9.95*/19.9V
Short circuit current	I_{sc}	7.8*/3.9A

* The Shell SP75 may be reconfigured in the field for 6V operation

Typical data at low irradiance

The relative reduction of module efficiency at an irradiance of 200W/m² in relation to 1000W/m² both at 25°C cell temperature and AM 1.5 spectrum is 7%.

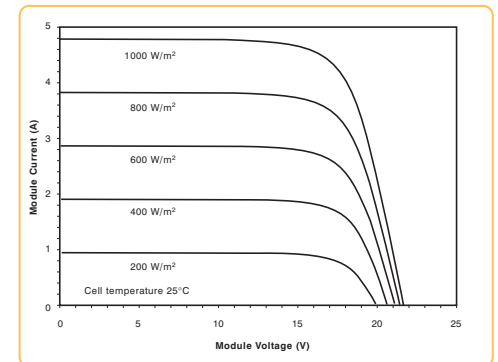
Temperature coefficients

αP_{mpp}	-0.45 %/°C
αV_{mpp}	-76 mV/°C
αI_{sc}	+2 mA/°C
αV_{oc}	-76 mV/°C

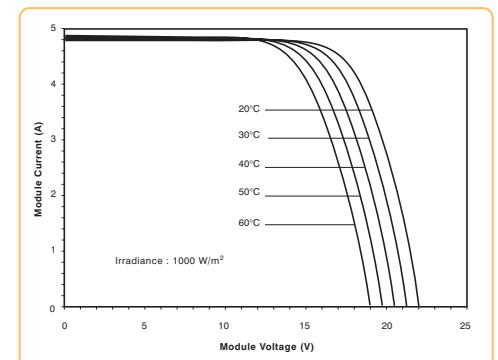
Maximum system voltage: 600 Vdc

Typical I/V Characteristics

The I/V graph below shows the typical performance of the solar module at various levels of irradiance.



The I/V graph below shows the typical performance of the solar module at various cell temperatures.



References in this Product Information Sheet to 'Shell Solar' are to companies and other organizational entities within the Royal Dutch/Shell Group of Companies that are engaged in the photovoltaic solar energy business. Shell Solar was set up in 1999 and has its principal office in Amsterdam, the Netherlands.

For further information on all Shell Solar products contact:

Shell Solar
4650 Adohr Lane, Camarillo CA 93012
805-482-6800 Fax 805-388-6511
Web www.shell.com/renewables

V2/SP75/05/02/US



APPENDIX “B”

**REPETITIVE AVALANCHE AND dv/dt RATED
 HEXFET® TRANSISTORS
 THRU-HOLE (TO-204AA/AE)**

**IRF150
 JANTX2N6764
 JANTXV2N6764
 [REF:MIL-PRF-19500/543]
 100V, N-CHANNEL**

Product Summary

Part Number	BVDSS	RDS(on)	ID
IRF150	100V	0.055Ω	38A

The HEXFET® technology is the key to International Rectifier's advanced line of power MOSFET transistors. The efficient geometry and unique processing of this latest "State of the Art" design achieves: very low on-state resistance combined with high transconductance; superior reverse energy and diode recovery dv/dt capability.

The HEXFET transistors also feature all of the well established advantages of MOSFETs such as voltage control, very fast switching, ease of paralleling and temperature stability of the electrical parameters.

They are well suited for applications such as switching power supplies, motor controls, inverters, choppers, audio amplifiers and high energy pulse circuits.



Features:

- Repetitive Avalanche Ratings
- Dynamic dv/dt Rating
- Hermetically Sealed
- Simple Drive Requirements
- Ease of Paralleling

Absolute Maximum Ratings

	Parameter		Units
ID @ VGS = 10V, TC = 25°C	Continuous Drain Current	38	A
ID @ VGS = 10V, TC = 100°C	Continuous Drain Current	24	
IDM	Pulsed Drain Current ①	152	
PD @ TC = 25°C	Max. Power Dissipation	150	W
	Linear Derating Factor	1.2	W/°C
VGS	Gate-to-Source Voltage	±20	V
EAS	Single Pulse Avalanche Energy ②	150	mJ
IAR	Avalanche Current ①	38	A
EAR	Repetitive Avalanche Energy ①	15	mJ
dv/dt	Peak Diode Recovery dv/dt ③	5.5	V/ns
TJ	Operating Junction	-55 to 150	°C
TSTG	Storage Temperature Range		
	Lead Temperature	300 (0.063 in. (1.6mm) from case for 10s)	
	Weight	11.5 (typical)	g

For footnotes refer to the last page

Electrical Characteristics @ T_j = 25°C (Unless Otherwise Specified)

	Parameter	Min	Typ	Max	Units	Test Conditions
BV _{DSS}	Drain-to-Source Breakdown Voltage	100	—	—	V	V _{GS} = 0V, I _D = 1.0mA
ΔBV _{DSS} /ΔT _J	Temperature Coefficient of Breakdown Voltage	—	0.13	—	V/°C	Reference to 25°C, I _D = 1.0mA
R _{DS(on)}	Static Drain-to-Source On-State Resistance	—	—	0.055 0.065	Ω	V _{GS} = 10V, I _D = 24A ^④ V _{GS} = 10V, I _D = 38A ^④
V _{GS(th)}	Gate Threshold Voltage	2.0	—	4.0	V	V _{DS} = V _{GS} , I _D = 250μA
g _{fs}	Forward Transconductance	9.0	—	—	S (r̄)	V _{DS} > 15V, I _{DS} = 24A ^④
I _{DSS}	Zero Gate Voltage Drain Current	—	—	25 250	μA	V _{DS} = 80V, V _{GS} = 0V V _{DS} = 80V V _{GS} = 0V, T _J = 125°C
I _{GSS}	Gate-to-Source Leakage Forward	—	—	100	nA	V _{GS} = 20V
I _{GSS}	Gate-to-Source Leakage Reverse	—	—	-100	nA	V _{GS} = -20V
Q _g	Total Gate Charge	50	—	125	nC	V _{GS} = 10V, I _D = 38A V _{DS} = 50V
Q _{gs}	Gate-to-Source Charge	8.0	—	22	nC	
Q _{gd}	Gate-to-Drain ('Miller') Charge	25	—	65	nC	
t _{d(on)}	Turn-On Delay Time	—	—	35	ns	V _{DD} = 50V, I _D = 38A, V _{GS} = 10V, R _G = 2.35Ω
t _r	Rise Time	—	—	190		
t _{d(off)}	Turn-Off Delay Time	—	—	170		
t _f	Fall Time	—	—	130		
L _S + L _D	Total Inductance	—	6.1	—	nH	Measured from the center of drain pad to center of source pad
C _{iss}	Input Capacitance	—	3700	—	pF	V _{GS} = 0V, V _{DS} = 25V f = 1.0MHz
C _{oss}	Output Capacitance	—	1100	—		
C _{rss}	Reverse Transfer Capacitance	—	200	—		

Source-Drain Diode Ratings and Characteristics

	Parameter	Min	Typ	Max	Units	Test Conditions
I _S	Continuous Source Current (Body Diode)	—	—	38	A	
I _{SM}	Pulse Source Current (Body Diode) ^①	—	—	152		
V _{SD}	Diode Forward Voltage	—	—	1.9	V	T _j = 25°C, I _S = 38A, V _{GS} = 0V ^④
t _{rr}	Reverse Recovery Time	—	—	500	rS	T _j = 25°C, I _F = 38A, di/dt ≤ 100A/μs
Q _{RR}	Reverse Recovery Charge	—	—	2.9	μC	V _{DD} ≤ 30V ^④
t _{on}	Forward Turn-On Time	Intrinsic turn-on time is negligible. Turn-on speed is substantially controlled by L _S + L _D .				

Thermal Resistance

	Parameter	Min	Typ	Max	Units	Test Conditions
R _{thJC}	Junction to Case	—	—	0.83	°C/W	Typical socket mount
R _{thJA}	Junction to Ambient	—	—	30		

For footnotes refer to the last page

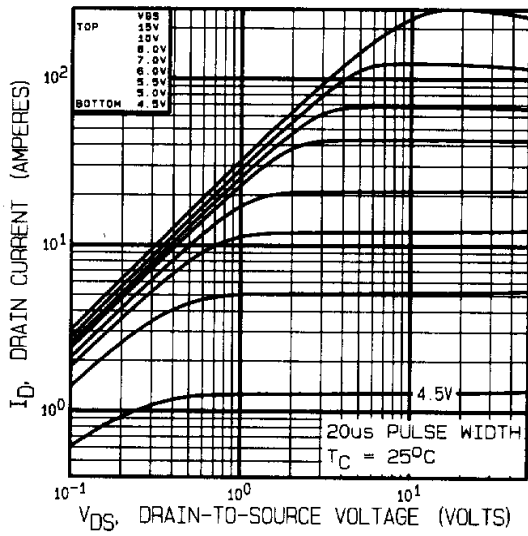


Fig 1. Typical Output Characteristics

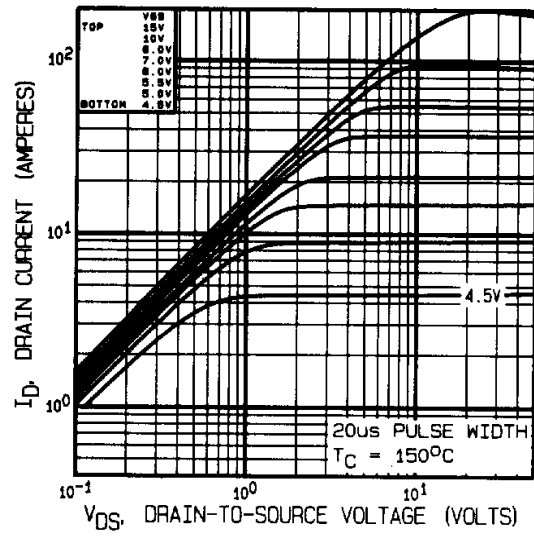


Fig 2. Typical Output Characteristics

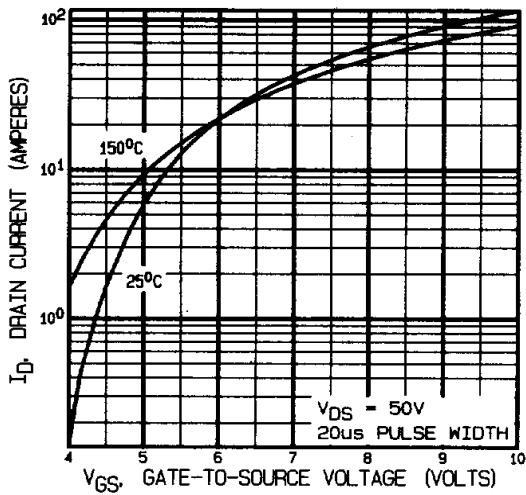


Fig 3. Typical Transfer Characteristics

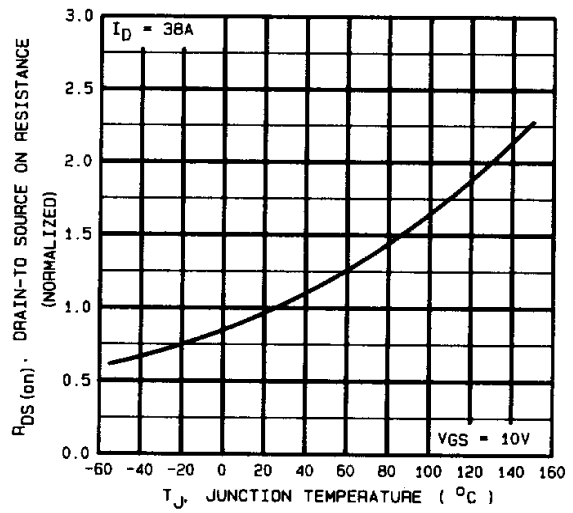


Fig 4. Normalized On-Resistance Vs. Temperature

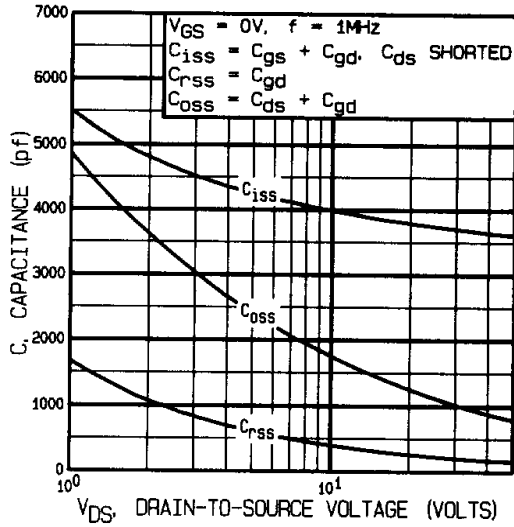


Fig 5. Typical Capacitance Vs. Drain-to-Source Voltage

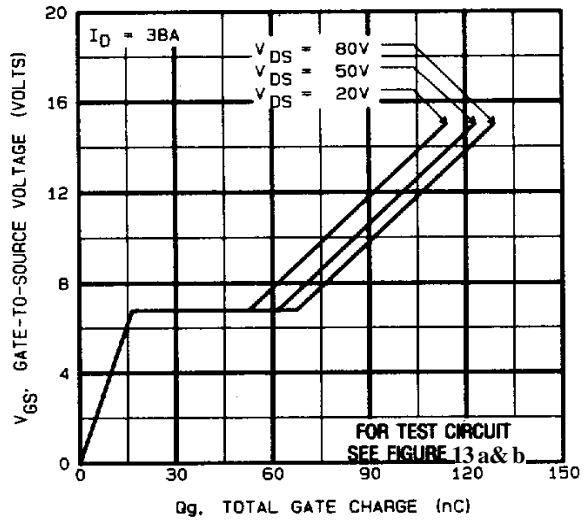


Fig 6. Typical Gate Charge Vs. Gate-to-Source Voltage

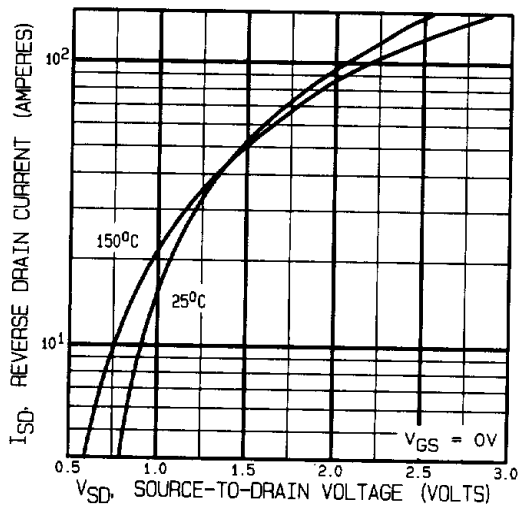


Fig 7. Typical Source-Drain Diode Forward Voltage

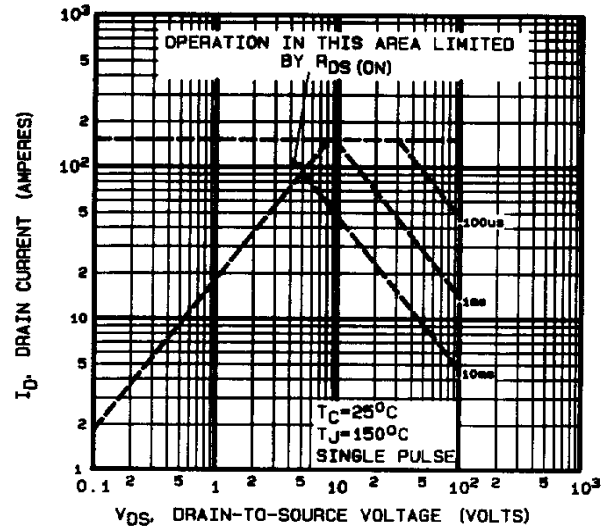


Fig 8. Maximum Safe Operating Area

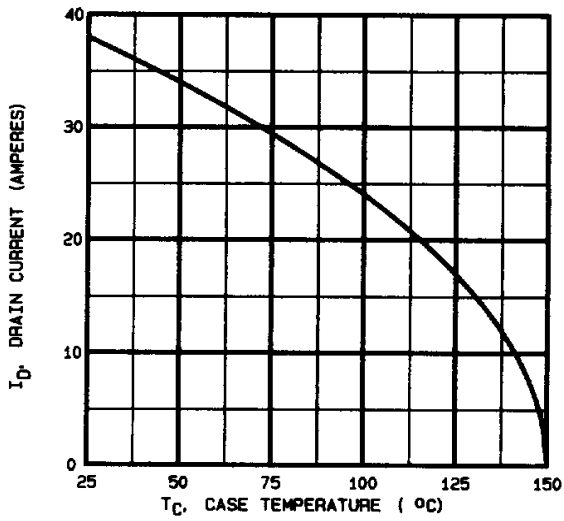


Fig 9. Maximum Drain Current Vs. Case Temperature

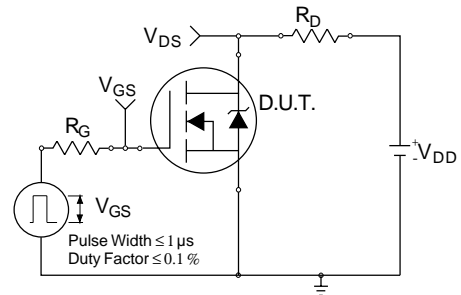


Fig 10a. Switching Time Test Circuit

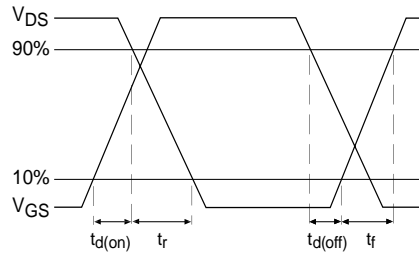


Fig 10b. Switching Time Waveforms

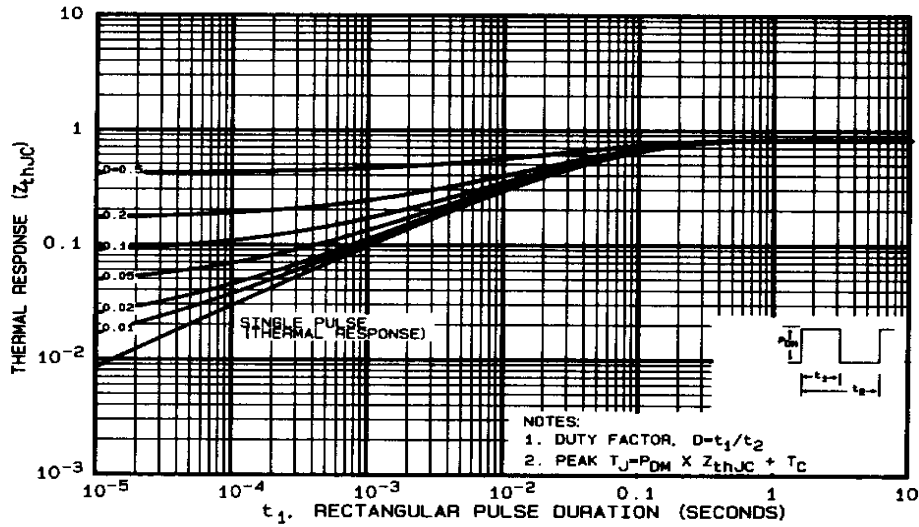


Fig 11. Maximum Effective Transient Thermal Impedance, Junction-to-Case

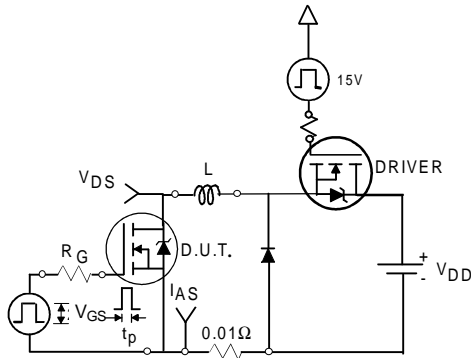


Fig 12a. Unclamped Inductive Test Circuit

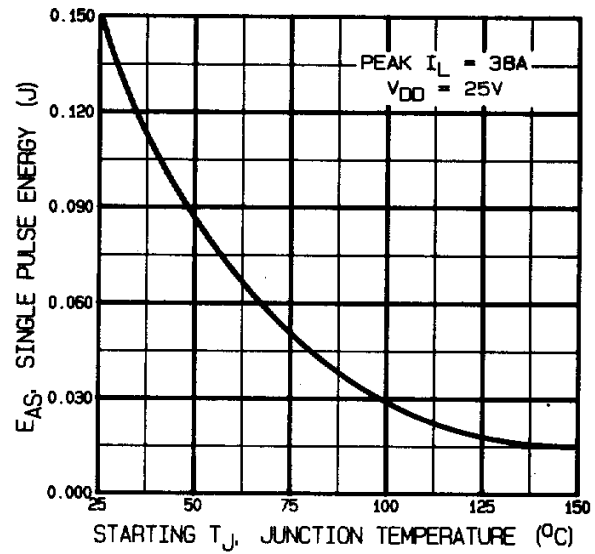


Fig 12c. Maximum Avalanche Energy Vs. Drain Current

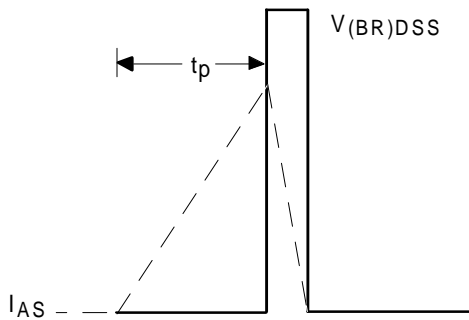


Fig 12b. Unclamped Inductive Waveforms

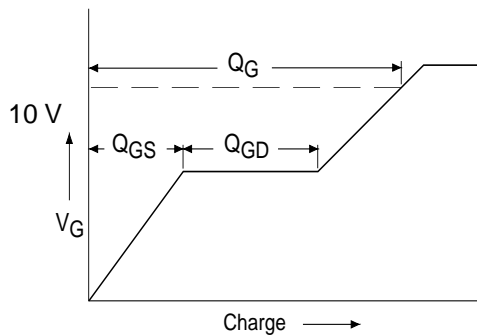


Fig 13a. Basic Gate Charge Waveform

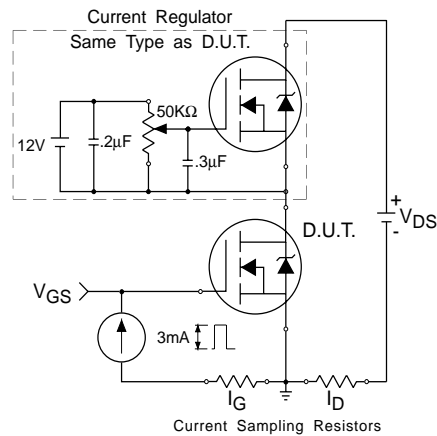
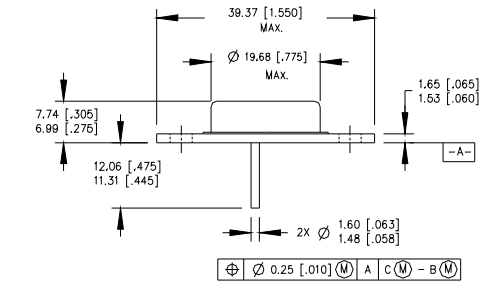


Fig 13b. Gate Charge Test Circuit

Foot Notes:

- ① Repetitive Rating; Pulse width limited by maximum junction temperature.
- ② $V_{DD} = 50V$, starting $T_J = 25^\circ C$, Peak $I_L = 38A$, $V_{GS} = 10V$
- ③ $I_{SD} \leq 38A$, $di/dt \leq 300A/\mu s$, $V_{DD} \leq 100V$, $T_J \leq 150^\circ C$
Suggested $R_G = 2.35 \Omega$
- ④ Pulse width $\leq 300 \mu s$; Duty Cycle $\leq 2\%$

Case Outline and Dimensions —TO-204AE (Modified TO-3)

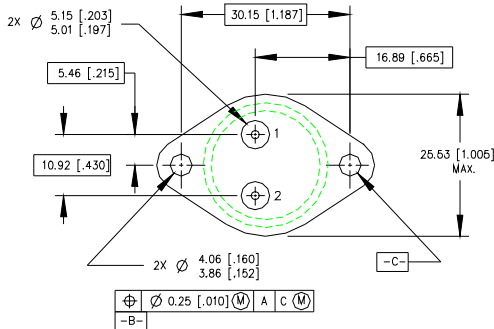


PIN ASSIGNMENTS

- 1 - SOURCE
- 2 - GATE
- 3 - DRAIN (CASE)

NOTES:

1. DIMENSIONING & TOLERANCING PER ANSI Y14.6M-1982.
2. CONTROLLING DIMENSION: INCH.
3. DIMENSIONS ARE SHOWN IN MILLIMETERS [INCHES].
4. OUTLINE CONFORMS TO JEDEC OUTLINE TO-204AE.



APPENDIX “C”

DATA SHEET

NE/SA/SE555/SE555C

Timer

Product data
Supersedes data of 1994 Aug 31

2003 Feb 14

Timer

NE/SA/SE555/SE555C

DESCRIPTION

The 555 monolithic timing circuit is a highly stable controller capable of producing accurate time delays, or oscillation. In the time delay mode of operation, the time is precisely controlled by one external resistor and capacitor. For a stable operation as an oscillator, the free running frequency and the duty cycle are both accurately controlled with two external resistors and one capacitor. The circuit may be triggered and reset on falling waveforms, and the output structure can source or sink up to 200 mA.

FEATURES

- Turn-off time less than 2 μ s
- Max. operating frequency greater than 500 kHz
- Timing from microseconds to hours
- Operates in both astable and monostable modes
- High output current
- Adjustable duty cycle
- TTL compatible
- Temperature stability of 0.005% per $^{\circ}$ C

APPLICATIONS

- Precision timing
- Pulse generation
- Sequential timing
- Time delay generation
- Pulse width modulation

PIN CONFIGURATION

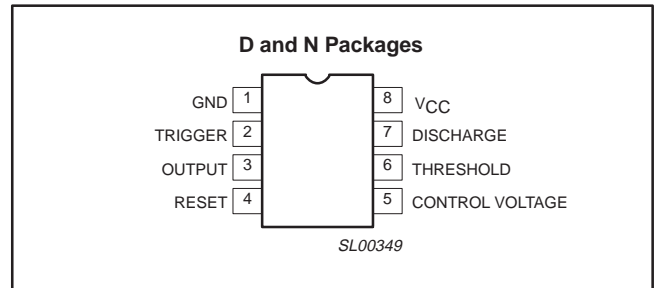


Figure 1. Pin configuration

BLOCK DIAGRAM

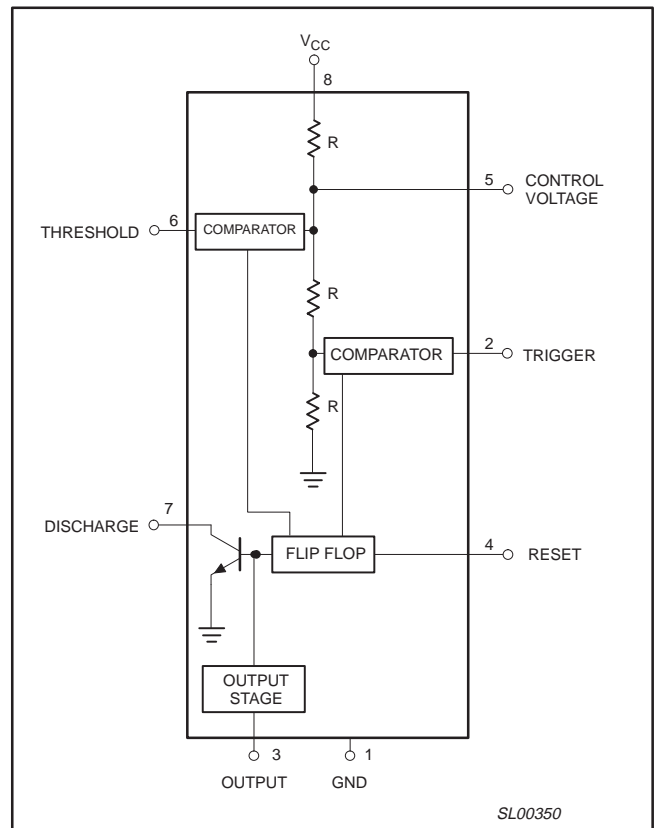


Figure 2. Block Diagram

ORDERING INFORMATION

DESCRIPTION	TEMPERATURE RANGE	ORDER CODE	DWG #
8-Pin Plastic Small Outline (SO) Package	0 to +70 $^{\circ}$ C	NE555D	SOT96-1
8-Pin Plastic Dual In-Line Package (DIP)	0 to +70 $^{\circ}$ C	NE555N	SOT97-1
8-Pin Plastic Small Outline (SO) Package	-40 $^{\circ}$ C to +85 $^{\circ}$ C	SA555D	SOT96-1
8-Pin Plastic Dual In-Line Package (DIP)	-40 $^{\circ}$ C to +85 $^{\circ}$ C	SA555N	SOT97-1
8-Pin Plastic Dual In-Line Package (DIP)	-55 $^{\circ}$ C to +125 $^{\circ}$ C	SE555CN	SOT97-1
8-Pin Plastic Dual In-Line Package (DIP)	-55 $^{\circ}$ C to +125 $^{\circ}$ C	SE555N	SOT97-1

Timer

NE/SA/SE555/SE555C

EQUIVALENT SCHEMATIC

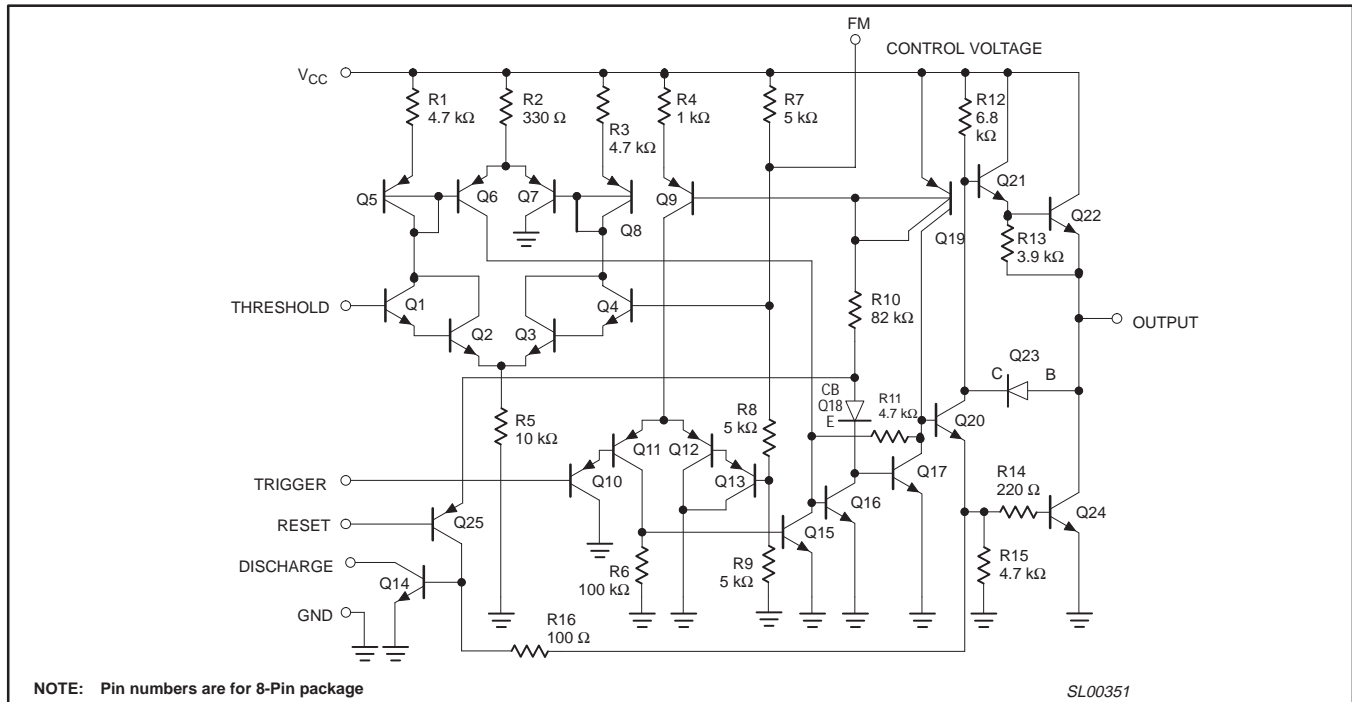


Figure 3. Equivalent schematic

ABSOLUTE MAXIMUM RATINGS

SYMBOL	PARAMETER	RATING	UNIT
V _{CC}	Supply voltage		
	SE555	+18	V
	NE555, SE555C, SA555	+16	V
P _D	Maximum allowable power dissipation ¹	600	mW
T _{amb}	Operating ambient temperature range		
	NE555	0 to +70	°C
	SA555	-40 to +85	°C
	SE555, SE555C	-55 to +125	°C
T _{stg}	Storage temperature range	-65 to +150	°C
T _{SOLD}	Lead soldering temperature (10 sec max)	+230	°C

NOTE:

- The junction temperature must be kept below 125 °C for the D package and below 150°C for the N package. At ambient temperatures above 25 °C, where this limit would be derated by the following factors:
 D package 160 °C/W
 N package 100 °C/W

Timer

NE/SA/SE555/SE555C

DC AND AC ELECTRICAL CHARACTERISTICS

$T_{amb} = 25\text{ }^{\circ}\text{C}$, $V_{CC} = +5\text{ V}$ to $+15\text{ V}$ unless otherwise specified.

SYMBOL	PARAMETER	TEST CONDITIONS	SE555			NE555/SA555/SE555C			UNIT
			Min	Typ	Max	Min	Typ	Max	
V_{CC}	Supply voltage		4.5		18	4.5		16	V
I_{CC}	Supply current (low state) ¹	$V_{CC} = 5\text{ V}$, $R_L = \infty$ $V_{CC} = 15\text{ V}$, $R_L = \infty$		3 10	5 12		3 10	6 15	 mA mA
t_M $\Delta t_M/\Delta T$ $\Delta t_M/\Delta V_S$	Timing error (monostable) Initial accuracy ² Drift with temperature Drift with supply voltage	$R_A = 2\text{ k}\Omega$ to $100\text{ k}\Omega$ $C = 0.1\text{ }\mu\text{F}$		0.5 30 0.05	2.0 100 0.2		1.0 50 0.1	3.0 150 0.5	 % ppm/ $^{\circ}\text{C}$ %/V
t_A $\Delta t_A/\Delta T$ $\Delta t_A/\Delta V_S$	Timing error (astable) Initial accuracy ² Drift with temperature Drift with supply voltage	$R_A, R_B = 1\text{ k}\Omega$ to $100\text{ k}\Omega$ $C = 0.1\text{ }\mu\text{F}$ $V_{CC} = 15\text{ V}$		4 0.15	6 500 0.6		5 0.3	13 500 1	 % ppm/ $^{\circ}\text{C}$ %/V
V_C	Control voltage level	$V_{CC} = 15\text{ V}$ $V_{CC} = 5\text{ V}$	9.6 2.9	10.0 3.33	10.4 3.8	9.0 2.6	10.0 3.33	11.0 4.0	 V V
V_{TH}	Threshold voltage	$V_{CC} = 15\text{ V}$ $V_{CC} = 5\text{ V}$	9.4 2.7	10.0 3.33	10.6 4.0	8.8 2.4	10.0 3.33	11.2 4.2	 V V
I_{TH}	Threshold current ³			0.1	0.25		0.1	0.25	μA
V_{TRIG}	Trigger voltage	$V_{CC} = 15\text{ V}$ $V_{CC} = 5\text{ V}$	4.8 1.45	5.0 1.67	5.2 1.9	4.5 1.1	5.0 1.67	5.6 2.2	 V V
I_{TRIG}	Trigger current	$V_{TRIG} = 0\text{ V}$		0.5	0.9		0.5	2.0	μA
V_{RESET}	Reset voltage ⁴	$V_{CC} = 15\text{ V}$, $V_{TH} = 10.5\text{ V}$	0.3		1.0	0.3		1.0	V
I_{RESET}	Reset current Reset current	$V_{RESET} = 0.4\text{ V}$ $V_{RESET} = 0\text{ V}$		0.1 0.4	0.4 1.0		0.1 0.4	0.4 1.5	 mA mA
V_{OL}	LOW-level output voltage	$V_{CC} = 15\text{ V}$ $I_{SINK} = 10\text{ mA}$ $I_{SINK} = 50\text{ mA}$ $I_{SINK} = 100\text{ mA}$ $I_{SINK} = 200\text{ mA}$		0.1 0.4 2.0 2.5	0.15 0.5 2.2		0.1 0.4 2.0 2.5	0.25 0.75 2.5	 V V V V
		$V_{CC} = 5\text{ V}$ $I_{SINK} = 8\text{ mA}$ $I_{SINK} = 5\text{ mA}$		0.1 0.05	0.25 0.2		0.3 0.25	0.4 0.35	 V V
V_{OH}	HIGH-level output voltage	$V_{CC} = 15\text{ V}$ $I_{SOURCE} = 200\text{ mA}$ $I_{SOURCE} = 100\text{ mA}$	13.0	12.5 13.3			12.5 13.3		 V V
		$V_{CC} = 5\text{ V}$ $I_{SOURCE} = 100\text{ mA}$	3.0	3.3		2.75	3.3		 V
t_{OFF}	Turn-off time ⁵	$V_{RESET} = V_{CC}$		0.5	2.0		0.5	2.0	μs
t_R	Rise time of output			100	200		100	300	ns
t_F	Fall time of output			100	200		100	300	ns
	Discharge leakage current			20	100		20	100	nA

NOTES:

- Supply current when output high typically 1 mA less.
- Tested at $V_{CC} = 5\text{ V}$ and $V_{CC} = 15\text{ V}$.
- This will determine the max value of $R_A + R_B$, for 15 V operation, the max total $R = 10\text{ M}\Omega$, and for 5 V operation, the max. total $R = 3.4\text{ M}\Omega$.
- Specified with trigger input HIGH.
- Time measured from a positive-going input pulse from 0 to $0.8 \times V_{CC}$ into the threshold to the drop from HIGH to LOW of the output. Trigger is tied to threshold.

Timer

NE/SA/SE555/SE555C

TYPICAL PERFORMANCE CHARACTERISTICS

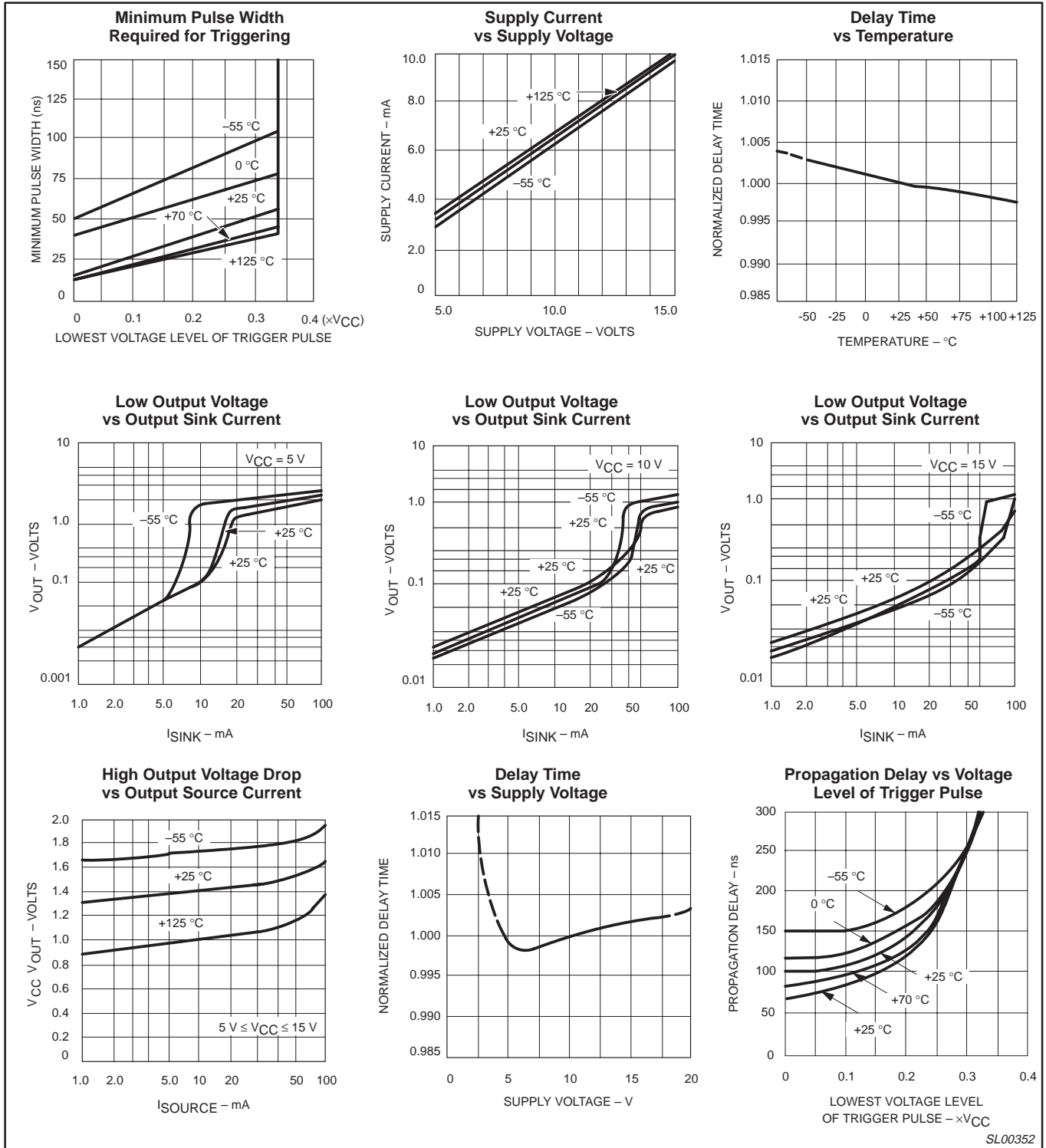


Figure 4. Typical Performance Characteristics

Timer

NE/SA/SE555/SE555C

TYPICAL APPLICATIONS

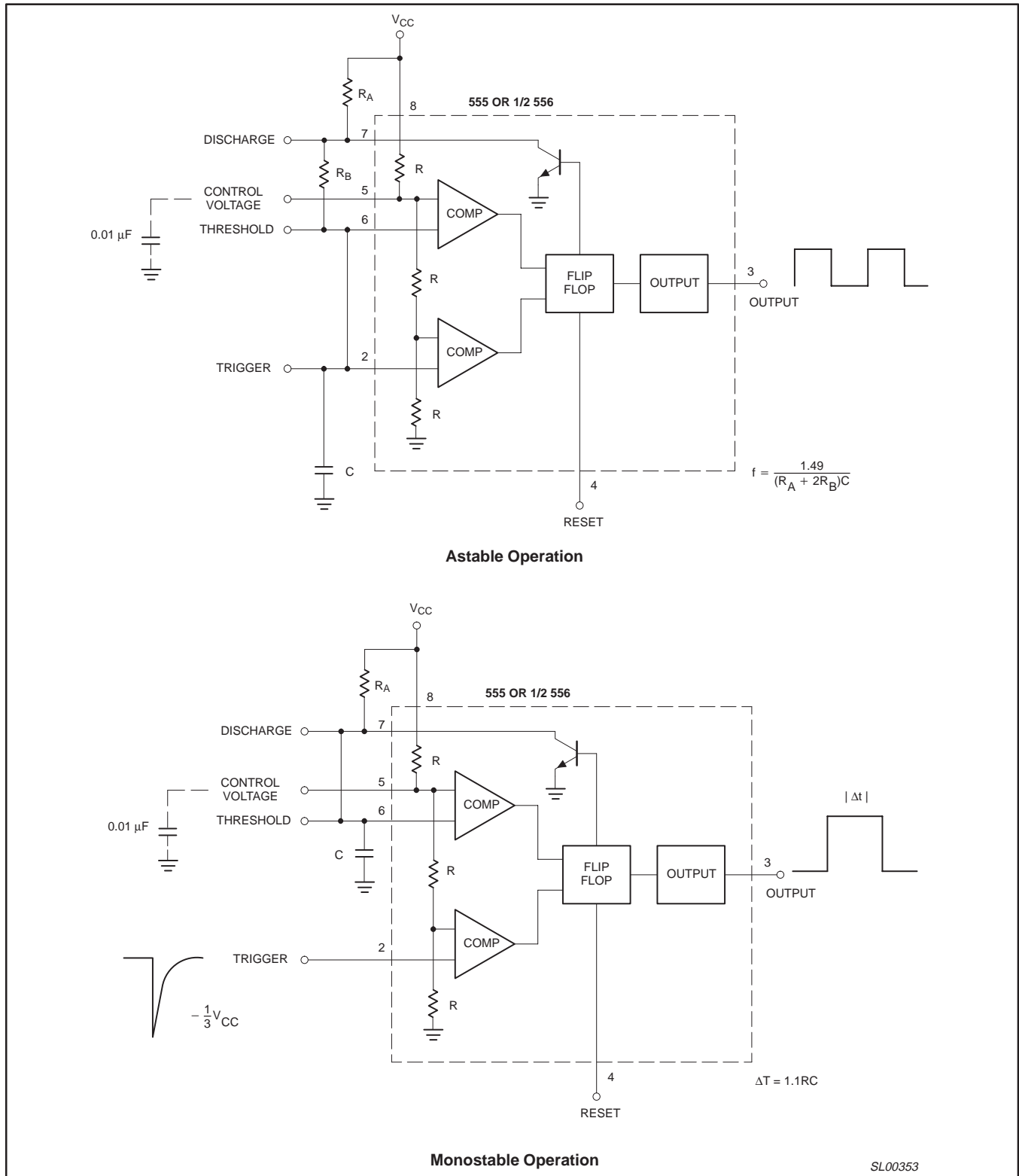


Figure 5. Typical Applications

TYPICAL APPLICATIONS

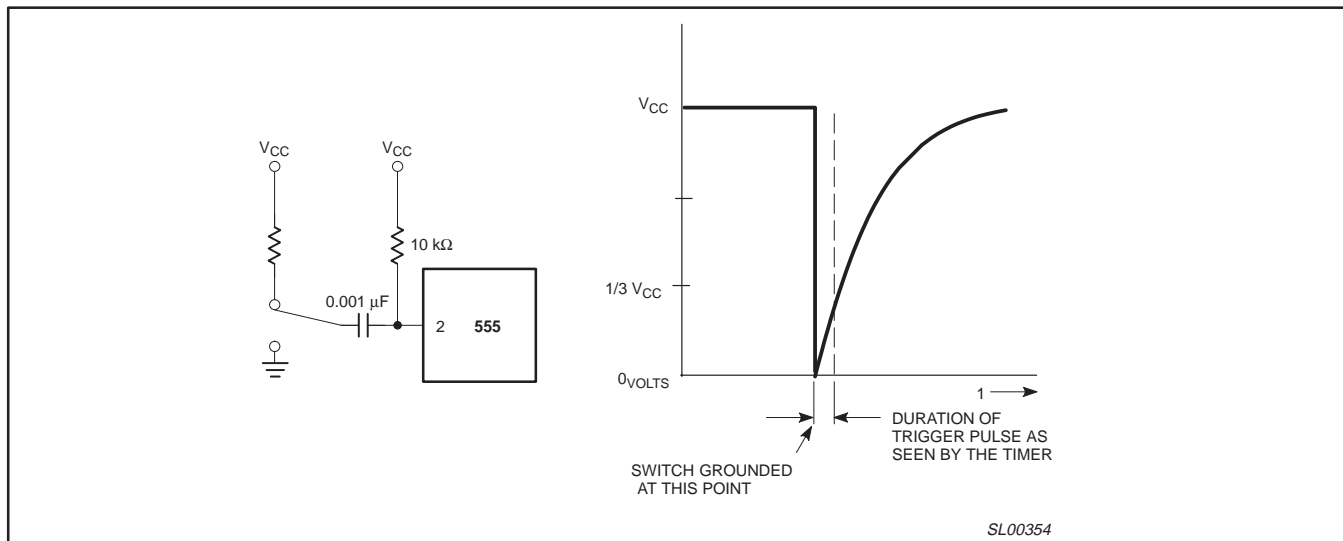


Figure 6. AC Coupling of the Trigger Pulse

Trigger Pulse Width Requirements and Time Delays

Due to the nature of the trigger circuitry, the timer will trigger on the negative going edge of the input pulse. For the device to time out properly, it is necessary that the trigger voltage level be returned to some voltage greater than one third of the supply before the time out period. This can be achieved by making either the trigger pulse sufficiently short or by AC coupling into the trigger. By AC coupling the trigger, see Figure 6, a short negative going pulse is achieved when the trigger signal goes to ground. AC coupling is most frequently used in conjunction with a switch or a signal that goes to ground which initiates the timing cycle. Should the trigger be held low, without AC coupling, for a longer duration than the timing cycle the output will remain in a high state for the duration of the low trigger signal, without regard to the threshold comparator state. This is due to the predominance of Q₁₅ on the base of Q₁₆, controlling the state of the bi-stable flip-flop. When the trigger signal then returns to a high level, the output will fall immediately. Thus, the output signal will follow the trigger signal in this case.

Another consideration is the “turn-off time”. This is the measurement of the amount of time required after the threshold reaches 2/3 V_{CC} to turn the output low. To explain further, Q₁ at the threshold input turns on after reaching 2/3 V_{CC}, which then turns on Q₅, which turns on Q₆. Current from Q₆ turns on Q₁₆ which turns Q₁₇ off. This allows current from Q₁₉ to turn on Q₂₀ and Q₂₄ to given an output low. These steps cause the 2 μs max. delay as stated in the data sheet.

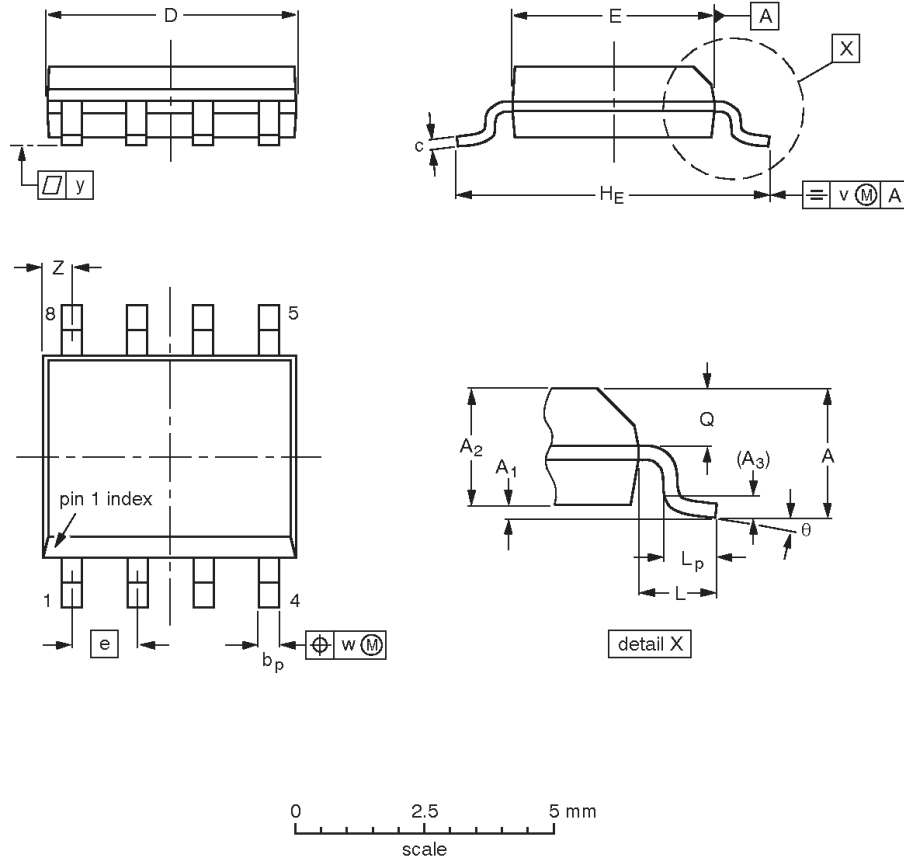
Also, a delay comparable to the turn-off time is the trigger release time. When the trigger is low, Q₁₀ is on and turns on Q₁₁ which turns on Q₁₅. Q₁₅ turns off Q₁₆ and allows Q₁₇ to turn on. This turns off current to Q₂₀ and Q₂₄, which results in output high. When the trigger is released, Q₁₀ and Q₁₁ shut off, Q₁₅ turns off, Q₁₆ turns on and the circuit then follows the same path and time delay explained as “turn off time”. This trigger release time is very important in designing the trigger pulse width so as not to interfere with the output signal as explained previously.

Timer

NE/SA/SE555/SE555C

S08: plastic small outline package; 8 leads; body width 3.9 mm

SOT96-1



DIMENSIONS (inch dimensions are derived from the original mm dimensions)

UNIT	A max.	A ₁	A ₂	A ₃	b _p	c	D ⁽¹⁾	E ⁽²⁾	e	H _E	L	L _p	Q	v	w	y	Z ⁽¹⁾	θ
mm	1.75	0.25 0.10	1.45 1.25	0.25	0.49 0.36	0.25 0.19	5.0 4.8	4.0 3.8	1.27	6.2 5.8	1.05	1.0 0.4	0.7 0.6	0.25	0.25	0.1	0.7 0.3	8° 0°
inches	0.069	0.010 0.004	0.057 0.049	0.01	0.019 0.014	0.0100 0.0075	0.20 0.19	0.16 0.15	0.050	0.244 0.228	0.041	0.039 0.016	0.028 0.024	0.01	0.01	0.004	0.028 0.012	

Notes

1. Plastic or metal protrusions of 0.15 mm maximum per side are not included.
2. Plastic or metal protrusions of 0.25 mm maximum per side are not included.

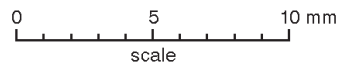
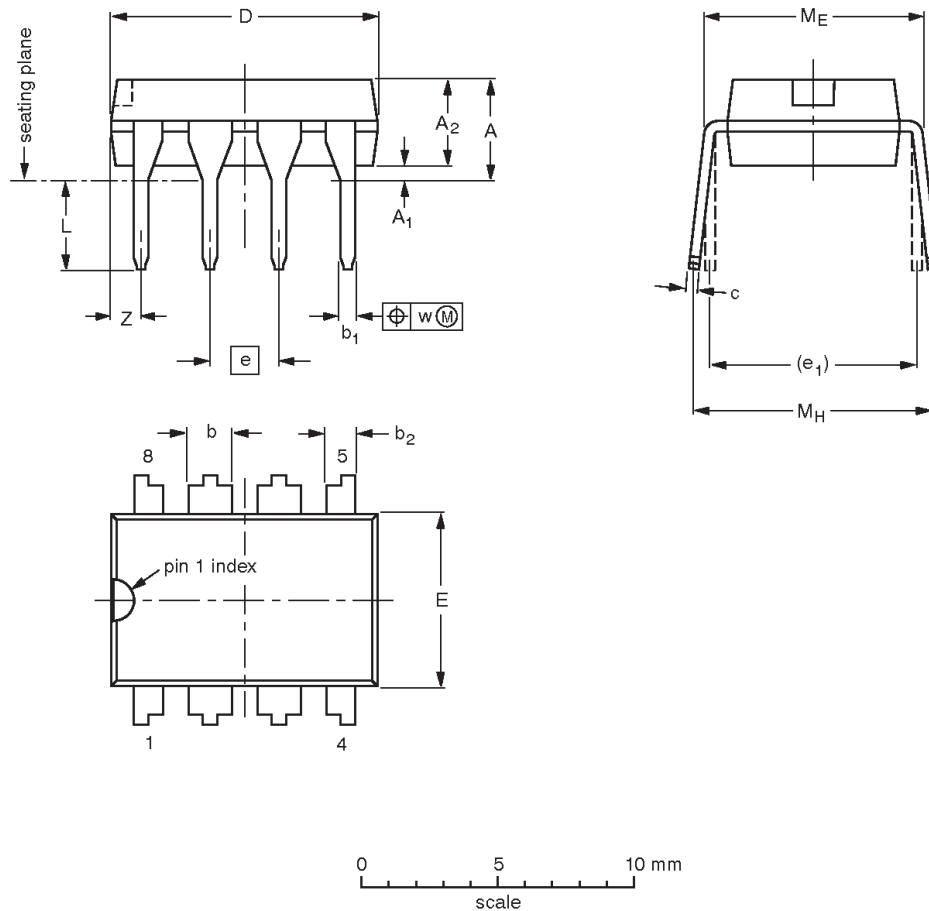
OUTLINE VERSION	REFERENCES				EUROPEAN PROJECTION	ISSUE DATE
	IEC	JEDEC	EIAJ			
SOT96-1	076E03	MS-012				97-05-22 99-12-27

Timer

NE/SA/SE555/SE555C

DIP8: plastic dual in-line package; 8 leads (300 mil)

SOT97-1



DIMENSIONS (inch dimensions are derived from the original mm dimensions)

UNIT	A max.	A ₁ min.	A ₂ max.	b	b ₁	b ₂	c	D ⁽¹⁾	E ⁽¹⁾	e	e ₁	L	M _E	M _H	w	Z ⁽¹⁾ max.
mm	4.2	0.51	3.2	1.73 1.14	0.53 0.38	1.07 0.89	0.36 0.23	9.8 9.2	6.48 6.20	2.54	7.62	3.60 3.05	8.25 7.80	10.0 8.3	0.254	1.15
inches	0.17	0.020	0.13	0.068 0.045	0.021 0.015	0.042 0.035	0.014 0.009	0.39 0.36	0.26 0.24	0.10	0.30	0.14 0.12	0.32 0.31	0.39 0.33	0.01	0.045

Note

1. Plastic or metal protrusions of 0.25 mm maximum per side are not included.

OUTLINE VERSION	REFERENCES				EUROPEAN PROJECTION	ISSUE DATE
	IEC	JEDEC	EIAJ			
SOT97-1	050G01	MO-001	SC-504-8			95-02-04 99-12-27

Timer

NE/SA/SE555/SE555C

REVISION HISTORY

Rev	Date	Description
2	20030214	Product data (9397 750 11129); ECN 853-0036 29156 of 06 November 2002. Supersedes Product specification dated August 31, 1994. Modifications: <ul style="list-style-type: none">• Remove all cerdip information from the data sheet. Package type discontinued.• 'Absolute maximum ratings' table: T{SOLD} rating changed from '+300 °C' to '+230 °C'.
	19940831	Product specification; ECN 853-0036 13721 of 31 August 1994. (Filename = NE_SA555X.pdf)

Timer

NE/SA/SE555/SE555C

Data sheet status

Level	Data sheet status ^[1]	Product status ^{[2] [3]}	Definitions
I	Objective data	Development	This data sheet contains data from the objective specification for product development. Philips Semiconductors reserves the right to change the specification in any manner without notice.
II	Preliminary data	Qualification	This data sheet contains data from the preliminary specification. Supplementary data will be published at a later date. Philips Semiconductors reserves the right to change the specification without notice, in order to improve the design and supply the best possible product.
III	Product data	Production	This data sheet contains data from the product specification. Philips Semiconductors reserves the right to make changes at any time in order to improve the design, manufacturing and supply. Relevant changes will be communicated via a Customer Product/Process Change Notification (CPCN).

[1] Please consult the most recently issued data sheet before initiating or completing a design.

[2] The product status of the device(s) described in this data sheet may have changed since this data sheet was published. The latest information is available on the Internet at URL <http://www.semiconductors.philips.com>.

[3] For data sheets describing multiple type numbers, the highest-level product status determines the data sheet status.

Definitions

Short-form specification — The data in a short-form specification is extracted from a full data sheet with the same type number and title. For detailed information see the relevant data sheet or data handbook.

Limiting values definition — Limiting values given are in accordance with the Absolute Maximum Rating System (IEC 60134). Stress above one or more of the limiting values may cause permanent damage to the device. These are stress ratings only and operation of the device at these or at any other conditions above those given in the Characteristics sections of the specification is not implied. Exposure to limiting values for extended periods may affect device reliability.

Application information — Applications that are described herein for any of these products are for illustrative purposes only. Philips Semiconductors make no representation or warranty that such applications will be suitable for the specified use without further testing or modification.

Disclaimers

Life support — These products are not designed for use in life support appliances, devices, or systems where malfunction of these products can reasonably be expected to result in personal injury. Philips Semiconductors customers using or selling these products for use in such applications do so at their own risk and agree to fully indemnify Philips Semiconductors for any damages resulting from such application.

Right to make changes — Philips Semiconductors reserves the right to make changes in the products—including circuits, standard cells, and/or software—described or contained herein in order to improve design and/or performance. When the product is in full production (status 'Production'), relevant changes will be communicated via a Customer Product/Process Change Notification (CPCN). Philips Semiconductors assumes no responsibility or liability for the use of any of these products, conveys no license or title under any patent, copyright, or mask work right to these products, and makes no representations or warranties that these products are free from patent, copyright, or mask work right infringement, unless otherwise specified.

Contact information

For additional information please visit
<http://www.semiconductors.philips.com>. Fax: +31 40 27 24825

© Koninklijke Philips Electronics N.V. 2003
 All rights reserved. Printed in U.S.A.

Date of release: 02-03

For sales offices addresses send e-mail to:
sales.addresses@www.semiconductors.philips.com

Document order number:

9397 750 11129

Let's make things better.

This datasheet has been download from:

www.datasheetcatalog.com

Datasheets for electronics components.



جمهورية العراق
وزارة التعليم العالي والبحث العلمي
جامعة النهرين
كلية العلوم

استخدام طريقة لتتبع نقطة الطاقة القصوى على اساس درجة الحرارة للسطوح الكهروضوئية باستخدام برنامج *PSPICE*

رسالة

مقدمة الى كلية العلوم \ جامعة النهرين
كجزء من متطلبات نيل درجة ماجستير في علوم الفيزياء

من قبل

حارث محمد سعيد حامد
بكالوريوس جامعة النهرين ٢٠١٤

بإشراف

أ.م.د. زينب منذر يونس

الخلاصة

أستخدم برنامج المحاكاة PSPICE لتصميم نموذج خلية شمسية عند طاقة 75 واط وتيار 4.8 أمبير وعند فولتية مقدارها 21 فولت وبعد ذلك تم دراسة سلوك وخصائص ذلك النموذج عند ظروف بيئية مختلفة مثل تغيير شدة الأشعاع الشمسي ودرجة الحرارة المحيطة بالإضافة الى تغيير درجة حرارة سطح اللوح الشمسي.

وتم تصميم هذا النموذج بحيث يمكن أستداعائه من مكتبة ال PSPICE كمصدر جاهز لأستعمالة في أغراض مختلفة.

يهدف هذا البحث الى دراسة تأثير درجة حرارة سطح اللوح الشمسي على الخواص الخارجة من اللوح الشمسي وسيتم أستخدام معادلة رياضية لتقدير درجة حرارة سطح اللوح الشمسي وأستخدامها ليعمل اللوح الشمسي في نقطة الطاقة القصوى سوف يتم تصميم رافع فولتية DC-DC لزيادة كفاءة النظام الشمسي. وسيتم بعد ذلك رافع فولتية DC-DC لزيادة كفاءة النظام الكهروضوئي.

المغير الرفع (DC-DC Boost converter) سيرفع فولتية اللوح الشمسي الى 34 فولت لكل تغير يحصل في درجة حرارة سطح اللوح الشمسي التي تتراوح بين 300 درجة مطلقة الى 350 درجة مطلقة.